MARMARA UNIVERSITY
INSTITUTE FOR GRADUATE STUDIES IN PURE AND APPLIED SCIENCES

ARTIFICIAL INTELLIGENCE APPLICATION IN INTEGRATED GASIFICATION SOLID OXIDE FUEL CELL CYCLE

SENEM SEZER

MASTER THESIS
Department of Chemical Engineering

Thesis Supervisor
Asst. Prof. Dr. Uğur ÖZVEREN

ISTANBUL, 2021

MARMARA UNIVERSITY
INSTITUTE FOR GRADUATE STUDIES IN PURE AND APPLIED SCIENCES

ARTIFICIAL INTELLIGENCE APPLICATION IN INTEGRATED GASIFICATION SOLID OXIDE FUEL CELL CYCLE

SENEM SEZER

(524518003)

MASTER THESIS

Department of Chemical Engineering

Thesis Supervisor

Asst. Prof. Dr. Uğur ÖZVEREN

ISTANBUL, 2021

ACKNOWLEDGEMENT

I would like to express my sincere appreciation to my dissertation advisor, Asst. Prof. Dr. Uğur ÖZVEREN, for his continuous support, encouragement and motivation throughout my graduate study and accomplishment of this thesis. His guidance helped me in all time for our research. Without his supports and experiences my graduate study would not have been as much as valuable.

I would also like to sincerely thank to Furkan KARTAL for his precious supports and contributions throughout the thesis. I am grateful to him for his good friendship and collaboration during my graduate study. My appreciation also extends to Halime YAKIŞIK and all colleagues in Modeling Laboratory for their supports.

I am thankful to Marmara University Scientific Research Projects Coordination Unit under grant number FEN-C-YLP-250919-0272 for their financial support to carry out this study. I would also like to sincerely thank to Türk Petrol Vakfı for their scholarship during my thesis.

Finally, I also want to express my gratitude to all my family for all patience and prayer.

June, 2021 **Senem SEZER**

TABLE OF CONTENTS

ACKNOWLEDGEMENT i

ÖZET iv

ABSTRACT v

SYMBOLS vi

ABBREVIATIONS viii

LIST OF TABLES x

LIST OF FIGURES xi

1. INTRODUCTION 1

2. LITERATURE 5

2.1. Gasification 5

2.1.1. Design Parameters 7

2.2. Gasifier Types 9

2.2.1. Fixed Bed Gasifiers 9

2.2.2. Fluidized Bed Gasifiers 9

2.2.3. Entrained Flow Gasifiers 11

2.3. Fuel Cells 12

2.3.1. SOFC 14

2.4. Modeling of Integrated Gasification-SOFC system 16

2.5. Artificial Neural Network 17

3. Materials and Methods 19

3.1. Fuel Characterization 19

3.2. Gasification Process 22

3.2.1. Development of BFBG Model in Aspen Plus 22

3.3. SOFC Process 28
3.3.1. Development of SOFC Model in Aspen Plus 28
3.4. Development of Integrated BFBG-SOFC Model 37
3.5. Development of the ANN Models 40
3.5.1. ANN Model Topology 40
3.5.2. Training Process 41
3.5.3. Error Evaluation of the ANN model 43
4. RESULTS AND DISCUSSION 45
4.1. Model Validation Results of BFBG 45
4.2. Model Validation Results of SOFC 47
4.3. Parametric Study for Integrated BFBG-SOFC Model 49
4.3.1. Effect of the Gasification Temperature on Syngas Composition 50
4.3.2. Effect of the S/B Ratio on Syngas Composition 53
4.3.3. Effect of the Gasification Temperature on SOFC 56
4.3.4. Effect of S/B Ratio on SOFC 59
4.3.5. Effect of Anode Temperature on SOFC 62
4.4. ANN Model Results 65
4.4.1. Input Selection of the ANN Models 65
4.4.2. Structure of ANN Models 68
4.4.3. Performance Assessment of the ANN Models 70
5. CONCLUSION 78
REFERENCES 80

ÖZET

GAZLAŞTIRICI İLE ENTEGRE EDİLMİŞ KATI OKSİT YAKIT HÜCRESİ ÇEVRİMİNDE YAPAY ZEKA UYGULAMASI

Fosil kaynakların hızla tükenmesi ve çevre üzerindeki zararlı etkileri nedeniyle, enerji üretiminde yenilenebilir ve çevre dostu kaynakların kullanılması büyük önem taşımaktadır. Yüksek enerji talebini verimli dönüşüm yöntemleri kullanarak karşılayabilecek bir kaynak olan biyokütlenin kullanımı son yıllarda oldukça ilgi görmektedir. Biyokütle gazlaştırma, daha az emisyona neden olan ve verimli dönüşüm sağlayan umut vadeden bir teknolojidir.

Gazlaştırma prosesinden üretilen yüksek H_2 içerikli gaz ürünü, doğrudan elektrik üretiminde kullanılmaya uygun bir yapıdadır. Katı oksit yakıt hücresi (KOYH) biyokütle türevi yakıtlar için en uygun tip olduğu varsayılan elektrokimyasal reaksiyonlar kullanarak kimyasal enerjiyi elektriğe dönüştürebilen cihazlardır. Literatürde entegre olarak çalışan gazlaştırıcı-KOYH sistemleriyle ilgili birçok çalışma bulunmasına rağmen bu sistemler hala geliştirilmekte olup yüksek verimde enerji elde etmek için uygun dizayn parametreleri ve çalışma koşulları üzerinde çalışmalar yapılmaktadır. Gazlaştırma ve KOYH sisteminin sıfır boyutlu (termodinamik) yöntem kullanılarak modellenmesi, proses davranışını belirlemenin en basit yoludur. Yapay sinir ağı (YSA), termodinamik tabanlı gazlaştırma ve KOYH sistemlerini temsil etmek için son yıllarda oldukça popüler olan modelleme yöntemlerinden biridir.

Bu tezde, Aspen Plus simülasyonu kullanılarak YSA modellerinin eğitimi için veri üretmek üzere entegre bir kabarcıklı akışkan yataklı gazlaştırıcı ve KOYH modeli oluşturulmuştur. YSA modelleri, giriş parametresi olarak biyokütle türleri ve çalışma koşulları kullanılarak elektriksel verim, net voltaj ve akım yoğunluğu açısından performans parametrelerini tahmin etmiştir. Sonuçlar, geliştirilen YSA modellerinin çıktı parametrelerini yüksek doğrulukla tahmin ettiğini göstermektedir.

ABSTRACT

ARTIFICIAL INTELLIGENCE APPLICATION IN INTEGRATED GASIFICATION SOLID OXIDE FUEL CELL CYCLE

Due to the rapid consumption of fossil resources and their harmful effects on the environment, it is very important to use renewable and environmentally friendly sources for energy production. The use of biomass, which is a resource that can meet the high energy demand through efficient conversion methods, has attracted much attention in recent years. Biomass gasification is a promising technology that produces fewer emissions and enables efficient conversion.

The high hydrogen content gasification is suitable for direct use in power generation. The solid oxide fuel cell (SOFC) can convert the chemical energy into electricity, which is probably the most suitable fuel cell type for biomass-derived fuels. The integrated gasification SOFC systems are still under development to determine suitable design parameters and operating conditions for high energy efficiency. Modeling the Gasifier-SOFC cycles using the thermodynamic method is the simplest way to determine the process behavior. Artificial neural networks (ANN) are one of the modeling methods that are popular nowadays to represent the thermodynamic based gasification and SOFC systems.

In this dissertation, an integrated bubbling fluidized bed gasifier and SOFC model was built to generate data for training the ANN models with Aspen Plus simulation. The ANN models predicted the performance parameters in terms of electrical efficiency, net voltage and current density using the biomass types and operating conditions as input parameters. The results show that the developed ANN models estimated the output parameters with high accuracy.

SYMBOLS

A : Ampere

C : Carbon

CO_2 : Carbon dioxide

CH_4 : Methane

C_xH_y : Higher hydrocarbons

Cl : Chlorine

CO : Carbon monoxide

C/mol : Coulomb/mol

F : Faraday constant

f : Fugacity

G^T : Total Gibbs free energy

H_2 : Hydrogen

HCl : Hydrogen chloride

H_2S : Hydrogen sulfur

h : hour

J : Joule

kg : kilogram

kW : Kilowatt

m : Meter

mV : Millivolt

NH_3 : Ammonia

NOx : Nitrogen oxides

N_2 : Nitrogen

n_i : Number of moles

O_2 : Oxygen

P : Ambient pressure (atm)

P^0 : Partial pressure (atm)

P_{syngas} : Inlet pressure of syngas

P_{SOFC} : SOFC operating pressure

R : Universal gas constant (J/mol K)

R^2 : Coefficient of determination

SOx : Sulfur oxides

T : Temperature (°C)

U_a : Air utilization factor

U_f : Fuel utilization factor

wt% : Weight percentage

y_i : Mole fraction

μ_i : Chemical potential

λ_k : Lagrange multiplier

φ_i : Fugacity coefficient

$\Delta\bar{g}_f$: Gibbs free energy of formation

ABBREVIATIONS

AFC **:** Alkaline fuel cell

ANN **:** Artificial neural network

AI **:** Artificial Intelligence

AC **:** Ash

ACP **:** AC power

BFBG **:** Bubbling fluidized bed gasifier

DCP **:** DC Power

EE **:** Overall electrical efficiency

FFBP **:** Feed forward back propagation

FC **:** Fixed carbon

I **:** Current

j **:** Current density

LHV_{fuel} **:** Energy content of fuel

L-M **:** Levenberg-Marquardt

LNN **:** Layered neural network

MLP **:** Multilayer perceptron

MSE **:** Mean-square error

ME **:** Mean error

MAPE **:** Mean absolute percentage error

MRAE **:** Mean relative absolute error

MCFC **:** Molten carbonate fuel cell

MC **:** Moisture

MNN **:** Modular neural network

PEMFC **:** Polymer electrolyte membrane fuel cell

PAFC **:** Phosphoric acid fuel cell

RMSE **:** Root mean square error

RNN **:** Recurrent neural network

RBFNN **:** Radial basis function neural network

S/B **:** Steam to biomass

SCR **:** Steam to carbon ratio

SOFC **:** Solid oxide fuel cell

SRK **:** Soave - Redlich – Kwong

UN **:** United Nations

VM **:** Volatile matter

$\mathbf{V_{id}}$ **:** Ideal voltage value

$\mathbf{V_{Nr}}$ **:** Nernst voltage

$\mathbf{V_a}$ **:** Activation losses

$\mathbf{V_o}$ **:** Ohmic losses

$\mathbf{V_c}$ **:** Concentration losses

$\mathbf{V_{act}}$ **:** Actual voltage value

LIST OF TABLES

Table 2.1 Thermo-chemical conversion processes 5
Table 2.2 Fuel cell types based on electrolyte characteristics 13
Table 3.1 Proximate and ultimate analysis results of biomass samples (dry basis) 20
Table 3.2 Definition of the gasification steps in Aspen Plus 27
Table 3.3 Definition of blocks in the SOFC model 31
Table 3.4 Equations for voltage losses 34
Table 3.5 Model design parameters for voltage losses 36
Table 3.6 Model geometry and material parameters 37
Table 4.1 Operating conditions of the validation data sets. 45
Table 4.2 Operating parameters of the SOFC model in literature study. 47
Table 4.3 SOFC model validation results. 48
Table 4.4 Operating parameters of BFBG-SOFC system 49
Table 4.5 Input parameters for the ANN model devolopment 66
Table 4.6 Specifications of the ANN models 69
Table 4.7 Error evaluation results 77

LIST OF FIGURES

Figure 2.1 Gasification zones in gasifier [13] 6
Figure 2.2 Fuel conversion process in BFBG..... 11
Figure 2.3 SOFC system..... 12
Figure 2.4 Tubular SOFC [82]..... 15
Figure 3.1 Flowsheet of the BFBG in Aspen Plus 23
Figure 3.2 Flow diagram of tubular SOFC in Aspen Plus..... 29
Figure 3.3 Integrated BFBG-SOFC model..... 38
Figure 3.4 Perceptron structure..... 41
Figure 4.1 Comparison of the model and experimental works..... 46
Figure 4.2 Change of gas concentrations in syngas according to temperature (S/B:0.7) 52
Figure 4.3 Change of gas concentrations in syngas according to S/B ratio (Gasifier Temperature: 800 °C)..... 55
Figure 4.4 Effect of the BFBG temperature on SOFC 58
Figure 4.5 Effect of S/B ratio on SOFC 61
Figure 4.6 Effect of anode temperature on SOFC..... 64
Figure 4.7 Correlation matrix for input and output parameters of the ANN models. .. 67
Figure 4.8 MLP structure of the developed ANN models..... 69
Figure 4.9 Performance analysis of training, test and validation data sets in terms of MSE..... 71
Figure 4.10 R^2 plot during ANN models training 73
Figure 4.11 R^2 plot during ANN models testing 74
Figure 4.12 R^2 plot during ANN models validation..... 74
Figure 4.13 Error histogram plots..... 76

1. INTRODUCTION

The world energy consumption will continue to rise at an accelerated rate in the coming decades [1]. The United Nations (UN) projects that the world population will grow to over 9 billion by 2040. This considerable increase in population will lead to a similar increase in demand for clean and consistent energy resources. Traditionally, fossil fuels have been used to generate electricity using various technologies in gas turbine, internal combustion engine and steam turbine plants. However, the rapid depletion of fossil fuels poses a major threat to economic growth and energy security [2]. Therefore, the replacement of conventional fuels with alternative energy sources is taken great interest [3]. In addition to carbon dioxide (CO_2) emissions, use of fossil sources also releases sulfur oxides (SOx) and nitrogen oxides (NOx) pollutants, which have negative impacts on the ecosystem [4].

Among the alternative energy sources such as wind, hydrothermal, solar, etc., biomass has received considerable attention with its highest potential considering energy efficiency. Moreover, CO_2 neutral characteristic and negligible nitrogen and sulfur content makes biomass a charming option from environmental point of view. Unlike fossil fuels, biomass is regenerated quickly and includes a wide variety of waste materials derived from plants and animals [5]. Further, the technologies based on biomass are provided a great contribution to the sustainable progress especially in developing countries. In Europe, about 13.6% of the biomass sources are used to generate electricity, 73.8% and 12.6% to produce heat and biofuels for heating and transport respectively in 2015 [6]. The biomass should be converted into the gaseous or liquid forms to provide better performance of its applications [7]. In this regard, there are many options based on thermochemical routes such as pyrolysis, combustion, and gasification.

Gasification is a promising pathway that converts carbonaceous materials into a gaseous product consisting mainly of combustible (hydrogen (H_2), methane (CH_4), carbon monoxide (CO)) and non-combustible (CO_2, nitrogen) gases. Gasification is a prominent route considering its higher energy recovery, lower pollutant emissions and lower content of tar and char in the final product [8]. Performance of the gasification process has been investigated by means of quantity and quality of syngas [9-11]. The design and operating

conditions of the gasification process such as gasifier type, heat source, pressure and gasification agent are determined according to the type and quantity of feedstock and the desired product composition [12]. Selection of the proper gasifier type is one of the key parameters to obtain the produced gas with higher efficiency. The various gasifier configurations which are entrained flow, fluidized bed and fixed bed are classified into according to their distinguishing features. Gasification in fluidized bed are preferable due to its excellent heat and mass transfer and better carbon conversion efficiency and capability of handle a wide range of particle sizes. [13]. Fluidized bed gasifiers can be divided into two subcategories, namely bubbling and circulating bed gasifiers. Comparing the fluidized bed gasifiers from the point of view of processing and design, the bubbling bed gasifier is considered to be the simpler type. The gasification agent, which can be steam, air, oxygen and their mixtures in a certain amount, is supplied to the system as an oxidant to react with the carbonaceous materials in the gasification process. The gasification agent that promotes the gasification reactions has an extreme effect on the syngas composition. The use of steam as an oxidant results in the production of a syngas with relatively high H_2 content, in contrast, the use of oxygen or air as a gasification agent results in obtaining a syngas with higher CO_2 and CO and lower H_2 and contents [14].

The syngas generated from the gasification process is a suitable component to form chemicals and fuels for the chemical industries and power generation. Between the diverse combined process systems to generate power by utilizing syngas, fuel cell-based systems are considered as the most promising one. Fuel cells are the electrochemical devices that can convert chemical energy into electricity by using electrochemical reactions with less harmful emissions at higher efficiency [15]. Solid oxide fuel cell (SOFC) is kind of the fuel cell type that operated higher temperature compared to another types. Besides, it is supposed the most convenient type for biomass derived fuels due to its higher operating temperature that leads to flexibility to several fuel and tolerant to contaminants [16].

Even though the integrated gasification and SOFC system is considered more efficient than other heat and power technologies, it is needed to develop and optimize to get over the problems related to design and operating parameters. Experiments need extra time and cost to specify the effect of the operating parameters on the integrated system. Thus, the modeling

of the gasification and SOFC system provides the reliable approach to specify the suitable configuration and optimum values of the operating conditions [17, 18]. The research related to modeling have usually conducted by using zero-dimensional (thermodynamic) method. The thermodynamic model is the simplest way to estimate the process behavior [19]. The gasification and SOFC are represented as a complex series of reactions. Aspen Plus is the mostly used software to model the systems on the basis of mass and energy balance [20]. Therefore, using the thermodynamic principles during the developing of the integrated gasification and SOFC model ensure to obtain the output parameters such as syngas composition, cell voltage, cell power and efficiencies etc. with simple and reliable way.

Artificial neural network (ANN) is another modeling method that is popular nowadays to obtain process outputs for thermodynamic based gasification or SOFC systems [21]. ANN models are able to develop a pattern for the input and output parameters of the system through their prior experience. Compared to other methods, ANN creates a faster response, regardless of the complexity of the model.

In the previous research studies about gasifier integrated SOFC have been modeled many times by using Aspen Plus [22-27]. However, ANN model has not been studied in the literature to optimize the process and examine the influence of the process parameters on the desired outputs for integrated gasifier and SOFC process [16, 28-31].

The main objectives of this study were:

- To develop a new ANN model with high generalization capability for an integrated gasification and SOFC system for bubbling fluidized bed gasifier based on a thermodynamic approach using data generated from the Aspen Plus model, which is validated with experimental data.
- To examine the effects of operating parameters and feedstock types on the performance parameters of the integrated gasification and SOFC system by means of artificial intelligence.
- To contribute to the literature using alternative energy technologies with a novel ANN approach.

In this dissertation, an integrated bubbling fluidized bed gasifier and SOFC model was

designed to generate data for the training and testing processes of the ANN models using Aspen Plus. The effects of the biomass types and operating parameters were investigated on the outputs of the system by performing sensitivity analysis. The input parameters of the models were selected in a wide range in order to the create comprehensive models that predict the performance parameters in terms of electrical efficiency, net voltage and current density. The results show that the developed ANN model has been predicted the output parameters with high accuracy.

In the following chapter, a literature review on gasification, fuel cells and modeling methods have been discussed. In the third chapter, the methodology of this work has been presented, in particular the Aspen Plus models of gasification and SOFC based on thermodynamic calculations and development of the ANN. Finally, the modeling results of the integrated gasification and ANN system for several cases have been examined. In the last part, the conclusions obtained from this work have been presented with suggestions for future studies.

2. LITERATURE

2.1. Gasification

Thermochemical conversion methods of carbonaceous solids consist of three diverse processes such as combustion, gasification and pyrolysis [32-34]. Depending on their operating conditions, oxidizing agent and final products, they are summarized in Table 2.1. Gasification is a thermochemical conversion process in which a carbonaceous solid is partially oxidized with air, steam or CO_2 to produce a gaseous mixture of CO, H_2, CO_2 and CH_4 named as syngas [35]. The fuels (except ash) are entirely converted into gaseous products during gasification.

Table 2.1 Thermo-chemical conversion processes

Process	Oxidizer	Temperature (°C)	Primary Products
Pyrolysis	-	200-700	Char, tar, liquid
Gasification	O_2, CO_2, H_2O	700-1300	H_2,CO, CO_2, ash
Combustion	O_2	700-1400	CO_2, ash

Unlike the other conversion methods, the syngas (H_2 and CO) produced during gasification can be utilized as fuel for electricity generation and as feedstock for chemicals [36]. In addition, gasification has the following advantages over the other methods [37]:

- Generation of useful products from wastes and trashy materials.
- Utilization of different types of raw materials (coal, agricultural, poultry, forest, petrochemical and municipal wastes).
- Negligible emissions in the syngas.

Gasification consists of two distinctive stages: in the first stage the solid fuels are heated until phase change occurred in their internal structure, and in the second stage char decomposes into the gases CO and H_2. In real applications, the sharp boundaries are not always clear, but they are evaluated separately. These stages, which are assumed to occur sequentially, are explained in detail as follows. [38].

Drying: The first step where the fuel sample meets the gasifier is drying [33]. Drying ensures

the removal of moisture due to mass transfer and requires a heat source. The temperature is about 150 °C during the process that takes place [19]. The moisture contained in the inherent composition of the solid fuel is reduced at this stage without chemical reactions.

Pyrolysis: Thermal decomposition of solid fuels begins in the pyrolysis stage, the temperature range of 200-500 °C in the absence of oxidizing agent [39]. Organic volatiles are released, and primary char and tar are formed. The char produced is used to rise the energy content of the feedstock before the gasification stage.

Gasification: In the gasification or reduction stage, the tar formed in the pyrolysis stage is cracked into gases. Secondary tar is formed and cracked into gases consecutively. Heterogeneous and homogeneous gas phase reactions take place [40].

Combustion: The unstable products of pyrolysis are combusted with immensely exothermic reactions. The oxidation reactions of the combustible gases occur rapidly [41].

A schematic representation of the decomposition process of the solid fuel in the gasification process is shown in Figure 2.1.

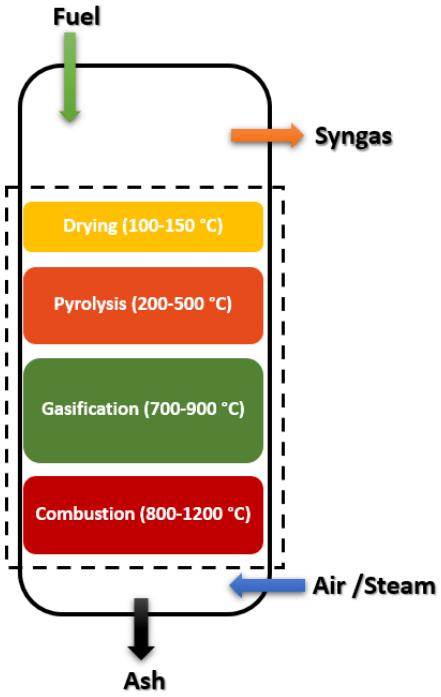


Figure 2.1 Gasification zones in gasifier [13]

Several number of endothermic and exothermic reactions form in the gasification [42, 43]. The heat needed for the endothermic reactions is provided by the oxidation reactions that occur in the combustion step or by an external source. The reactions involving solid carbon, called heterogeneous reactions, are given as (2.1), (2.2), (2.3), (2.4), and (2.5). The main products of these reactions are CO and H_2.

Boudouard reaction: $C + CO_2 \leftrightarrow 2CO$	+172 kJ/mol	(2.1)
Water-gas reaction: $C + H_2O \leftrightarrow CO + H_2$	+131 kJ/mol	(2.2)
Hydrogasification: $C + 2H_2 \leftrightarrow CH_4$	−74.8 kJ/mol	(2.3)
Carbon partial oxidation: $C + 0.5O_2 \rightarrow 2CO$	−111 kJ/mol	(2.4)
Carbon oxidation: $C + O_2 \rightarrow CO_2$	−394 kJ/mol	(2.5)

Homogenous reactions that occur in the gasification are presented as below:

Carbon monoxide oxidation: $CO + 0.5O_2 \rightarrow CO_2$	−283 kJ/mol	(2.6)
Steam methane reforming: $CH_4 + H_2O \leftrightarrow CO + 3H_2$	+206 kJ/mol	(2.7)
Methane partial oxidation: $CH_4 + 2O_2 \leftrightarrow CO_2 + 2H_2O$	−803 kJ/mol	(2.8)
Water-gas shift reaction: $CO + H_2O \leftrightarrow CO_2 + H_2$	−41.2 kJ/mol	(2.9)

The composition and yield of the gas produced are influenced by many parameters related to the design and operating parameters of the gasification process, as well as the type and amount of feedstock and oxidant.

2.1.1. Design Parameters

2.1.1.1. Gasification Agent

Depending on the type of gasification agent, the gas produced has different chemical and physical properties such as composition, calorific value [12]. Gasification processes are classified into air gasification, carbon dioxide gasification, steam gasification, supercritical steam gasification and oxygen gasification according to the gasification agent [14]. The commonly used gasification processes are explained below.

Air gasification: Air is the commonly used gasification agent because it is cheap and available at any place and time without the need for complicated industrial utilities and infrastructure [44]. The gas produced has a relatively low calorific value as it contains up to 60% N_2 gas and other by-products such as CO_2, tar and hydrocarbons [45].

Oxygen Gasification: Since the production of pure oxygen has a high cost and some safety issues, oxygen gasification is not a widely preferred type. The gas produced by oxygen gasification has higher calorific value compared to air gasification however it has higher content of CO_2 and CO in the syngas [12, 13].

Steam Gasification: Compared to air and pure oxygen gasification, steam gasification is more economical than pure oxygen gasification and has higher calorific value than air gasification. Steam gasification offers higher hydrogen content in the syngas related to advanced steam methane reforming and shift reactions [46, 47].

2.1.1.2. Heat Source of Gasification

Although the exothermic step (combustion) in the gasification process occurs, many of the gasification steps (drying, pyrolysis, and gasification) are endothermic and require heat. The required heat can be supplied from an external heat source or exothermic reactions. The gasification temperature can be adjusted by the gasification agent, with air or oxygen [48]. For the steam gasification process, an external heat source should be placed to provide the required heat. Even though steam gasification produces a syngas with higher heating value, the economic and operational constraints can be challenging. Therefore, the amount and temperature of steam entering the gasifier should be designed to minimize energy input. Moreover, regardless of the gasification agent, an external heating element is available if the gasification temperature needs to be above 850 °C [49]. There are two main process types based on thermal coupling.

Allothermal Gasification: This type of process is referred to as heating the fuel is provided by an external source such as hot bed materials or heat exchangers [50]. The heat generated is transferred from the outside to the inside of the reactor.

Autothermal Gasification: Autothermal process means the required heat is generated inside the reactor by exothermic reactions [51]. Using the heat from combustion part is the more economical way to drive gasification reactions but the temperature is not as easy to control compared to the allothermal process.

2.2. Gasifier Types

Gasifier is a type of reactor in which the solid fuel and oxidant react with each other. The selection of the right type of gasifier is commonly basis of fuel characteristics, capacity, and economic aspects. The direction in which the fuel and oxidizing agent are in contact with the reactor and with each other is essential. According to their individual design, gasifier types are classified as fluidized bed, entrained flow and fixed bed [52].

2.2.1. Fixed Bed Gasifiers

Fixed bed gasifiers can be classified as three types according to the direction of feed and syngas: Downdraft, Updraft and Crossdraft. This type of gasifier has attracted most attention due to its simple and low-cost design [53]. Especially in downdraft gasifier, the tar content is very low because the oxidizing agent and fuel move in the same direction [54]. The produced gas from downdraft gasifier is directly utilized in the internal combustion engines or gas turbines after cleaning small amount of tar [19]. On the other hand, gasifying agent and fuel feed move in opposite direction in updraft gasifiers. Updraft gasifiers are capable of processing fuels with high ash and moisture content, but the final product is obtained with high tar content [55]. Therefore, the syngas from updraft gasifier can be used in direct combustion as a simple application that does not require cleaning.

2.2.2. Fluidized Bed Gasifiers

Fluidized bed gasifiers are separated into two main types: bubbling and circulating. A fine bed material such as sand, silica behaves like a fluid and can be well mixed with the fuel and gas in the fluidized bed gasifier [56]. This fluidization process takes place when a fluid is passed through a granular medium. This is a promising approach and gives them more uniform temperature distribution and flawless heat and mass transfer capability compared to

fixed bed gasifiers [57]. They are also flexible to utilize various type of fuels. The main advantage of fluidized bed gasifiers over fixed bed is the higher conversion rate of solid fuels [33]. However, the design configuration of fluidized bed is more complex and requires higher capital cost than fixed bed.

2.2.2.1.Bubbling Fluidized Bed Gasifier

In a typical bubbling fluidized bed gasifier (BFBG), the fuel feed is send from the top while the gasifying agent is fed from the lower part of the reactor [58]. First, the recently fed solid particles come into contact with the hot bed material, then the particles quickly reach the bed temperature [59]. The generated gas exits at the top of the gasifier. The BFBG has a simpler operation and design than the circulating type. The fluidizing agent, which operates the gas velocity of the BFBG lower than 1 m/s, lifts the fuel particles [60]. The main part of the conversion takes place almost exclusively in the bubbling region and few amounts of tar is cracked in the freeboard. The use of BFBG is a rather useful technique to produce H_2-rich syngas under steam atmosphere. The thermal decomposition of the feedstock is very satisfactory due to the high operating temperature, which is about 850 °C [61]. Equivalence ratio and steam to biomass ratio of the system are fluctuated between 0.2-0.4 and 0-1, respectively. Difference of circulating fluidized bed reactor according to BFBG, unreacted char and gas are fed to the reactor as recycle through a cyclone in the circulating bed reactor. Like other fluidized bed gasifiers, the main features of BFBG are intense gas-particle interaction, complex chemical reactions and high particle concentration [62]. Although it has many advantages such as good scale-up potential, there are some drawbacks of BBFG such as lower conversion than circulating bed gasifiers and relatively higher tar content than downdraft gasifiers [63]. The thermochemical conversion process of biomass sample in BFBG is presented in Figure 2.2.

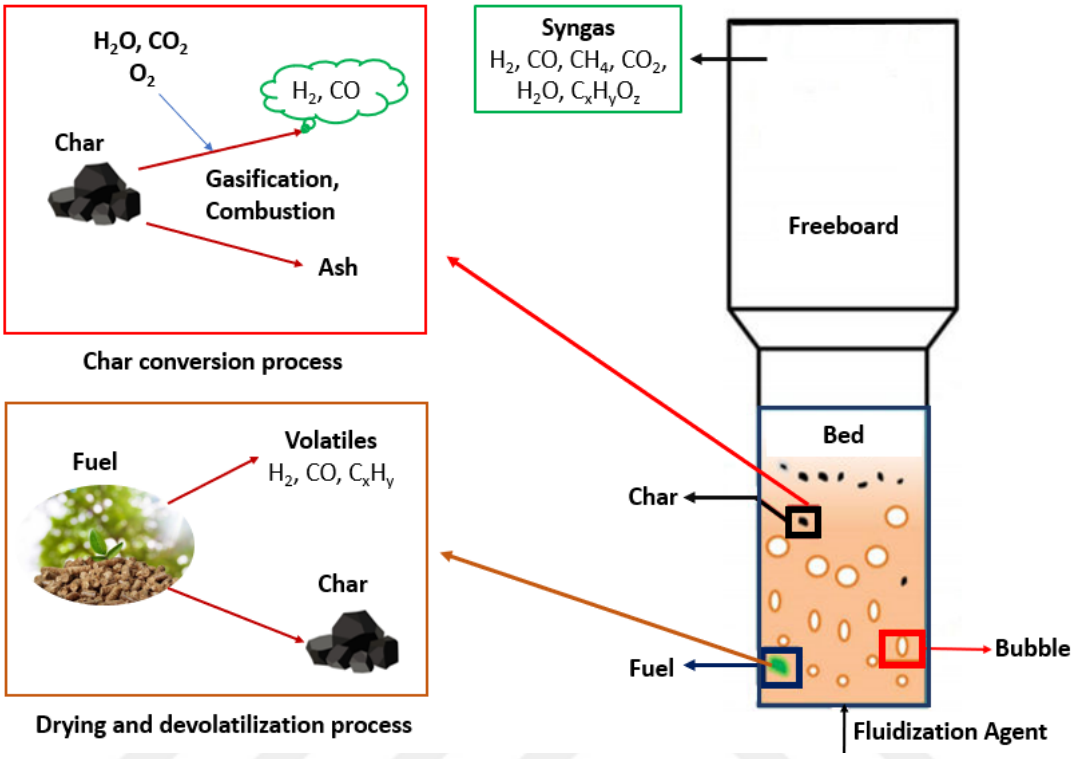


Figure 2.2 Fuel conversion process in BFBG

2.2.3. Entrained Flow Gasifiers

The fuel is entrained in a very short residence time by a gas stream [64]. Entrained flow gasifiers can be a good alternative for large-scale applications because they operate at relatively high temperatures and feed rates [65]. Due to the high operating temperatures, the tar produced as a result of the gasification process can be neglected and the char conversion efficiency is very high [52].

Entrained-flow gasifiers typically exhibit the following characteristics [66, 67]:

- Solid fuels with high carbon content are used.
- It requires high oxidation and therefore most entrainment gasifiers must blow oxygen instead of blowing air.
- There is a single temperature profile throughout the reactor.
- Above ash slagging temperatures
- Short reactor residence time

- High carbon conversion, but low cold gas efficiency
- High level of sensible heat in product gas, heat recovery is required to improve efficiency.
- Environmentally most benign; produced syngas consists of mainly H_2, CO and CO_2 with trace of other contaminants which can be removed downstream of the reactor; glassy slag is inert and easily disposed.

2.3. Fuel Cells

Fuel cells are devices that can generate electrical energy from the conversion of chemical energy based on electrochemical reactions [68]. The simple construction of a fuel cell includes an electrolyte layer between an anode and a cathode. In a typical fuel cell, fuels in the gas phase and oxidant that can be oxygen or air are repeatedly fed into the anode and cathode, respectively [69]. The ions of the oxidant or fuel produced by electrochemical reactions in the cathode and anode transfer to the opposite side of the electrolyte. As a result, electrons are moved by load and electric current is generated on the electrolyte side. The direction of the ions determines the direction of the escaping gas. The operating principle of the fuel cell is shown in Figure 2.3.

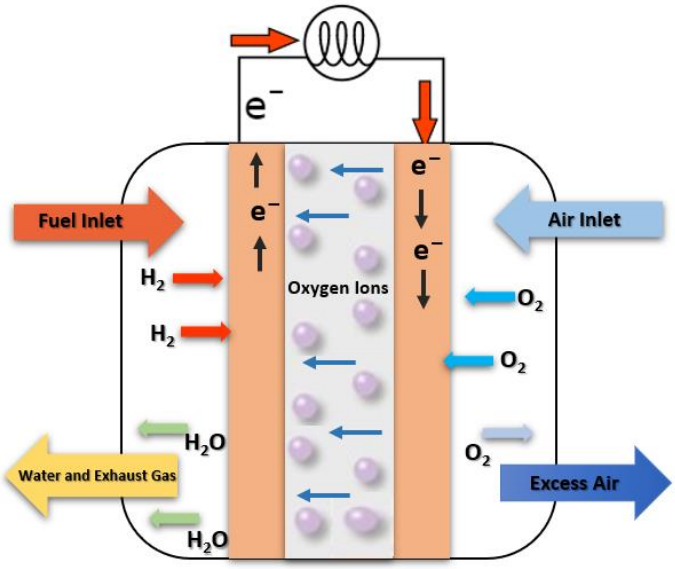


Figure 2.3 SOFC system

Fuel cells are commonly categorized by the electrolyte used, such as alkaline fuel cell (AFC),

SOFC, molten carbonate fuel cell (MCFC), polymer electrolyte membrane fuel cell (PEMFC), and phosphoric acid fuel cell (PAFC) [70]. Fuel cells have some features that make them superior as power generation devices. They have very low detrimental effects for the environment (low noise and gas emissions) and higher efficiency compared to the conventional systems [71, 72]. Moreover, unlike batteries, recharged of the system are not needed the operations continue as long as the fuel is provided. In Table 2.2, different fuel cell types are compared based on their electrolyte properties according to their individual advantages and operating conditions [72].

Table 2.2 Fuel cell types based on electrolyte characteristics.

	AFC	**MCFC**	**PEMFC**	**PAFC**	**SOFC**
Electrolyte	potassium hydroxide	molten salt (sulphate, nitrate, carbonates)	polymer	phosphoric acid	ceramic oxide
Efficiency	50-70%	40-55%	35-60%	35-50%	45-60%
Operating Temperature	50–200°C	630–650°C	50–80°C	160–210°C	600–1000°C
Anode Gas	H_2	H_2, CH_4	H_2	H_2	H_2, CH_4
Cathode Gas	Air - O_2	Air - O_2	Air - O_2	Air - O_2	Air - O_2

According to the classification of fuel cells, it can be shown that there are large differences in the operating temperature with respect to the resistance of the electrolyte material. The efficiencies of the high operating temperature fuel cells can increase 20% by heat recovery [69]. Therefore, SOFCs are the most convenient type for cogeneration and integrated power generation. In addition, SOFC fuel cells are the best candidates for gasifier-fuel cell cycles, with their low tolerance for inlet gas compositions [73].

2.3.1. SOFC

SOFC is one of the most promising fuel cell types that differs from the others in many ways [74]. Firstly, their structure consists entirely of solid materials. Secondly, they operate at higher temperatures than others, this feature makes them highly tolerant to impurities. Internal reforming exists for the conversion of hydrocarbons to H_2 within the cell [75]. SOFC is capable of using CO as fuel due to its high operating temperature [76]. The use of electrocatalysts is not required. The main implementation field of SOFC is stationary power generation, it is useful for large-scale applications [77, 78]. However, it can also be used as an auxiliary power generator in transportation applications such as motor vehicles [79, 80].
The basic operating principles of the fuel cell are also valid for the SOFC as well. A SOFC comprises strict ceramic electrolyte which made of zirconia, and two electrodes. O_2 molecules from the air stream are ionized by the electrochemical reactions and the oxygen ions from the cathode to the anode side through the electrolyte [81]. The H_2 and CO molecules react with the oxygen at the anode in this way electrical current, CO_2 and water vapor are formed. The anode and cathode half reactions are presented as following:

Anode: $H_2 + O^{-2} \rightarrow H_2O + 2e^-$ (2.10)

Anode: $CH_4 + 4O^{-2} \rightarrow 2H_2O + CO_2 + 8e^-$ (2.11)

Anode: $CO + O^{-2} \rightarrow CO_2 + 2e^-$ (2.12)

Cathode: $1/2O_2 + 2e^- \rightarrow O^{-2}$ (2.13)

SOFCs are classified based on their cell and stack design (planar, tubular, monolithic), temperature level (low, intermediate and high), type of support (self and external), flow configuration (co-flow, cross-flow, counter-flow) and type of fuel reforming (external and internal). The view of the tubular fuel cell is presented in Figure 2.4.

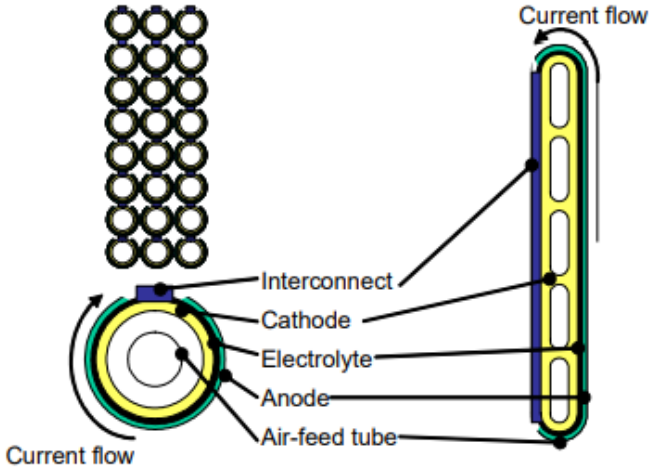


Figure 2.4 Tubular SOFC [82]

The discovery of SOFC came after Nernst's work on solid oxide electrolyte in 1899 [71]. Over the years, many researchers carried out their studies to improve fuel cell technologies. NASA invested a considerable amount of money in H_2-based fuel cells in 1960 in connection with the space program. Subsequently, the governments agencies of the US, Japan and Canada outstandingly raised their investments in fuel cell research [83]. Progress in materials technology and rising energy costs have forced the development of SOFC design and performance. The 220 kW SOFC with 60% efficiency that considered the most successful application, was built by Siemens Westinghouse in the last decades [84, 85].

To increase the performance of SOFC, researchers have conducted studies to optimize the operating parameters and develop more efficient materials [86-88]. Combined cycle or cogeneration applications of SOFC have received considerable attention in recent years. Ghaffarpour et al. [89] studied an integrated gasification, SOFC, gas turbine and organic Rankine cycle plant and concluded that the current density of the SOFC and the biomass flow rate were the parameters that influenced the energy efficiency of the hybrid plant. Colpan et al. [90] developed a thermodynamic model for a SOFC using syngas as fuel produced by the gasification process. They investigated the impact of the SOFC operating parameters on the electrical efficiency and cell voltage. Gadsbøll et al. [91] conducted an experimental work for a combined gasification and SOFC system to investigate the commercial potential of this system, and the results depicted that the electrical efficiency reached up to 46.4%.

2.4. Modeling of Integrated Gasification-SOFC system

Modeling is a helpful tool for optimization and design of a complex gasification and SOFC system. Instead of time consuming and expensive experiments, modeling provides a comprehensive examination to analyze the process behavior [20]. The operating parameters such as temperature, pressure, feed rates of fuel and oxidizing agent of the system are optimized in a short time with good accuracy and minimum financial cost [92]. Thermodynamic method is the simplest among the various modeling approaches, the system is thought of as a black box [58]. In the black box models, mass and heat balances are solved for the whole system or calculations can be conducted for specific regions of the system supported by some assumptions.

Thermodynamic models use equilibrium relationship on the basis of equilibrium point of the reactions in the system. They are better suited to focus on the calculation of the operating parameters. These models are categorized as stoichiometric and non-stoichiometric based on the equilibrium constant and minimization of Gibbs free energy, respectively [93]. The possible reactions of the system should be inserted with their conversion rates and stoichiometric coefficients if the stoichiometric method is chosen for the modeling approach. Because of the complexity of the processes, such as gasification, the definition of all possible reactions is very difficult and some of the significant reactions are neglected. No specific reactions are included to be solved, so only the elemental composition of the input is needed in the non-stoichiometric method [7]. Even if the reactions are not known exactly, all possible reactions, which are independent of their complexity, are formed in the system [94]. The solutions of this method can provide various mathematical programming algorithms on the basis of the minimization of Gibbs free energy. Process simulation programs have the ability to solve this type of models. Aspen Plus®, developed at Massachusetts Institute of Technology in the US Department of Energy, is an equation-oriented process simulation software that can be used to optimize existing systems and simulate new plants under specific conditions [95]. Recently, Islam Md. [96] developed a fluidized bed gasifier model using Aspen Plus simulator and investigated the effect of the five different gasifying agents on the syngas composition and quality of syngas.

Hauck et al. [18] presented a newly developed model for a reversible SOFC in Aspen Plus simulation. The important model parameters, inlet gas composition, temperature and pressure were evaluated by conducting parametric studies. The results depicted that the model parameters strongly influence the performance of the SOFC.

Doherty W. [97] investigated the feasibility of the biomass gasification and SOFC system as a combined power and heat process on the basis of a thermodynamic and economic approach using Aspen Plus. The integrated gasification and SOFC system achieved high efficiency, but the results of the economic analysis depict that this system was not commercially viable at that time because of the expensive biomass fuel prices and capital costs.

2.5. Artificial Neural Network

Artificial intelligence (AI) leads to create intelligent systems that have the ability to respond and work like human brains [98]. Artificial neural networks (ANN) as an AI approach have been developed by inspiring of the structure and functioning of biological neural systems. ANNs use computational and statistical methods without requiring a mathematical equation or description to acquire knowledge and recognize patterns through past experiences and inferences [99]. Apart from problem solving ability, it has other skills like learning, reasoning, understanding, perception and awareness of surroundings. ANN is applied in extensive fields such as computer science, nanotechnology, biomedical, biotechnology, pharmaceutical, and biological and chemical engineering etc [100].

The learning ability of the model rely on the network structure and training process. ANN is made up many numbers of neurons, which are the fundamental part of the network structure. Determining the appropriate structure is directly related to the complexity of the problem [101]. The number of neurons and their connections affects the mechanism of computations [102, 103]. Among the different network structures such as modular neural network (MNN), layered neural network (LNN), feedback or recurrent neural network (RNN), radial basis function neural network (RBFNN), which differ in the interactions and connections of the neurons, feedforward neural network (FFNN) is most commonly used for prediction, classification and approximation applications [98]. Besides, the choice of activation

functions (hyperbolic tangent sigmoid, logarithmic tangent sigmoid, linear, binary step and elliot symmetric sigmoid) and training algorithms (Gradient descent, Newton's method, Levenberg-Marquardt, Quasi-newton method) have a strong impact on the performance of ANN. Compared to other modeling techniques, ANNs offers non-linearity in an excellent manner [104]. Further, they have ability to:

- handle multiple inputs and outputs modeling,
- spent less computational time,
- work with noisy data,
- update the model with new data.

ANN is particularly suitable for predicting complex system outputs. Therefore, it can be implemented for the gasification and SOFC process as a relatively new segment of modeling.

Kartal et al. [105] predicted the LHV of syngas generated from circulating fluidized bed gasifier. Using large data sets from Aspen Plus, the ANN model was developed, and outputs depicted that the precited LHV of syngas was found in well agreement with the real values. The coefficient of determination values were obtained greater than 0.99. These results proved the high prediction capability of the ANNs on the nonlinear complex systems like gasification process.

Sezer et al. [106] developed an ANN model to predict syngas exergy value in bubbling fluidized bed gasifier. They evaluated the estimation performance of the model at the points that has highest H_2 concentration. The results illustrated that the training, test and extra validation data sets have similar values with the calculated exergy values. The study showed the superiority of the ANN model that developed a relationship between input and outputs of the system parameters without the complex and time-consuming calculations.

Milewski et al. [107] implemented an ANN, to simulate the SOFC. The ANN model was trained and tested with experimental data. Current density, air flow densities, anode thickness, anode porosity, electrolyte temperature and thickness, anode H_2 flow density were used as input parameters of ANN to predict the cell voltage. The test results depicted that ANN successfully represents the SOFC.

3. Materials and Methods

3.1. Fuel Characterization

Biomass is the widely available carbon-based fuel sources after oil and coal [108]. Biomass has high reactivity owing to its higher volatile content and more reactive char however it has lower calorific value because of lower C and higher O and H contents compared with the coal [109]. The higher rate of O and H in biomass decreases the energy content of biomass due to weaker bonds in C-O and C-H than C-C bonds, which have higher energy content [110]. Although biomass has lower calorific value, it also has lower fixed carbon and higher moisture contents. These natural characteristics represent low emission levels and make biomass a proper fuel. Biomass is classified into two main groups non-lignocellulosic and lignocellulosic. Lignocellulosic biomass types comprise of three major components such as hemicellulose, lignin and cellulose [111, 112]. The amount of these major components make the physicochemical characteristics of lignocellulosic biomass several [113]. Herbaceous and woody wastes, agricultural residues are the widely used and cost-effective lignocellulosic biomass species and usually chosen as an energy source [114, 115].

Proximate and ultimate analyzes are the most preferred methods for characterizing fuels. These methods are standardized by major standards institutions such as ASTM, ISO. Ash (AC), moisture (MC), volatile matter (VM) and fixed carbon (FC) contents in the fuel sample are determined by proximate analysis (weight percent, wt%). Generally, MC is obtained by measuring the weight of the sample before and after drying. The mass loss of the biomass sample during the defined time and temperature in a closed crucible gives the VM content. AC is specified by weighing the residual mass after complete combustion. The FC content is determined by subtracting the VM, MC and AC from 100.

$$FC = 100 - (VM + MC + AC) \quad (3.1)$$

The elemental composition of biomass, such as the C, N, O, H, and S contents (wt %), is determined by the ultimate analysis. The O content of fuels is obtained by subtracting the sum of the C, H, N and S contents from 100 %, as shown below [116, 117].

$$O = 100 - (N + C + S + H) \quad (3.2)$$

Investigation of the FC, MC, AC and VC of biomass creates a perspective on fuel quality and shows its convenience for the gasification process. Exclusively, FC content is the most substantial parameter to specify the thermal decomposition characteristics and energy potential of biomass. Conversely, ash that is the inorganic part of biomass, and moisture have a negative effect on the heating value of biomass. The biomass with higher MC is not suitable to be transported economically for thermochemical conversion. Volatiles are defined the components that can be combustible (H_2, C_xH_y gases or CO) or non-combustible (CO_2, NO_x or SO_2) gases, except moisture, which are released when biomass is heated even at relatively low temperatures. In some cases, S and N can be considered negligible because their amount in the biomass fuels is very low based on the basis of ultimate analysis results.

The selection of proper type of biomass sample for the gasification process in a particular type of gasifier is carried out according to these analysis outputs. The biomass samples selected for this study are illustrated in Table 3.1 with their material characteristics.

Table 3.1 Proximate and ultimate analysis results of biomass samples (dry basis)

	Fuel	**MC**	**FC**	**AC**	**VM**	**O**	**S**	**C**	**N**	**H**	Ref.
1	Almond Hulls	6.52	20.07	6.13	73.8	39.18	0.06	47.53	1.13	5.97	[118]
2	Cacao	9.33	19.82	8.26	71.92	31.47	0.06	48.24	2.79	9.18	[119]
3	Hazelnut Shell	13.00	27.31	0.75	71.94	45.21	0.81	47.06	0.33	5.84	[120]
4	Olive Kernels	8.76	19.52	2.58	77.90	39.01	0.28	51.31	1.00	5.82	[121]
5	Pistachio Shells	7.54	16.95	1.41	81.64	41.16	0.22	50.20	0.69	6.32	[118]
6	Sunflower Seed Husk	10.50	21.90	4.25	73.85	39.74	0.19	48.93	0.86	6.03	[122]
7	Palm Kernels	11.01	17.58	5.14	77.28	37.44	0.26	48.34	2.62	6.20	[123]
8	Olive Pomace	3.38	19.88	2.08	78.04	36.57	0.10	54.70	0.48	6.07	[124]
9	Cotton Husk	6.90	18.20	3.40	78.40	38.45	0.00	48.69	1.35	8.11	[125]
10	RDF	6.45	11.75	12.25	76.00	38.62	0.53	40.75	0.28	7.57	[126]
11	Corn Stover	5.00	14.55	7.35	78.10	39.67	0.11	46.50	0.56	5.81	[127]
12	Wheat Straw	10.50	17.79	3.41	78.80	44.17	0.12	45.97	0.55	5.78	[128]

13	Eucalyptus Wood	4.00	18.80	0.80	80.40	41.78	0.02	51.20	0.20	6.00	[129]
14	Willow Wood	11.10	19.30	2.10	78.60	40.80	0.10	49.30	1.10	6.60	[130]
15	Poplar Wood	6.74	12.26	1.60	86.14	41.08	0.02	50.82	0.59	5.89	[118]
16	Chestnut Tree	8.20	22.69	4.90	72.41	41.33	0.26	45.48	2.10	5.93	[131]
17	Pine Chips	10.25	17.80	0.60	81.60	45.61	0.28	47.86	0.09	5.56	[131]
18	Walnut Shell	8.70	18.70	2.30	79.00	45.37	0.10	45.89	0.21	6.13	[131]
19	Red Oak Wood	14.76	17.69	1.03	81.28	42.33	0.03	50.03	0.21	6.37	[132]
20	Hemlock Wood	8.40	25.50	2.50	72.00	37.83	0.10	53.63	0.19	5.75	[133]
21	Pine Sawdust	8.00	17.16	0.55	82.29	41.11	0.57	50.54	0.15	7.08	[134]
22	Barley Straw	11.50	18.50	5.30	76.20	41.29	0.10	46.78	0.66	5.87	[125]
23	Balsam Bark	8.40	20.00	2.60	77.40	38.47	0.10	52.60	0.19	6.04	[125]
24	Coconut Shell	4.40	23.00	3.20	73.80	41.72	0.09	49.47	0.10	5.42	[125]
25	Groundnut Shell	7.90	22.70	3.40	73.90	39.02	0.00	49.17	1.16	7.25	[125]
26	Maple Bark	8.40	19.40	4.00	76.60	39.65	0.10	49.92	0.38	5.95	[125]
27	Spruce Wood	6.70	18.30	0.50	81.20	40.99	0.10	52.04	0.30	6.07	[125]
28	Grpae Seeds	6.29	27.87	6.04	66.09	37.75	0.00	48.33	1.93	5.95	[125]
29	Mustard Husk	5.60	23.30	4.10	72.60	42.59	0.19	43.92	0.38	8.82	[125]
30	Alfalfa Straw	9.30	15.80	5.30	78.90	38.64	0.19	47.25	2.65	5.97	[125]

For this study, different types of biomasses from agricultural, forestry and industrial wastes were used considering their availability and abundance. These biomass samples are thought compatible for gasification application in BFBG because they have relatively low MC. Regardless of their origin, the biomass samples were selected in a wide range based on their characterization results. The main aim of these selection is to provide a comprehensive database for the ANN model. 30 biomass samples were used along the training, test and validation processes of ANN models.

3.2. Gasification Process

3.2.1. Development of BFBG Model in Aspen Plus

In this part, the development of the BFBG model for biomass gasification in the Aspen Plus simulation program is presented. Aspen Plus uses its chemical component database and library, which contains various unit operations, to simulate models traditionally related to vapor-liquid processes, such as chemical, petroleum refining, petrochemical, and oil and gas industries [135, 136]. However, it is also capable of simulating solid-phase processes like coal and biomass processing, polymers, pulp and paper [136]. The wide database in terms of thermodynamic properties, chemical reactions and reaction kinetics allows accurate prediction of process parameters and behaviors. The simulation model is established by determining the chemical components and describing the flowsheet with material and energy flows and unit operations (heaters, reactors, pumps, etc.). Calculator block and Fortran subroutines can be used to conduct calculations and design specifications that are not present in the unit operations [137]. Optimization and investigation of the effect of operating parameters can be performed using model analysis tools such as optimization sensitivity and analysis sections.

Generally, complex thermodynamic systems like gasification are divided into subprocesses (drying, pyrolysis, gasification and combustion) in order to simulate them via Aspen Plus. All steps of the gasification process should be represented one by one to make the system as close as possible to the real application. Drying zone, pyrolysis zone, combustion zone and gasification zone are the main parts of the gasification process as mentioned above and are simulated sequentially by linking unit operation blocks to each other. The sequential modular approach is carried out to solve each block in the process. Gasification has a number of complex and different types of chemical reactions (homogeneous, heterogeneous, endothermic, exothermic), which makes the modeling of the process very difficult. The equilibrium model allows to model and predict the products of gasification reactions in a simple way. In the present work, a thermodynamic equilibrium model was developed to represent the gasification process in Aspen Plus® simulation software (V11 aspenONE

Engineering Suite). The assumptions listed below were considered in the simulation of the gasification process to produce a realistic model:

- The process reaches to steady state conditions.

- No heat and pressure losses occur.

- Devolatilization of the fuel is instantaneous.

- Char consists only of carbon.

- Ash does not react as it is assumed to be inert.

- The reactions reach chemical equilibrium within a reasonable residence time.

- The syngas contains H_2, CH_4, CO_2, H_2O, CO gases.

- Hydrogen sulfur (H_2S) and hydrogen chloride (HCl) are formed by the S and chlorine (Cl) that inherently present in the biomass.

- Each gases act as ideal gases.

The flow diagram of the BFBG model in Aspen Plus can be seen in Figure 3.1. The gasification process was shown from the beginning of the fuel supply to the end of the production of syngas. The description of each part of the gasification was detailed by using different reactors and blocks.

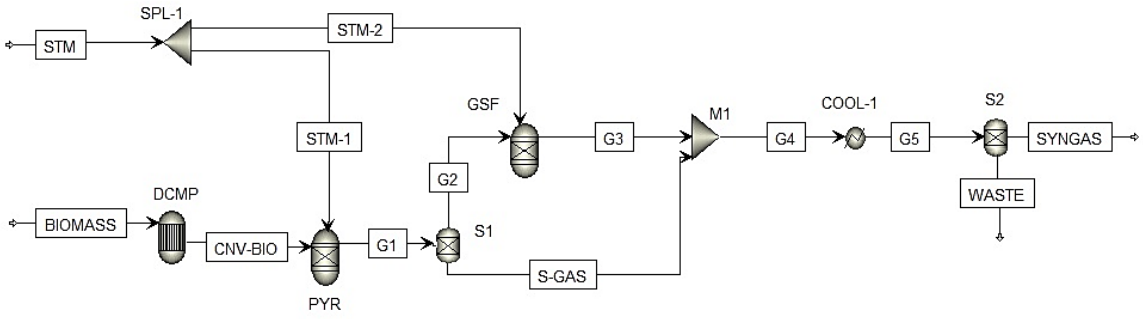


Figure 3.1 Flowsheet of the BFBG in Aspen Plus

In this study, two types of components take place: conventional and nonconventional. To determine the physical properties of the conventional components (H_2, O_2, H_2O, CO_2, CH_4...) already present in the Aspen Plus library, the Soave - Redlich - Kwong (SRK) equation of

state with the free water method (STEAMNBS) proposed in the Aspen Plus User's Guide was selected.

HCOALGEN and DCOALIGT was chosen as the physical property method for the non-conventional components to perform the enthalpy and density calculations respectively. The non-conventional components are currently not available in the Aspen Plus library and should be defined according to their physical and chemical properties. In the present work, biomass and ash were introduced as non-conventional components because of their heterogenous structure. The biomass samples were made known to the system in terms of their material characterization results (proximate, ultimate and sulfate analyzes).

3.2.1.1. Gasification Steps

In real applications, the gasification steps take place within the BFBG without the sharp distinctions. However, there is no reactor or block in Aspen Plus to simulate all the reactions and steps that take place in the BFBG as only a stand-alone unit. Therefore, the simulation model of the BFBG should be represented individually to create a reliable and realistic model. Accordingly, the BFBG model was developed considering the four steps: drying, pyrolysis, gasification and combustion.

The partitioning of gasification into different steps is not sufficient to create a well-developed model because the gasification reactions are complex and instantaneous. For this reason, approaches to minimization the Gibbs free energy (non-stoichiometric) or the equilibrium constant (stoichiometric) are used to develop equilibrium-based models. A simplified model using one of these approaches gives better results with higher certainties and accuracies with respect to the gasification reactions. The non-stoichiometric method is simpler than the stoichiometric way because it is not necessary to identify all possible reactions, equilibrium constants, or convergence rates [138]. Pyrolysis, gasification and oxidation which are the main parts of the gasification were carried out based on the principle of minimization Gibbs free energy.

For multicomponent systems, Gibbs free energy is minimized when the thermodynamic equilibrium condition occurs at stable temperature and pressure. Gibbs free energy of a given

system is described as follows [139, 140]:

$$G^T = \sum_{i=1}^{N} n_i \mu_i \quad (3.3)$$

$$\mu_i = G_i^0 RT + \ln\left(\frac{f_i}{f_i^0}\right) \quad (3.4)$$

G^T stands for the total Gibbs free energy, μ_i and n_i are the chemical potential and the number of moles of species i, respectively. R depicts the universal gas constant; T is temperature and f_i represents the fugacity of each species. The superscript *0* depicts the standard thermodynamic quantity.

$$\Delta G_{fi}^0 + RTln\frac{y_i \varphi_i P}{P^0} + \sum_k \lambda_k \alpha_{ik} = 0 \quad (3.5)$$

Here ΔG_{fi}^0 is standard Gibbs free energy and y_i stands for the standard mole fraction of gas species *i*. φ_i represents the fugacity coefficient P, P^0 are the ambient and partial pressures respectively. The Lagrange's undetermined multiplier method is implemented where λ_k is the Lagrange multiplier and *k* element stands for each molecule of species *i* and a_{ik} represents the number of atoms.

Drying and Pyrolysis

After defining the fuel sample on the basis of its ultimate and proximate analysis results as nonconventional component, thermodynamic conditions and flow rate of the fuel was inputted. Biomass should be converted into a conventional form suitable for carrying out the reactions. Thus, it can be said that the thermal decomposition of biomass was started in this part. The convergence step was simulated using the yield reactor (RYIELD) named "DCMP", which can be seen in the BFBG flow diagram. The biomass sample is needed to be introduced into the simulation as a dry base, but the feedstock enter to the reactor should have the same moisture content as in its raw form. Therefore, the calculator (flow sheeting options in Aspen Plus) was used to calculate the conversion of dry basis ultimate analysis to wet basis in the "DCMP" reactor using the biomass moisture content already defined in the proximate

analysis. Based on the wet basis values of ultimate analysis, the calculator was also used to convert the biomass into conventional components (H_2, N_2, H_2O, C and Cl_2...). The main aim of this reactor is to convert the non-conventional form of biomass to the conventional form with respect to the mass yields of each component, considering the ultimate analysis outputs in wet basis. This stage can be considered as the first part of the pyrolysis. Consequently, the stream "CNV-BIO" leaves from the "DCMP" reactor in conventional form.

The function of the following block named "PYR" represents the drying and pyrolysis sections using Gibbs reactor (RGIBBS). In this step, the temperature is usually set between 200-500 °C. In this case, the temperature was set at 300 °C and the second step of thermal decomposition started with pyrolysis. It was not necessary to simulate drying as a separate part, because the moisture and other volatiles can release in the pyrolysis part. Steam was preferred as the gasifying agent as it produces higher H_2 content in the syngas. The pure steam flow “STM” was fed into the system through the "SPL-1" block at 250 °C and atmospheric pressure. The inlet flow of steam was split into two streams at a specific ratio to establish a steam atmosphere in the pyrolysis and gasification reactors. “STM-1” was sent to the "PYR" reactor without changing its thermodynamic conditions. The moisture and volatiles were released and charcoal was formed according to the reactions that occur in the pyrolysis part based on the principle of minimizing Gibbs free energy. The exit stream "G1" was formed mainly from CH_4, H_2O, CO_2 and smaller amount of C_2H_2, CO and C_2H_6 as a result of gas and solid phase reactions in the "PYR" reactor. "S1" block was placed to separate certain amount of CH_4 to avoid its complete depletion. Because CH_4 reaches the chemical equilibrium in the “GSF” reactor which set at high temperature and cannot be seen in the syngas. In addition, other gases that do not contribute to the gasification reactions were also separated via the S1 block. The "G2" stream was sent directly to the "GSF" reactor to perform gasification reactions. The separated gas called "S-GAS" was flowed into exit stream without any interaction with the gasification part.

Gasification and Oxidation

In the gasification part, the main gasification and oxidation reactions take place, namely water-gas shift, Boudouard and steam-methane reforming. The "G2" stream enters the "GSF" reactor, where the reactions are carried out according to the principle of minimization of Gibbs free energy at a temperature beyond 700 °C. Additional stream “STM-2” was flowed to the reactor to provide pure steam at the same thermodynamic conditions as the inlet steam (250 °C and atmospheric pressure) for the "GSF" reactor.

The gas formed with undesired by-products and water at the same temperature as the "GSF" reactor. The exit stream "G3" was mixed with the "S-GAS" which was separated from the "G1" after the pyrolysis step using the "M1" block. Then the "PG2" was passed through the "COOL-1" block to obtain the gas mixture the temperature at 500°C. From this stream, the unwanted by-products (H_2S, N_2, ash) and moisture should be removed. For this purpose, the "S2" block was used for the separation process and the "SYNGAS" stream was produced containing only the gases H_2, CO, CH_4 and CO_2. The blocks and reactors are shortly listed in Table 3.2.

Table 3.2 Definition of the gasification steps in Aspen Plus

Part	Simulation Name	Definition
DCMP	RYIELD	Nonconventional biomass is converted into conventional form.
PYR	RGIBBS	Pyrolysis step occurs in this reactor.
GSF	RGIBBS	Gasification step takes place in this reactor.
SPL-1	FSPLIT	Steam is split between the two Gibbs reactors.
S1	SEP	Specific amount of gases is separated before gasification step.
COOL-1	HEATX	Temperature is fixed at 500°C
M1	MIXER	SG and PG2 streams are mixed.
S2	SEP	Ash, H_2S and N_2 water are removed from the produced gas

3.3. SOFC Process

3.3.1. Development of SOFC Model in Aspen Plus

SOFC modeling is a highly strategic research field to specify safe and optimal operating conditions [141]. Zero-dimensional models provide a more appropriate solution in terms of simplicity and speed. Further, zero-dimensional models do not require information about electrochemical parameters or material properties of the SOFC. Aspen Plus as a simulation package has been used for modeling SOFC and other type of fuel cells [18, 142, 143]. Although there is no ready-made module for fuel cells, the integration of the specific process units from the extensive library is used for modeling. In this chapter, the tubular SOFC configuration was modeled based on the equilibrium-based method using Aspen Plus simulation. The model works on the basis of principle of Gibbs free energy minimization. The SOFC models should meet the rapid technological progress in this field. Therefore, there is a need for models that are reliable and have fast computational skills. Because there is no present model in Aspen Plus to simulate SOFC as only one stack, the Fortran programming language linked to Aspen Plus subroutine was employed to conduct the calculations of the SOFC model. The model was developed to perform mass and heat balances and voltage calculation considering the ohmic, concentration and activation losses. There are the assumptions were used during the development of the SOFC model as follows:

- Pressure and heat losses in the unit operation blocks are negligible.
- All gasses are assumed to be ideal.
- The system conducts under steady state conditions.
- Shift and reforming reactions achieve chemical equilibrium.
- The air consists only of the gasses N_2 (79%) and O_2 (21%).

The tubular SOFC system has the highest potential considering its advanced technology and commercialization capacity. In the present study, a 120 kW tubular SOFC unit designed by Siemens Power Generation Inc. was selected to perform. This system has been used by many researchers in the literature [29, 144-146]. The SOFC was developed by combining different unit operation blocks. The flow diagram of the model is presented in Figure 3.2.

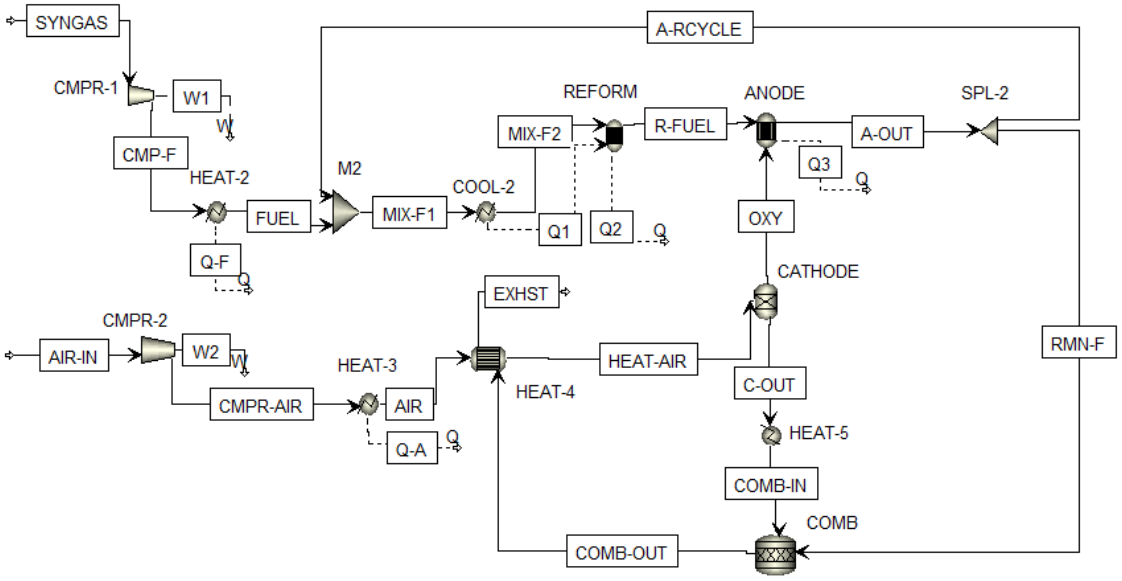


Figure 3.2 Flow diagram of tubular SOFC in Aspen Plus.

The "SYNGAS" stream was fed into the compressor block named "CMPR-1" to adjust the pressure of the fuel stream at desired value. The discharge value of the pressure was set with the P_{syngas}/P_{SOFC} ratio equals to 3 using the design specification block "D-1". The temperature, pressure and composition of the "SYNGAS" were inserted, but its initial flow rate changed by the design specification "D-5" with respect to the determined stack power. The compressed stream was heated by the heater block "HEAT-2" and then fed to the "M2" to mix them with the stream "A-RCYCLE", which is the recycle from the "ANODE" outlet. The pre-reformer of the SOFC stack was represented by the combination of the "COOL-2" block and the "REFORM" reactor. The main goal of the "COOL-2" is supplying the required heat to carry out the reforming reactions in "REFORM" from heat released by cooling. "COOL-2" changes discharge stream "MIX-F2" temperature until the net heat duty of the "REFORM" reactor was set to zero with "D-3" as it was operated adiabatically. Consequently, the mixed fuel stream was cooled to simulate the endothermicity of the reforming process. It is assumed that only H_2 can contribute to electrochemical reactions, so CH_4 and the other higher hydrocarbons are reformed, and CO is shifted to H_2 in the "REFORM" reactor via the following reactions:

Water-gas shift: $CO + H_2O \leftrightarrow CO_2 + H_2$ (3.6)

Steam reforming: $C_xH_z + xH_2O \leftrightarrow (z/2 + x)\ H_2 + xCO$ (3.7)

Afterward, the outlet stream flows along the "ANODE" reactor and mixes with the oxidant flow from the “CATHODE” reactor. There is no possibility to simulate the transfer of ions via the current model, so only one complete reaction was performed for the oxidant and fuel streams which is given below:

Complete reaction: $H_2 + 0.5O_2 \rightarrow H_2O$ (3.8)

The air compressor “CMPR-2” block was used to include the air into the system. The discharge pressure of the air was set as a bit higher than atmospheric pressure. It was inserted with its temperature and pressure values and composition. The molar flow rate of air was arranged using the design specification block “D-4” which changes the flow rate until the air utilization factor (U_a) is equal to 0.19. The compressed air stream was heated to the air preheating temperature using the heat exchanger block “HEAT-4”. The hot products supplied the required heat from the combustion reactions in “COMBUST” reactor. The air enters the block “CATHODE” at the desired temperature and pressure. The function of the “COTHODE” block is separation of the O_2 from the air. The split fraction of O_2 was arranged by the calculator block via equations as follows:

$$nH_{2,in} = nH_{2,syngas} + 1\ (nCO_{syngas}) + 4\ (nCH_{4,syngas}) + \ \ldots \quad (3.9)$$

$$Uf = \frac{nH_{2,cons}}{nH_{2,in}} \quad (3.10)$$

$$nO_{2,cons} = 0.5nH_{2,cons} \quad (3.11)$$

$$O_{2,split} = \frac{nO_{2,cons}}{nO_{2,in}} \quad (3.12)$$

$n_{H2,in}$ is the total molar flow rate of H_2 comprised in the syngas. $1(nCO_{syngas})$, $4(nCH_{4,syngas})$ and other higher hydrocarbon gasses give the molar flow rate of H_2 that can be generated by steam reforming and water gas shift reactions respectively. $nH_{2,cons}$ is calculated using the value of fuel utilization factor (U_f) 0.85. Then, $nO_{2,cons}$ is determined by half of $nH_{2,cons}$ using

Eq. (3.11). Consequently, $O_{2,split}$ is found using the ratio of $nO_{2,cons}$ to $nO_{2,in}$ from the molar flow rate of O_2 in air.

The complete reaction was carried out in the "ANODE" reactor using a certain amount of O_2 from "CATHODE". Then, a percentage of the out gas from the "ANODE" was recycled and the recycle ratio was adjusted with respect to the steam to carbon ratio (STC) as 1.8 using design specification block "D-2". Residual fuel from "ANODE" was sent to the stoichiometric reactor "COMB" to combust them with excess oxidant coming from "CATHODE". "HEAT-5" was used to preheat the inlet stream of the reactor "COMB". In this part, the stoichiometry and conversion rates of the combustion reactions should be inserted. The combustion reaction products flowed into the "HEAT-4" block to heat the air before entering the "CATHODE" block. The stack exhaust temperature (stream "EXHST") was specified as well. The unit operation blocks are defined in summary in Table 3.3.

Table 3.3 Definition of blocks in the SOFC model

Part	Aspen Plus® Name	Definition
CMPR-1	COMPR	Sets the operating pressure of SOFC.
CMPR-2		Rises the pressure of air a little higher than atmospheric pressure.
HEAT-2	HEATER	Provides preheating to the syngas.
HEAT-3		Provides preheating to the inlet air.
HEAT-5		Provides preheating to the excess air.
COOL-2	COOLER	Adjusts the fuel temperature.
M2	MIXER	Mixes the syngas with the recycling steam.
REFORMER	RGIBBS	Forms the water-gas shift and steam reforming process of methane and other hydrocarbons.
ANODE	RGIBBS	Simulates the electrochemical reactions.
CATHODE	SEP	Separates the oxygen for electrochemical reactions.
SPL-2	FSPLIT	Splits the stream to provide essential S/C ratio

COMB	RSTOIC	Simulates the combustion reactions of CO, H_2 and CH_4 from the anode outlet flow
HEAT-4	HEATX	Provides preheating of the air by using the exhaust gas from combustion reactions

3.3.1.1. Voltage Calculation

The first step of the voltage calculation is started based on its ideal performance. Then the voltage losses are calculated considering the non-ideal behavior to determine the actual voltage value. Ideal voltage value (V_{id}) is the statement of the standard potential where the voltage is at standard pressure as following [147]:

$$V_{id} = \frac{-\Delta \overline{g_f}}{2F} \tag{3.13}$$

The Gibbs free energy of formation ($\Delta \bar{g}_f$) depicts the highest electrical energy generated by a fuel cell without losses [148]. F represents the Faraday constant (96485 C/mol) and 2 illustrates the number of moles of electrons released in the anode half reaction. The Nernst voltage (V_{Nr}), known as the reversible or equilibrium potential, is found to be closer to the actual cell voltage than V_{id} as more realistic one. The V_{Nr} is obtained using the Nernst equation which shows how the V_{id} changes as a function of species gas pressure, concentration, etc. as seen in Eq. 3.14.

$$V_{Nr} = V_{id} + \frac{RT}{2F} ln \frac{P_{H_2} P_{O_2}^{0.5}}{P_{H_2O}} \tag{3.14}$$

where T is the average temperature of the inlet and outlet streams (K) of the SOFC, and R is the universal gas constant (8.314 J/mol K). P_i represents the partial pressure (bar) of each species. The partial pressures were calculated as mean values of the inlet and outlet streams of the cathode and anode. The voltage losses occur are due to the ohmic, activation and concentration losses.

The activation losses (V_a) because of the slow kinetics of the reactions taking place in the electrodes were calculated using the correlations in Eq. (3.17) and (3.18) that can be seen in

Table 3.4 [149]. The voltage is lost due to the energy barrier required to pass by the reactants. The R_A stands for the specific resistance at cathode and anode. k_{AN} and k_{CA} are the pre-exponential factors and E_{AN}, E_{CA} activation energy values for anode and cathode respectively, which are the terms represented in Table 3.4. P^0 was assumed to be 1 bar (reference pressure), P_i is the partial pressure of each species at the cathode and anode enter and exit streams. Compared to other fuel cell types the V_a is less important in SOFC owing to its relatively high operating temperature.

Electronic and ionic resistance to electron and ion flows in the fuel cell cause the ohmic losses (V_o) which is quite essential for the tubular SOFC because they dominant due to the long current flow roads. The equations were developed by Song et al.[150] for the calculation of ohmic losses in the tubular SOFC as can be seen in Eq. (3.19) - (3.22) in Table 3.4. The uniform current density and ionic flux are assumed in circumferential and radial directions. Current (I) and current density (j) are calculated in terms of H_2 consumed in electrochemical reactions using following equations:

$$I = 2 * F * (H_{2,cons} * \frac{1000}{3600}) \quad (3.15)$$

$$j = \frac{I}{A} \quad (3.16)$$

F is Faraday constant and $H_{2,cons}$ is calculated according to Eq. (3.10). The j is obtained as dividing the I value to SOFC active area (A) that is 96.0768 m^2. Aπ is the angle is concerned with the extent of electrical contact, and Bπ is the angle radians is interested with the interconnection while ρ_{AN}, ρ_{CA}, ρ_E and ρ_{Int} are the resistivity terms [151]. D_{mA} is another expression that seen in Eq (3.19), it represents the average diameter of the cell (m) obtained from the geometry parameters introduced in Table 3.6. w_{Int} (m) is the interconnection width and $t_{A,C,E,Int}$ (m) are the cell fragment thickness.

Table 3.4 Equations for voltage losses

Voltage Losses		Eq.
	Activation	
Anode	$\frac{1}{R_{A,A}} = \frac{2F}{R_g T_{OP}} k_{AN} \left(\frac{P_{H_2}}{P^0}\right)^m exp\left(\frac{-E_{AN}}{R_g T_{OP}}\right)$	(3.17)
Cathode	$\frac{1}{R_{A,C}} = \frac{4F}{R_g T_{OP}} k_{CA} \left(\frac{P_{O_2}}{P^0}\right)^m exp\left(\frac{-E_{CA}}{R_g T_{OP}}\right)$	(3.18)
	Ohmic	
Anode	$V_{O,A} = \frac{j\rho_{AN}(A\pi D_{mA})^2}{8t_A}$	(3.19)
Cathode	$V_{O,C} = \frac{j\rho_{CA}(\pi D_{mA})^2}{8t_C} A[A + 2(1 - A - B)]$	(3.20)
Interconnection	$V_{O,Int} = j\rho_{Int} \frac{t_{Int}}{w_{Int}} (\pi D_{mA})$	(3.21)
Electrolyte	$V_{O,E} = j\rho_E t_E$	(3.22)
	Concentration	
Anode	$V_{C,A} = \frac{R_g T_{OP}}{2F} ln\left[\frac{1 - (R_g T_{OP}/2F)(t_A/D_{A,eff} y^0_{H_2} P_{SOFC})j}{1 + (R_g T_{OP}/2F)(t_A/D_{A,eff} y^0_{H_2O} P_{SOFC})j}\right]$	(3.23)
Cathode	$V_{C,C} = \frac{R_g T_{OP}}{4F} ln\left[\frac{(P_{SOFC}/\delta_{O_2}) - \left[(P_{SOFC}/\delta_{O_2}) - y^0_{O_2} P_{SOFC}\right] exp\left[(R_g T_{OP}/4F)(\delta_{O_2} t_C / D_{C,eff} P_{SOFC})j\right]}{y^0_{O_2} P_{SOFC}}\right]$	(3.24)

Mass transfer constraints cause concentration loss (V_c) in porous electrodes. Diffusion with convection in the electrodes was assumed. The Eq. (3.25) and (3.26) were obtained from Fick's law of diffusion and also Knudsen and ordinary diffusion were taken account to calculate V_c [152]. Ordinary diffusion takes place when the material has a large pore diameter compared to the average free route of the gas particles, while Knudsen diffusion happens when the pore diameter is small. The effective diffusion coefficients for the cathode and anode were used to obtain the Knudsen and Ordinary diffusions. The following equations are established to find the effective Knudsen and diffusion (Knudsen) coefficients:

$$D_{K,eff} = D_K(\varepsilon/\exists) \tag{3.25}$$

$$D_K = 97r(T_{OP}/M_i)^{0.5} \quad (3.26)$$

The model parameters of electrode pore radius (r), porosity (ε) and tortuosity (∃) seen in the Eq (3.25) and (3.26) are presented in Table 3.5. The molecular weights of each gaseous component are represented by M_i where the i depicts the components (O_2, H_2O, N_2 or H_2). There are different methods calculating the ordinary diffusion coefficients developed by researchers [153, 154]. Among them, the simplest method was chosen for calculation considering its successful performance (mean error 5%) [155]. On the basis of kinetic theory of gasses, the ordinary diffusion coefficients for cathode and anode were calculated via the following equation:

$$D_{ik} = \frac{1\times10^{-7}T_{OP}^{1.75}(1/M_i+1/M_k)^{1/2}}{P(v_i^{1/3}+v_k^{1/3})^2} \quad (3.27)$$

where k and i stand for the gaseous components which compose of the gas mixtures at anode (H_2 and H_2O) and cathode (O_2 and N_2), *v* represents the volume of Fuller diffusion which represented in Table 3.4. The coefficient of the effective ordinary diffusion and coefficient of the overall effective diffusion was calculated respectively by equations as follows:

$$D_{ik,eff} = D_{ik}(\varepsilon/\exists) \quad (3.28)$$

$$\frac{1}{D_{i,eff}} = \frac{1}{D_{ik,eff}} + \frac{1}{D_{K,i,eff}} \quad (3.29)$$

Eventually, the diffusion coefficients of the anode and cathode were determined via Eq. 3.30 and 3.31 respectively:

$$D_{A,eff} = D_{H_2,eff}\left(\frac{y_{H_2O}^0 P_{SOFC}}{P_{SOFC}}\right) + D_{H_2O,eff}\left(\frac{y_{H_2}^0 P_{SOFC}}{P_{SOFC}}\right) \quad (3.30)$$

$$D_{C,eff} = D_{O_2,eff} \quad (3.31)$$

$$\delta_{O_2} = \frac{D_{K,O_2,eff}}{D_{K,O_2,eff}+D_{O_2-N_2,eff}} \quad (3.32)$$

y_i^0 is the average value of the molar fractions of the gaseous components in the inlet and outlet streams for the anode and cathode. The concentration losses are low when the air and fuel concentrations are in normal values.

The actual voltage value (V_{act}) was calculated by subtracting the total voltage losses from V_{Nr} using the following equation:

$$V_{act} = V_{Nr} - (V_o + V_a + V_c) \quad (3.33)$$

The calculations were described in the design specification block (D-5) that adjusts the flow rate of the fuel until the DC power of the SOFC stack is equal to 120 kW. The DC power (DCP) was obtained by multiplying the V_{act} value with current.

$$DCP = V_{act} \times I \quad (3.34)$$

Table 3.5 Model design parameters for voltage losses

Activation Loss	
k_A (A/m^2)	2.13×10^{8}
k_B (A/m^2)	1.49×10^{10}
m (slope)	0.25
E_A (J/mol)	110000
E_C (J/mol)	160000
Ohmic Loss	
A	0.804
B	0.13
Concentration Loss	
r (m)	5×10^{-7}
ε	0.5
∃	5.9

Table 3.6 Model geometry and material parameters

Geometry	
Cell Diameter (m)	0.022
Cell Length (m)	1.5
t_A, t_C, t_E, t_{Int} (m)	0.0001, 0.0022, 0.00004, 0.000085
w_{Int} (m)	0.009
Material Characteristics	
ρ_{AN} (Ω m)	$2.98\times10^{-5}\exp(-1392/T_{OP})$
ρ_{CA} (Ω m)	$8.114\times10^{-5}\exp(600/T_{OP})$
ρ_E (Ω m)	$2.94\times10^{-5}\exp(10350/T_{OP})$
ρ_{Int} (Ω m)	0.025

3.4. Development of Integrated BFBG-SOFC Model

The combined system models for power generation have been studied in the literature by many researchers [156-158]. It is expected that the system performance can be improved with integrated models. The waste heat can be used as a useful source in the combined systems. The syngas from the gasification process should be cleaned and the syngas temperature should be adjusted to a suitable value before entering the fuel cell [159].

In this study, the developed BFBG model was connected with the SOFC models in the Aspen Plus simulation environment. The BFBG is an attractive type due to its high energy and H_2 contents and low CO_2 and N_2 contents in the syngas related to its high conversion capacity. The higher content of N_2 and CO_2 gasses in the syngas negatively affects the SOFC performance and causes a drop in the V_{Nr} value. The equipment for applying effective syngas cleaning is generally expensive. The selection of reliable and relatively inexpensive equipment may be the major challenge in the design of the gasification system [160]. The impurities contained in the produced gas depend on different factors such as operating conditions, design specifications and fuel type. The type of contaminants present in syngas are found in different compositions and forms. Solid particles are one of the contaminant

types that contain ash, gasifier bed material and unreacted char. They cause clogging in the SOFC anode and system equipment may fail during long-term use. The Cl in the biomass can be converted to HCl during the gasification process. Even if the syngas includes very small amounts of HCl, it can cause corrosion and should be removed. The S in the biomass forms the H_2S and COS (carbonyl sulfide) which are potent poisons. In addition, they can convert into SOx gasses which have harmful effects on the environment and human health. The mixture of heavy hydrocarbons is composed the tar, an organic impurity with no exact definition. It can condense and accumulate on cold equipment surfaces thus carbon residue problem occurs in SOFC. The contaminants which include N compounds usually form ammonia (NH_3). Even though the SOFC can use the NH_3 as fuel by converting it to H_2, it was removed from the syngas to avoid the formation of NOx gasses that cause emissions. The blocks were added to the BFBG model to allow appropriate integration with the SOFC model. The integrated model in Aspen Plus simulation were presented in Figure 3.3.

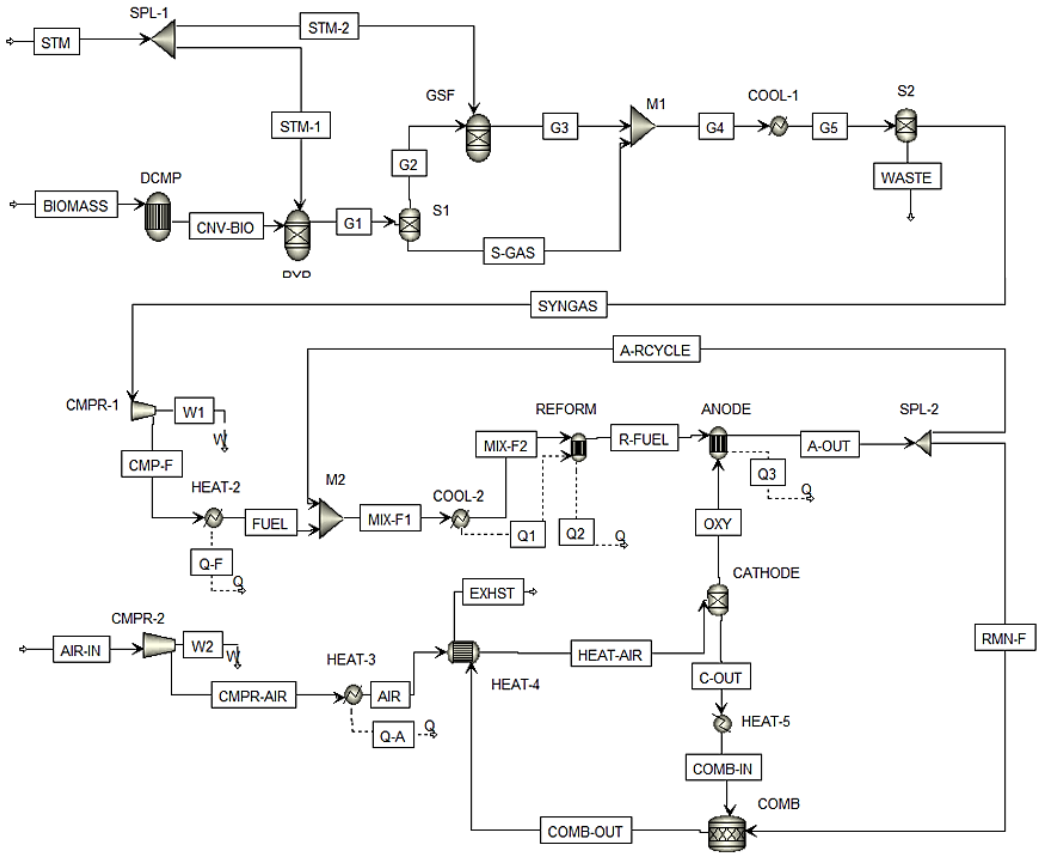


Figure 3.3 Integrated BFBG-SOFC model

The produced syngas was passed through the cooler block "COOL-1" to maintain a constant temperature value before the separation process. The temperature was set at 500°C and the output stream "G5" was fed to the separator block "S2". According to the assumptions mentioned in Section 3.2.1. char includes only the C (solid) and it may be present in very small amount as unreacted char in the syngas. The other solid impurity except the unreacted char is ash. Further H_2S, HCl and N compounds are the impurities that form in the gasifier. Addition of these, H_2O should also be removed from the syngas. The formation of tar is not possible because the simulation work on the basis of chemical equilibrium and higher hydrocarbons are converted into the small molecules. All impurities (H_2S, HCl, H_2O, unreacted char, N compounds, ash) were removed using the separator block "S2" and separated components were sent to the "WASTE" stream. The "SYNGAS" was generated from the top of the block "S2" as it consists of only H_2, CO, CH_4, CO_2 and trace amounts of propane (C_3H_8), ethane (C_2H_6) and butane (C_4H_{10}). The addition of the "COOL-1" and "S2" blocks to the system to obtain the syngas in suitable fuel form for the SOFC. Furthermore, some modifications were necessary to make the integrated BFBG-SOFC model run well. The variable of design specification block "D-5" was changed as the biomass flow rate to obtain the required amount of syngas. The biomass flow rate was changed until the DCP of the SOFC achieved 120 kW. The steam flow rate of the gasifier should be changed corresponding to the biomass flow rate to keep the steam to biomass (S/B) ratio constant. The calculator block "C-3" was used to calculate the steam flow rate according to the specific SBR value (0.5, 0.6, 0.7, 0.8, 0.9, 1.0, 1.1). Fortran code in D-5 block was also used to calculate the overall electrical efficiency (EE) of SOFC based on the energy content of fuel (LHV_{fuel}) which fed to SOFC and AC power (ACP). DCP is converted into the ACP with 0.92 conversion efficiency and EE is obtained via equation as follow:

$$EE = \frac{PDC*0.92}{1000} / \mathrm{LHV}_{fuel} \times 100 \qquad (3.35)$$

3.5. Development of the ANN Models

In the scope of this section an ANN model was developed using the data sets generated from the integrated BFBG-SOFC model in Aspen Plus simulation.

3.5.1. ANN Model Topology

ANN method plays an important role in creating an advanced AI approach [161]. Based on the basic principles of reasoning, critical thinking and remembering of ANN like human mind, it is capable of predicting the desired outcomes with respect to complicated systems [162]. An ANN includes of a group of artificial neurons lined up in layers that form the perceptron structure [163]. Computations are carried out and the output signal is produced in the perceptron which is the simple processing unit of an ANN. Each neuron generally has multiple input and output connections. The interactions between the neurons provide the flow of information. The neurons are activated when the input signal has enough intensity to overcome the bias value of the neurons. Then the received input signal is forwarded to the subsequent layer. The structure of the perceptron is presented in Figure 3.4.

The neurons arranged in multiple layers create the structure of a multilayer perceptron (MLP). The varying combinations of neuron connections make the network architecture different. Based on the connections, feedforward and feedback (recurrent) are grouped. MLP is also known as feed-forward neural network based on the directions of information flow. The MLP structure has many number of perceptron forming a layered structure (input, one or more hidden layers and output). The neurons in the input layer receive the input data and then transferred it to the hidden layers. The neuron number in the input layer refers to the input variable number. After processing the data and executing the calculations in the hidden layer the meaningful output is generated by the following output layer [164]. The number of hidden layers and neurons in the hidden layer related to the difficulty of the process affect the architecture and learning ability of the ANN. The neurons in the completely connected MLP structure have a numerical value called weight. The randomly appointed initial value of the weights is adjusted during the learning process. These topological features were arranged to perform the training process successfully.

3.5.2. Training Process

The training process is one of the essential parts that determines the prediction capability of the ANN model. Training is conducted by updating the network weights until the error value between the input and target datasets reaches the minimum. The training algorithm is used to minimize the error value and it should be selected appropriately with respect to the specific applications. The back propagation algorithm with feed forward network (FFBP) is one of the training algorithm that is often preferred in MLP structure [165, 166]. The back propagation algorithm propagates the error signal, which calculated from the target and predicted datasets, behind from the output to the input layers of the network. Then the bias and weight values are iteratively modified to reduce the error value by the FFBP algorithm.

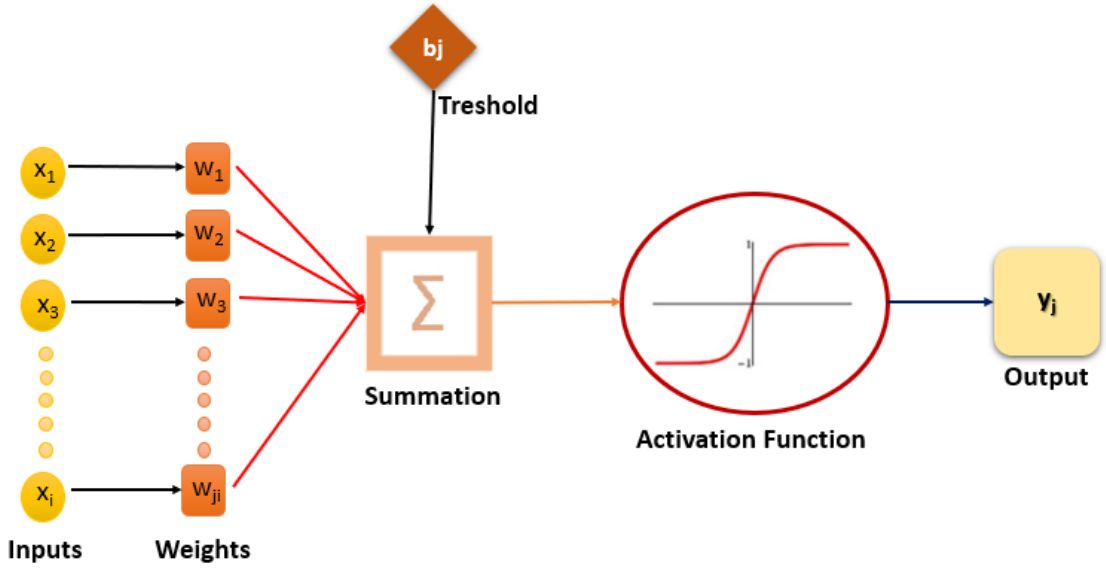


Figure 3.4 Perceptron structure

The input value (x_i) is multiplied by the network weight (w_{ji}), then the total value is summed with the bias value (b_j) to produce the output (y_j) of the ANN. The first values of the biases and weights are incidentally assigned. The y_j are described by the following equation:

$$y_j = z(\sum_{i=1}^{n} w_{ji} x_i + b_j) \tag{3.36}$$

The w_{ij} stands for the weights related to the connection between the nodes in the input (i) and

hidden (*j*) layers. *z* is called the activation or transfer function that activates the neurons and determines the response of the network corresponding to the input data. The activation function supplies the nonlinear transformation and promotes the expression capability to compute complex relationships [167]. The most commonly used activation functions according to the ANN structure consist of tangent sigmoid, ReLu, sigmoid, ELU, exponential, etc. In this study, the tangent sigmoid function was selected due to its faster training capacity, and higher sensitivity to small deviations. This function is the modified version of the sigmoid function. The output values are limited between -1 and +1 thus it has positive and negative responses, which is the important superiority over the sigmoid function (has only positive response). The equation of the tangent sigmoid function is represented by the following equation:

$$f(x) = (e^{x} - e^{-x}) / (e^{x} + e^{-x}) \tag{3.37}$$

Different optimization algorithms which use the performance function gradient is employed to regulate the weights and biases. The Levenberg-Marquardt (L-M) algorithm that provides a higher training speed even in the case of large data sets was preferred to optimize the network [168]. It carries out the combination of the superiorities of the gradient descent method (stable convergence) and Gauss-Newton algorithm (high convergence rate). The L-M method allows to reduce nonlinear function problems with an approximate solution using following equations for calculation of increment in weights [169]:

$$\Delta w = [\, J^{T} J + \lambda I \,]^{-1} \times J^{T} \times e \tag{3.38}$$

where I stands for the identity matrix a, J refers to the Jacobian matrix and vector network error were represented by

e. λ is a scalar which is to be adjusted using the decay rate according to the outputs.

3.5.3. Error Evaluation of the ANN model

The bias and weights values are updated to obtain a satisfactory result in the training part using the error value. The large data set should be used to train the ANN model and aid to fit the training data sets successfully. For this reason, using a large amount of data and evaluating the estimation performance of ANN are the methods applied to avoid the over-fitting problem. Mean-square error (MSE), mean error (ME), root mean square error (RMSE), mean absolute percentage error (MAPE) Mean Relative Absolute Error (MRAE) are the substantial criteria to assess the prediction capacity of ANN model. In this work, the MSE was used as a performance function during the development of the FFBP network model. The MSE has many advantages that make it the generally preferred statistical measure. First, the meaning of the error signal which has net physical meaning is defined in a natural way, it also has the simple calculations. It does not memorize and independent of another data, so it is calculated for each sample. The calculation of MSE value is expressed using the equation as follow:

$$MSE = \frac{\sum_{i=1}^{n}(C_i - P_i)^2}{n} \tag{3.39}$$

The ME, RMSE, MAPE and MRAE were preferred to check the forecasting capability of the ANN. They found via the equations as follows:

$$ME = \frac{\sum_{i=1}^{n}(C_i - P_i)}{n} \tag{3.40}$$

$$RMSE = \sqrt{\frac{\sum_{i=1}^{n}(C_i - P_i)^2}{n}} \tag{3.41}$$

$$MAPE = \frac{100\%}{n} \sum_{i=1}^{n} \left|\frac{(C_i - P_i)}{C_i}\right| \tag{3.42}$$

$$MRAE = \frac{1}{n} \sum_{i=1}^{n} \left|\frac{(C_i - P_i)}{(C_i - \overline{C_i})}\right| \tag{3.43}$$

where P_i stands for the predicted value, C_i represents the calculated value, $\bar{C}$ depicts the mean of the calculated values for the model and n is the size of data.

The coefficient of determination (R^2) is the uncertainty measure that has the statistical metric in range between 0 and 1. R^2 was used to visualize the estimation performance of the ANN model via the following equation:

$$R^2 = 1 - \frac{\sum_{i=1}^{n}(Y_{predicted} - Y_{actual})^2}{\sum_{i=1}^{n}(Y_{predicted} - Y_{mean})^2} \quad (3.44)$$

where "n" depicts the size of data, "$Y_{predicted}$" and "Y_{actual}" are the estimated and target values of the ANN model respectively, and "Y_{mean}" represents the avarage value of the target outputs.

4. RESULTS AND DISCUSSION

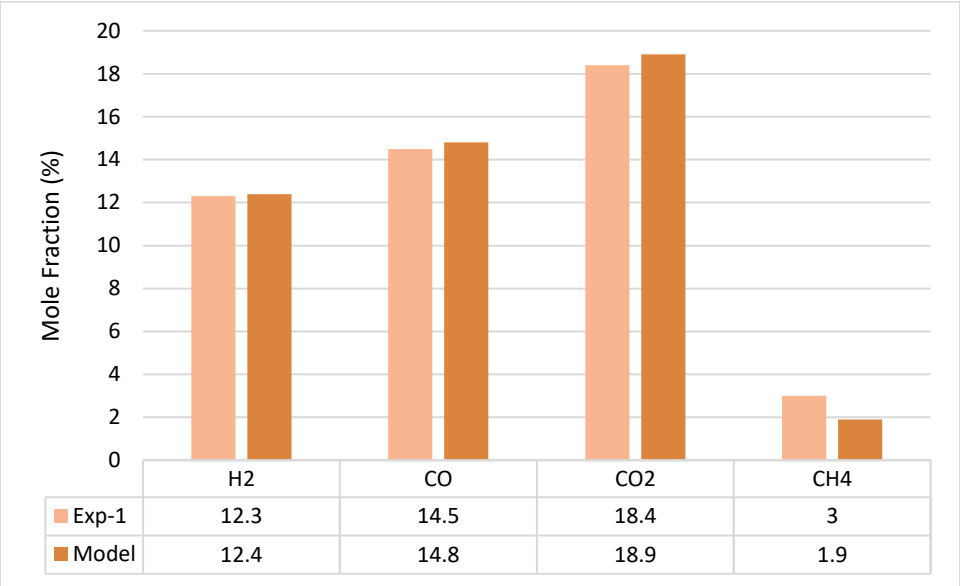
4.1. Model Validation Results of BFBG

The accuracy of the BFBG model should be approved after accomplishment of the model development. The reality of the developed process was tested using the experimental data sets from literature studies. Two different BFBGs were used to validate the model via following procedure. The operating conditions, fuel sample and gasification agents with their flow rates were described to system same as the experimental conditions which are presented in Table 4.1.

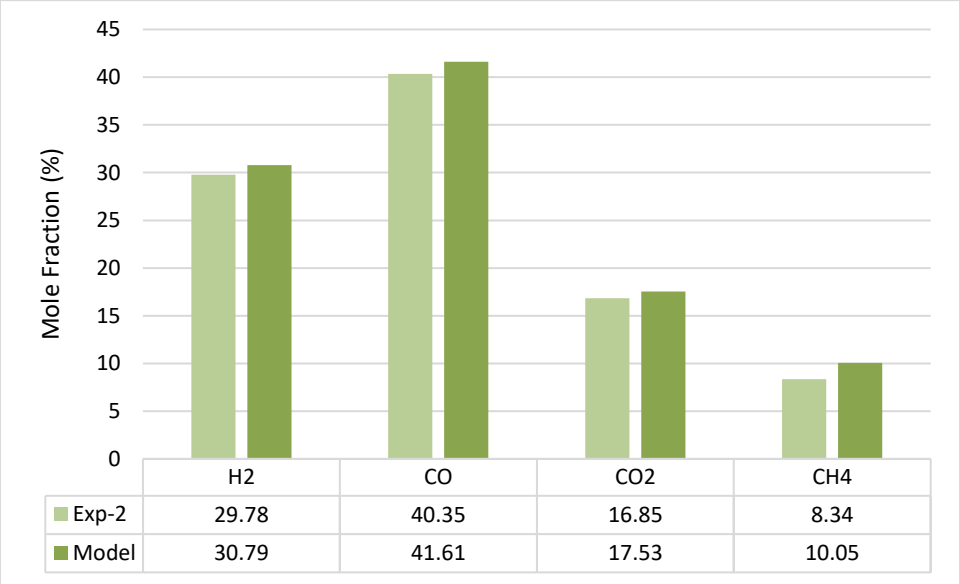
Table 4.1 Operating conditions of the validation data sets.

	1 [170]	**2 [134]**
Fuel Type	Rice Husk	Pine Sawdust
Gasification Agent	Steam, Air	Steam, Air
Fuel Feed Flow (kg/h)	2.5	0.445
Equivalence Ratio	0.35	0.22
S/B Ratio	0.5	1.35
Gasifier Temperature (°C)	850	800

The rice husk and pine sawdust as fuel samples were used for the first and second experimental works respectively. The air and steam at different amounts were preferred together for both studies. After conducting the simulation under same operating conditions with experiments, the syngas flows for molar fraction of H_2, CH_4, CO and CO_2 were compared and outputs were showed in Figure 4.1 (a) and (b).



(a)



(b)

Figure 4.1 Comparison of the model and experimental works

(a) First experimental work [170]

(b) Second experimental work [134]

Comparison results showed that the model works very well even there are slight differences between the mole fractions. These differences in results are in the acceptable range like the other literature studies [171, 172]. Although the model works based on some assumptions independent of the reaction kinetics and design of the reactor which mentioned in Section (3.2.1), the model showed the extraordinary simulation performance to represent the real gasification.

4.2. Model Validation Results of SOFC

The SOFC stack model was developed in Aspen Plus simulation based on the tubular SOFC technology. The developed SOFC model needs to validate with the experimental or approved data sets. Operating parameters of the SPGI 100 kW SOFC stack model was used to verify the model. System outputs were compared for the simulation and experimental works. The SOFC operating parameters are listed in Table 4.2.

Table 4.2 Operating parameters of the SOFC model in literature study.

Parameters	**Specifications**
Fuel inlet composition (%, mole)	CH_4 81.3%, C_2H_6 2.9%, C_3H_8 0.4%, C_4H_{10} 0.2%, N_2 14.3%, CO 0.9%
SOFC Operating Temperature (°C)	910
SOFC Operating Pressure (bar)	1.08
DCP output (kW)	120
Active Area (m^2)	96.1
Cell Number	1152
Inlet Air Temperature (°C)	630
Inlet Fuel Temperature (°C)	200
DC to AC inverter efficiency (%)	92
Uf, Ua	0.85, 0.19
STCR	2.5
P_{FUEL}/P_{SOFC}	3
Temperature difference between the exit of hot and cold stream in the ‘‘HEATEX3’’ block	10

Thermal Losses 2%

The operating parameters were set and fuel was introduced to system identically with the experimental work. The outputs were compared by means of the cell voltage, current density, gross AC efficiency and temperature and composition at the specific streams. Comparison results can be seen in the Table 4.3.

Table 4.3 SOFC model validation results.

Parameters	**Experimental-Literature [173]**	**Model – Literature [144]**	**Model – Literature [97]**	**Model Results**
Voltage (mV)	Not Available	700	683	683
Current Density (mA/cm^2)	180	178	182.86	189
Pre-reforming Temperature (°C)	550	536	535	544
Cathode Inlet Temperature (°C)	Not Available	821	823	826
Stack Exhaust Temperature (°C)	847	834	833	836
Anode Inlet Gas Composition (%, mole)	Not Available	27.9% H_2O, 23.1% CO_2, 27% H_2, 5.6% CO, 6.2% N_2, 10.1% CH_4	27.8% H_2O, 23.1% CO_2, 26.9% H_2, 5.6% CO, 6.2% N_2, 10.4% CH_4	27.8% H_2O, 23.1% CO_2, 26.9% H_2, 5.6% CO, 6.2% N_2, 10.4%CH_4
Anode Exhaust Gas Composition (%, mole)	48% H_2O, 28% CO_2, 14% H_2, 5% CO, 5% N_2	50.9% H_2O, 24.9% CO_2, 11.6% H_2, 7.4% CO, 5.1% N_2	50.9% H_2O, 24.9% CO_2, 11.6% H_2, 7.4% CO, 5.1% N_2	50.8% H_2O, 24.9% CO_2, 11.6% H_2, 7.4% CO, 5.1% N_2
Gross AC Efficiency (%, LHV)	50	52	51.28	51.19

The model outputs showed the well similarity with the experimental results. However, there are small deviations in the composition and temperature values, the model showed the remarkable performance in terms of voltage, current density, and gross AC efficiency.

After the successful validation studies for the BFBG and SOFC models. The integrated BFBG-SOFC model was used to generate data for the development of the ANN model.

4.3. Parametric Study for Integrated BFBG-SOFC Model

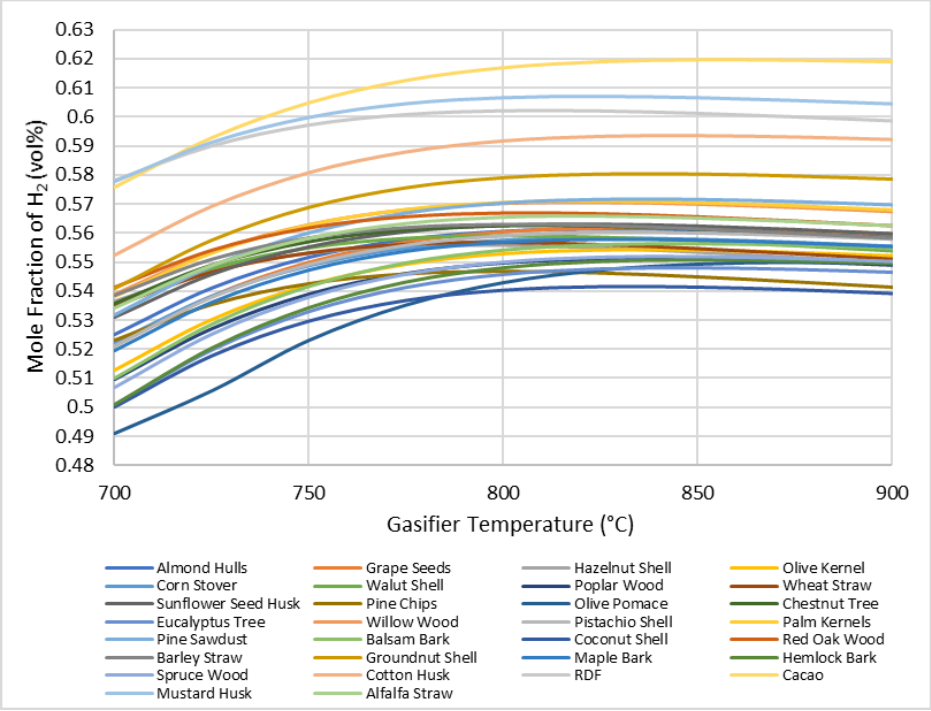
The output parameters of the BFBG and SOFC models are influenced by many parameters related to operating conditions and fuel types. Operating temperature and steam flow rate for the gasification process were selected the main parameters to evaluate the syngas composition at the gasifier exit. The composition of the fuel which fed to the SOFC is one of the important parameters for the system performance. Therefore, operating conditions and biomass samples which preferred for the BFBG are the considerable parameters for SOFC as well. Effect of steam to biomass ratio (S/B), BFBG temperature and anode temperature was examined on the EE, j and V_{act} of SOFC for 30 diverse biomass samples. The operating parameters for integrated BFBG-SOFC model was specified in Table 4.4.

Table 4.4 Operating parameters of BFBG-SOFC system

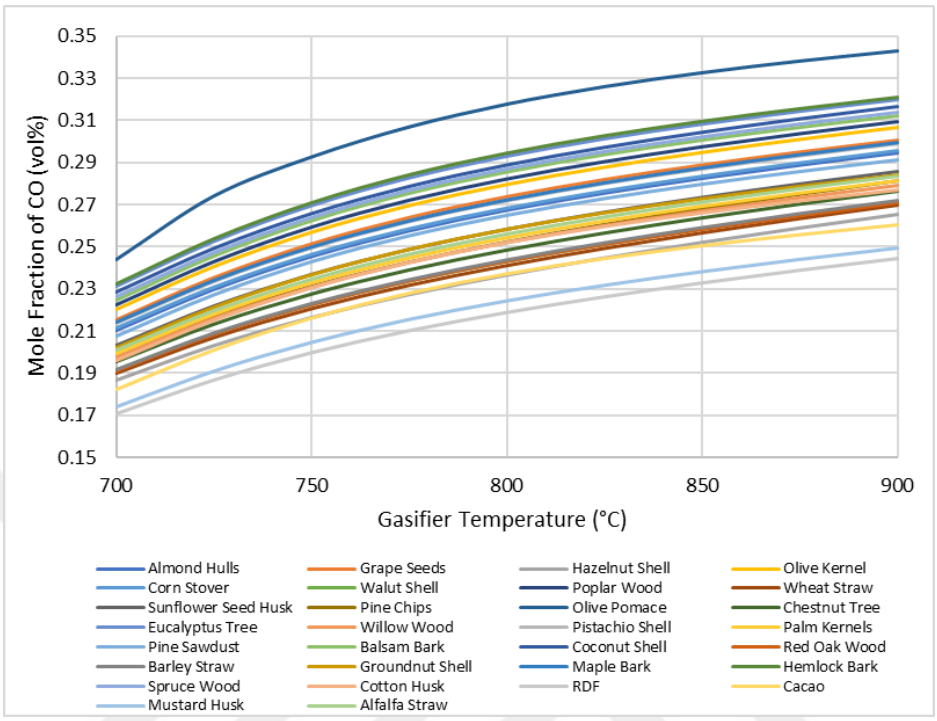
Parameters	**Value**
Gasifier Pressure (bar)	3
SOFC Pressure (bar)	1
U_f	0.85
U_a	0.19
DC to AC conversion efficiency	0.92
SCR	1.85
Active Area (m^2)	96.076
Power (kW)	120

4.3.1. Effect of the Gasification Temperature on Syngas Composition

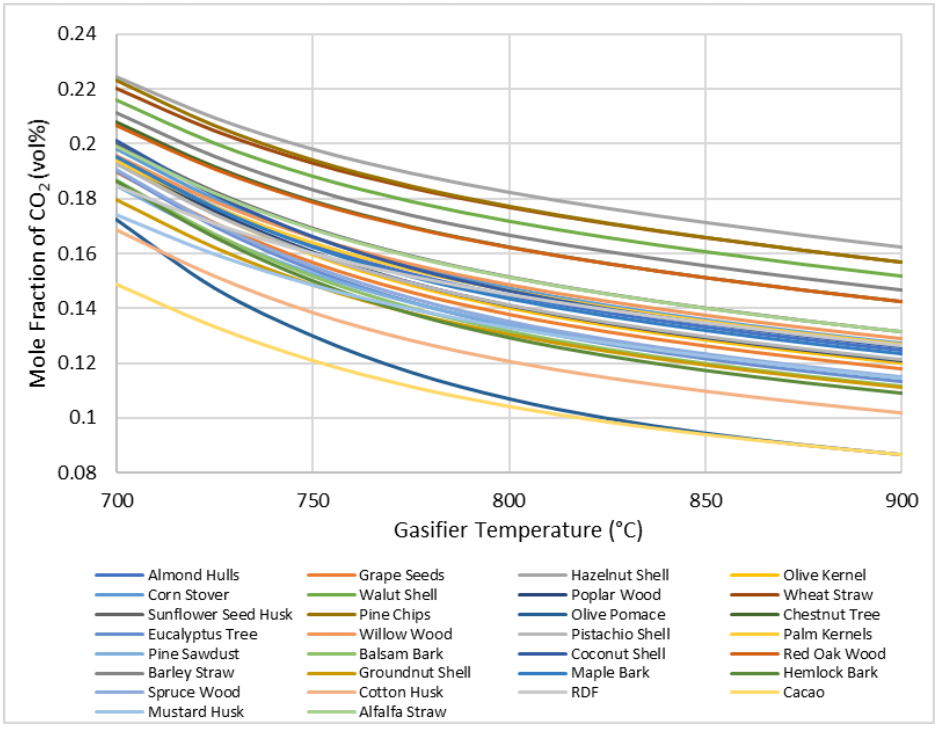
The operating temperature of gasification process is one of the key parameters that effects the syngas composition and quality as well. The equilibrium reactions occurred in the gasification are extremely influenced by the temperature because most of them are endothermic. Fluidized bed reactors for biomass gasification process are generally operated at lower than 1000 °C to prevent defluidization and agglomeration that occur as a result of ash softening. In this study, effect of gasifier temperature on the syngas composition was investigated using sensitivity analysis tool in Aspen Plus simulation. The simulation results are presented for the concentration change of the H_2, CO, CH_4 and CO_2 versus temperature that varied between 700-900 °C while the S/B ratio was kept stable as 0.7 in Figure 4.2.



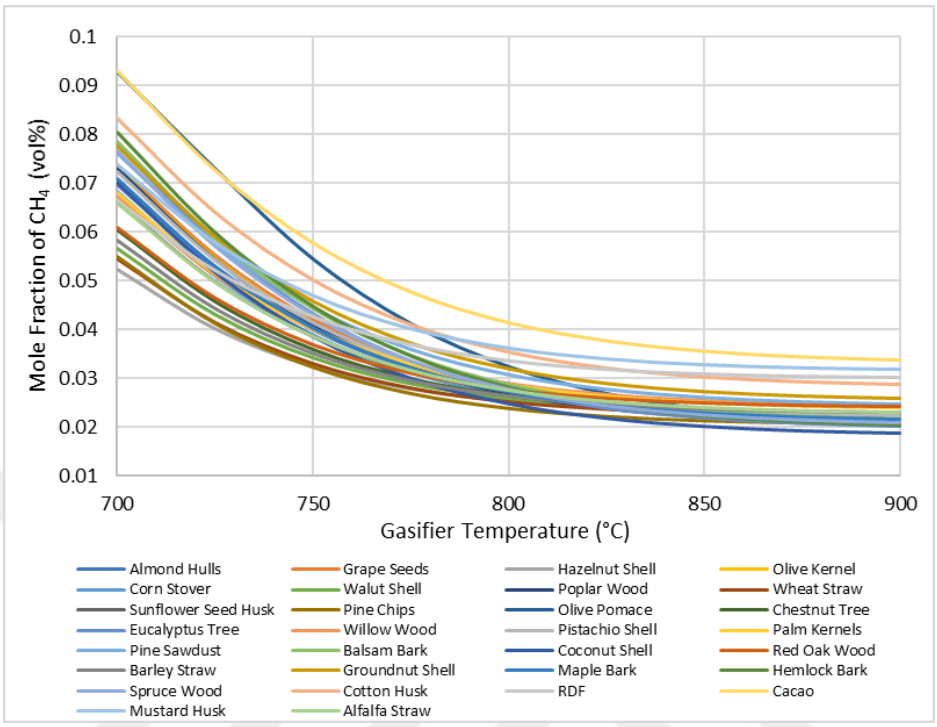
(a)


0.35
0.33
0.31
0.29
0.27
0.25
0.23
0.21
0.19
0.17
0.15
Mole Fraction of CO (vol%)
700
750
800
850
900
Gasifier Temperature (°C)
Almond Hulls
Grape Seeds
Hazelnut Shell
Olive Kernel
Corn Stover
Walut Shell
Poplar Wood
Wheat Straw
Sunflower Seed Husk
Pine Chips
Olive Pomace
Chestnut Tree
Eucalyptus Tree
Willow Wood
Pistachio Shell
Palm Kernels
Pine Sawdust
Balsam Bark
Coconut Shell
Red Oak Wood
Barley Straw
Groundnut Shell
Maple Bark
Hemlock Bark
Spruce Wood
Cotton Husk
RDF
Cacao
Mustard Husk
Alfalfa Straw

(b)


0.24
0.22
0.2
0.18
0.16
0.14
0.12
0.1
0.08
Mole Fraction of CO_2 (vol%)
700
750
800
850
900
Gasifier Temperature (°C)
Almond Hulls
Grape Seeds
Hazelnut Shell
Olive Kernel
Corn Stover
Walut Shell
Poplar Wood
Wheat Straw
Sunflower Seed Husk
Pine Chips
Olive Pomace
Chestnut Tree
Eucalyptus Tree
Willow Wood
Pistachio Shell
Palm Kernels
Pine Sawdust
Balsam Bark
Coconut Shell
Red Oak Wood
Barley Straw
Groundnut Shell
Maple Bark
Hemlock Bark
Spruce Wood
Cotton Husk
RDF
Cacao
Mustard Husk
Alfalfa Straw

(c)



(d)

Figure 4.2 Change of gas concentrations in syngas according to temperature (S/B:0.7)

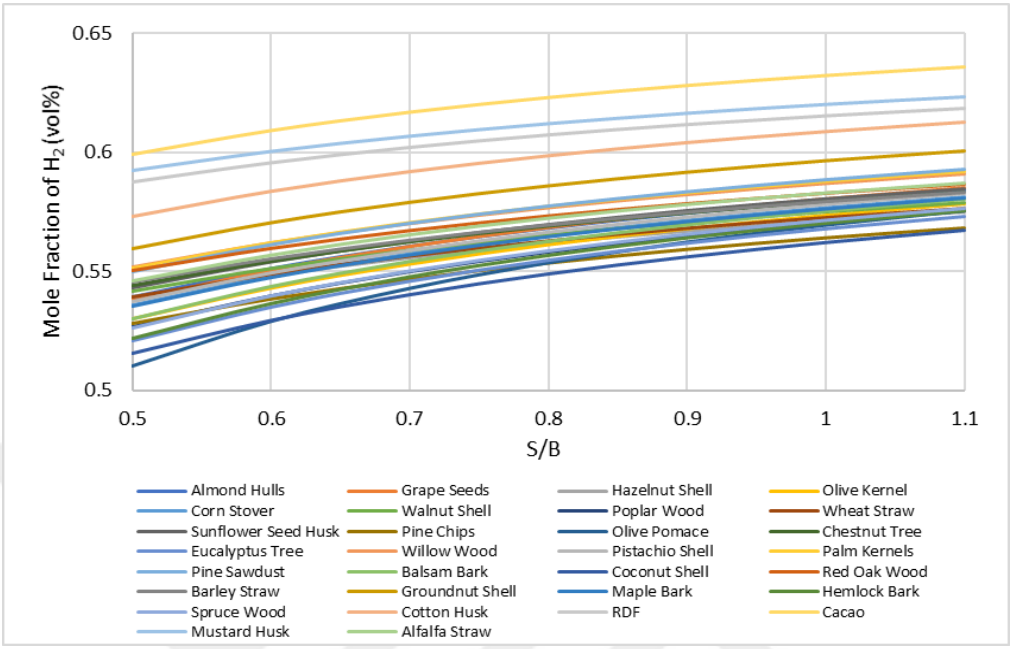
(a) H_2, (b) CO, (c) CO_2, (d) CH_4

As seen in Figure 4.2 the syngas composition was highly influenced by the temperature change. The results depicted that H_2 and CO concentrations enhanced with temperature while CH_4 and CO_2 concentrations reduced. Even if all samples showed similar behavior with temperature, their concentration changes were not same according to varying physicochemical characteristics of the biomass samples. Cacao sample showed highest H_2 concentration in syngas (61.98%) among the other samples. Mustard husk, RDF, cotton husk and groundnut shell samples followed it with higher H_2 content compared with others. H_2 concentrations in syngas achieved their maximum values when the temperature was changed between 750-850 °C inside the gasifier at different points for each biomass samples. Their CO concentrations in syngas also increased notably with temperature. Initially syngas contained more CO_2 and CH_4 than final for each biomass samples. Their concentrations in syngas dramatically decreased between the temperature 700-800 °C, the decreasing behavior continued slowly the temperature above 800 °C. The forward reactions of the endothermic

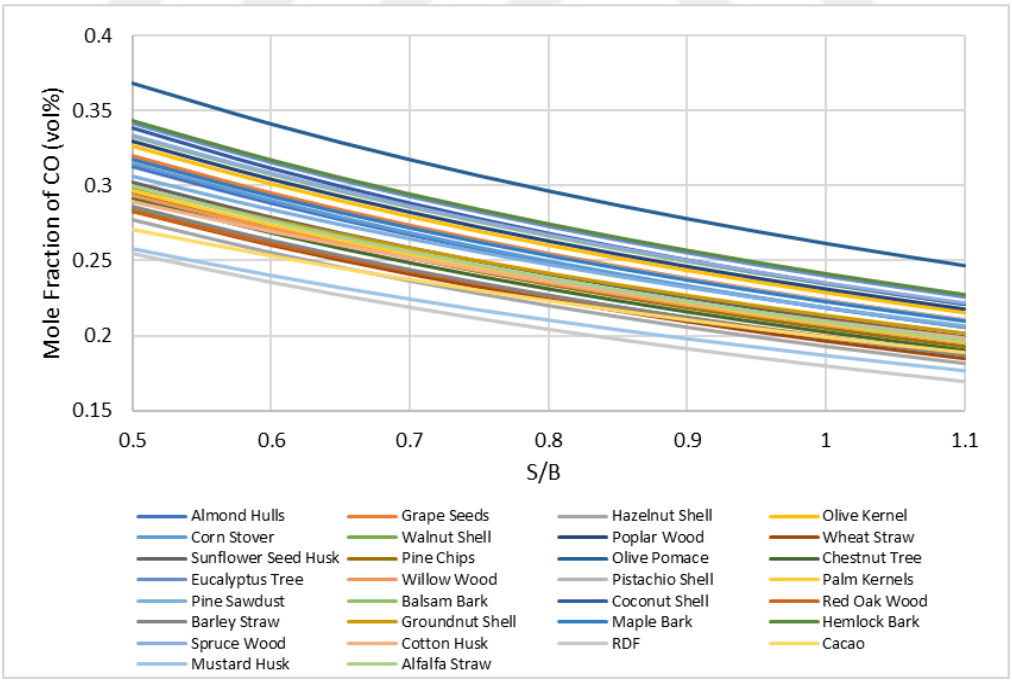
char conversion and steam-methane reforming reactions accelerated while the exothermic hydrogasification and methanation reactions oriented backward with temperature rise [51]. According to the above statement, results were found in well agreement with the Le Chatelier's principle [174]. Therefore, high temperature was attributed the decomposition of char and conversion of the CH_4 and other large hydrocarbons to small gasses such as H_2 and CO. As the gasifier temperature further rise, the concentration of CO_2 decreased, and CO increased because of extremely endothermic Boudouard Reaction. Similar trends of concentrations in syngas were also cited by many researchers in the previous works. Faraji and Saidi [175]. found the composition change of syngas from algal biomass gasification as same with these outputs. Monteiro et al [176]. also obtained the same trend in syngas composition using a CFD model. Couto et al [177]. investigated the effect of gasification temperature on the syngas quality in terms of composition and other parameters and they reported similar results for the change of syngas composition.

4.3.2. Effect of the S/B Ratio on Syngas Composition

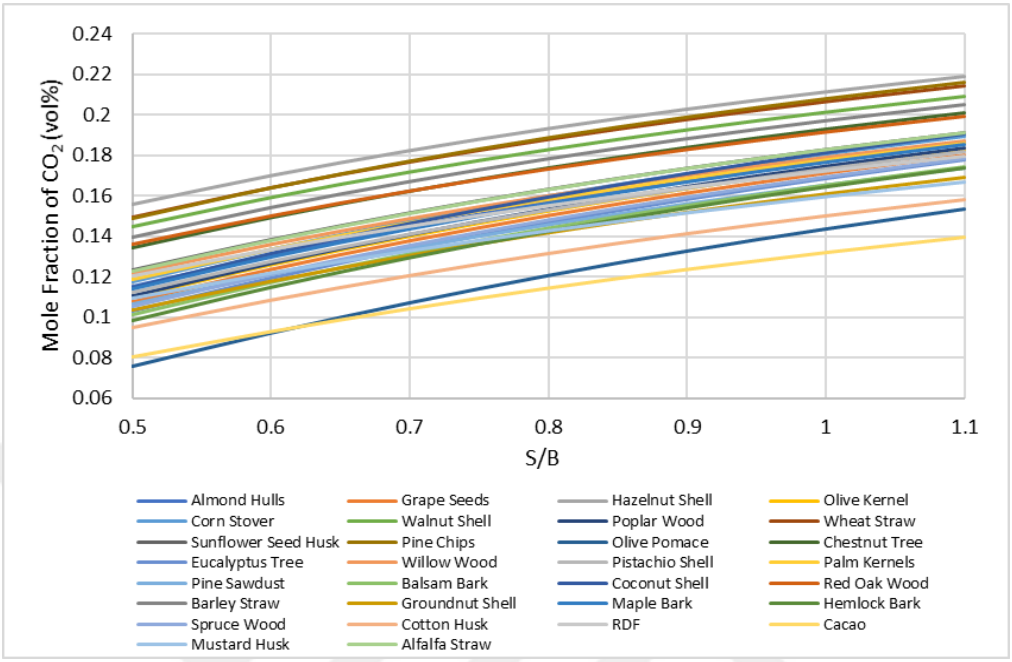
S/B ratio is a significant parameter having a notable influence on the syngas composition. It can be obtained from dividing of the mass flow rate of the steam to biomass feed flow rate [178]. Addition of the steam provides higher partial pressure for H_2O inside the gasifier. The higher partial pressure of H_2O encourages the forward reactions of the steam methane reforming, water gas and water-gas shift reactions. This behavior leads to increase production of H_2 and CO_2 and reduce of CO and CH_4. The results related to effect of S/B ratio on the gas concentrations in syngas are presented in Figure 4.3. for each biomass samples used in the present study. The evaluation range for S/B ratio was selected between 0.5 and 1.1 when the gasifier temperature fixed at 800 °C.


Mole Fraction of H_2 (vol%)
0.65
0.6
0.55
0.5
0.5
0.6
0.7
0.8
0.9
1
1.1
S/B
Almond Hulls
Grape Seeds
Hazelnut Shell
Olive Kernel
Corn Stover
Walnut Shell
Poplar Wood
Wheat Straw
Sunflower Seed Husk
Pine Chips
Olive Pomace
Chestnut Tree
Eucalyptus Tree
Willow Wood
Pistachio Shell
Palm Kernels
Pine Sawdust
Balsam Bark
Coconut Shell
Red Oak Wood
Barley Straw
Groundnut Shell
Maple Bark
Hemlock Bark
Spruce Wood
Cotton Husk
RDF
Cacao
Mustard Husk
Alfalfa Straw

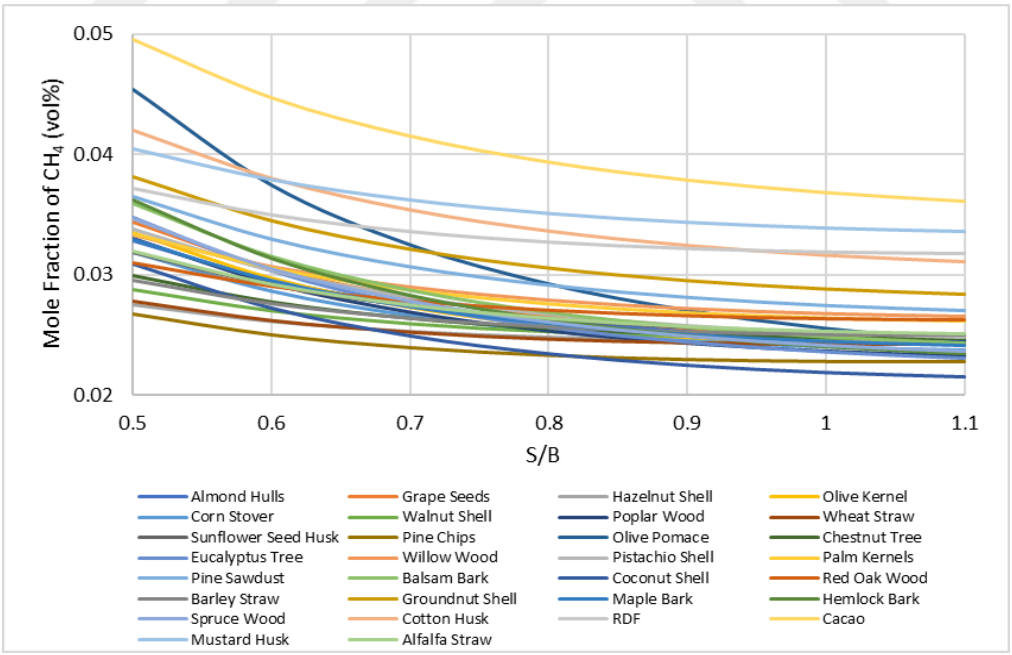
(a)


Mole Fraction of CO (vol%)
0.4
0.35
0.3
0.25
0.2
0.15
0.5
0.6
0.7
0.8
0.9
1
1.1
S/B
Almond Hulls
Grape Seeds
Hazelnut Shell
Olive Kernel
Corn Stover
Walnut Shell
Poplar Wood
Wheat Straw
Sunflower Seed Husk
Pine Chips
Olive Pomace
Chestnut Tree
Eucalyptus Tree
Willow Wood
Pistachio Shell
Palm Kernels
Pine Sawdust
Balsam Bark
Coconut Shell
Red Oak Wood
Barley Straw
Groundnut Shell
Maple Bark
Hemlock Bark
Spruce Wood
Cotton Husk
RDF
Cacao
Mustard Husk
Alfalfa Straw

(b)



(c)



(d)

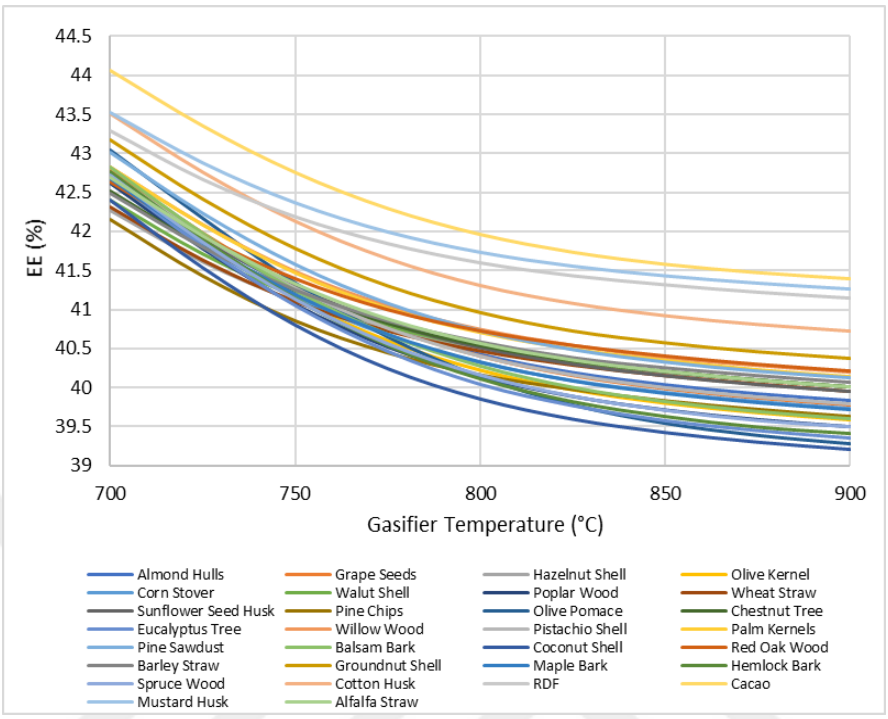
Figure 4.3 Change of gas concentrations in syngas according to S/B ratio (Gasifier Temperature: 800 °C)

(a) H_2, (b) CO, (c) CO_2, (d) CH_4

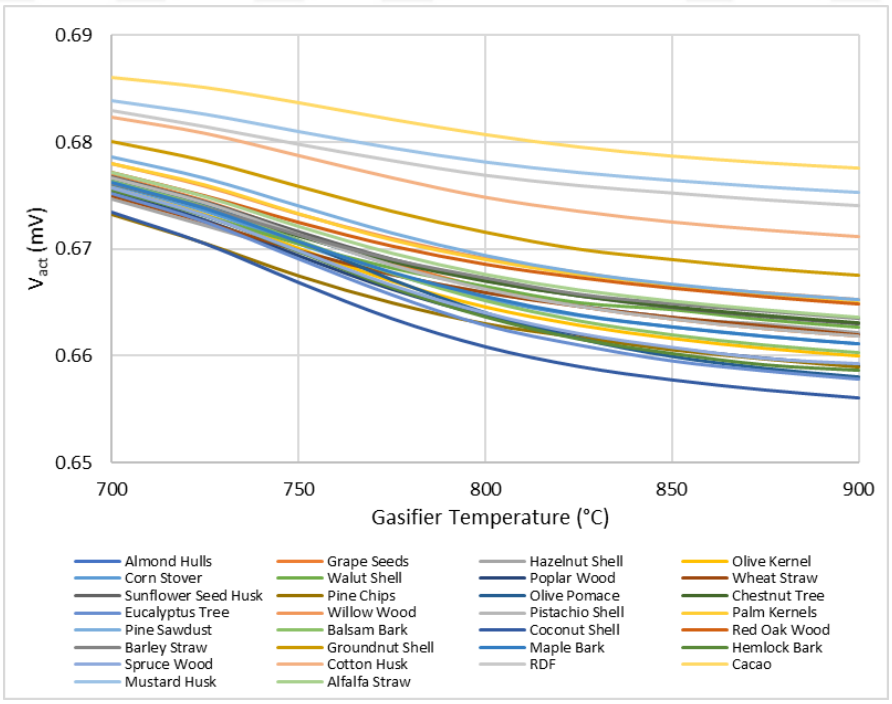
As seen in Figure 4.3, increasing steam amount showed the favorable effect on the H_2 concentration but it was also raised the CO_2 concentration which is the undesired product. Addition of more steam immensely supported the decomposition reactions of hydrocarbons thus the H_2 content of syngas upsurged and reached the 63.61% for cacao sample. Furthermore, CH_4 concentrations showed decreasing trend because of the extremely activated steam methane reforming reaction. The magnitudes of CO_2 and CO in syngas was mainly affected by the water-gas shift reaction and they showed opposite behavior for each biomass sample as seen in Figure 4.3 (b) and (c). All biomass samples showed similar trend, but the concentrations change had not been identical related to different physicochemical characteristics. Even if the studies were conducted under different operating conditions and fuel samples, they found in agreement with these outputs [179-181].

4.3.3. Effect of the Gasification Temperature on SOFC

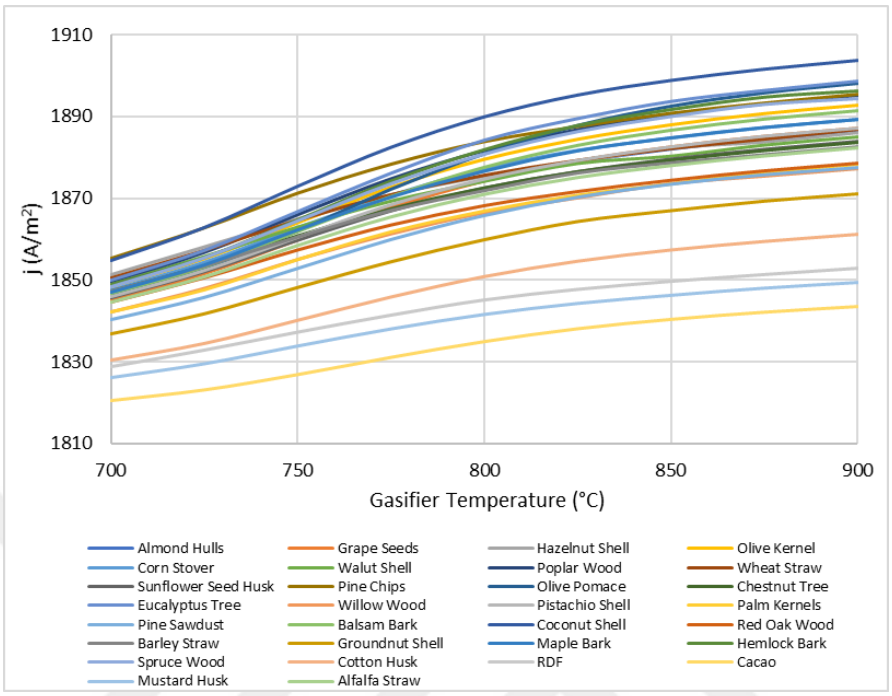
The whole system should be considered while discussing the influence of operating parameters for the performance evaluation. Gasification temperature was thought is the mainly effective parameter on the integrated BFBG-SOFC system because syngas composition was changed remarkably with temperature. The performance parameters of SOFC (EE, j and V_{act} and biomass feed flow) are calculated according to syngas composition and molar flow directly or indirectly. Therefore, effect of gasification temperature on the performance parameters of SOFC was investigated. The BFBG temperature was enhanced from 700 to 900 °C while the S/B ratio and anode temperature of SOFC were fixed at 0.7 and 910 °C respectively. Results can be seen in Figure 4.4 for each biomass samples.


44.5
44
43.5
43
42.5
42
41.5
41
40.5
40
39.5
39
EE (%)
700
750
800
850
900
Gasifier Temperature (°C)
Almond Hulls
Grape Seeds
Hazelnut Shell
Olive Kernel
Corn Stover
Walut Shell
Poplar Wood
Wheat Straw
Sunflower Seed Husk
Pine Chips
Olive Pomace
Chestnut Tree
Eucalyptus Tree
Willow Wood
Pistachio Shell
Palm Kernels
Pine Sawdust
Balsam Bark
Coconut Shell
Red Oak Wood
Barley Straw
Groundnut Shell
Maple Bark
Hemlock Bark
Spruce Wood
Cotton Husk
RDF
Cacao
Mustard Husk
Alfalfa Straw

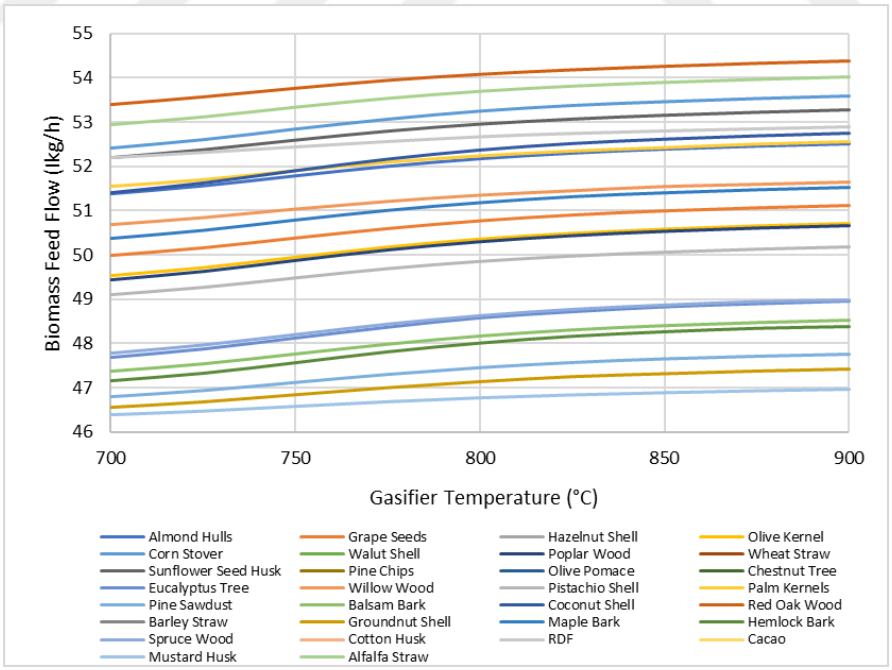
(a)


0.69
0.68
0.67
0.66
0.65
V_{act} (mV)
700
750
800
850
900
Gasifier Temperature (°C)
Almond Hulls
Grape Seeds
Hazelnut Shell
Olive Kernel
Corn Stover
Walut Shell
Poplar Wood
Wheat Straw
Sunflower Seed Husk
Pine Chips
Olive Pomace
Chestnut Tree
Eucalyptus Tree
Willow Wood
Pistachio Shell
Palm Kernels
Pine Sawdust
Balsam Bark
Coconut Shell
Red Oak Wood
Barley Straw
Groundnut Shell
Maple Bark
Hemlock Bark
Spruce Wood
Cotton Husk
RDF
Cacao
Mustard Husk
Alfalfa Straw

(b)



(c)



(d)

Figure 4.4 Effect of the BFBG temperature on SOFC

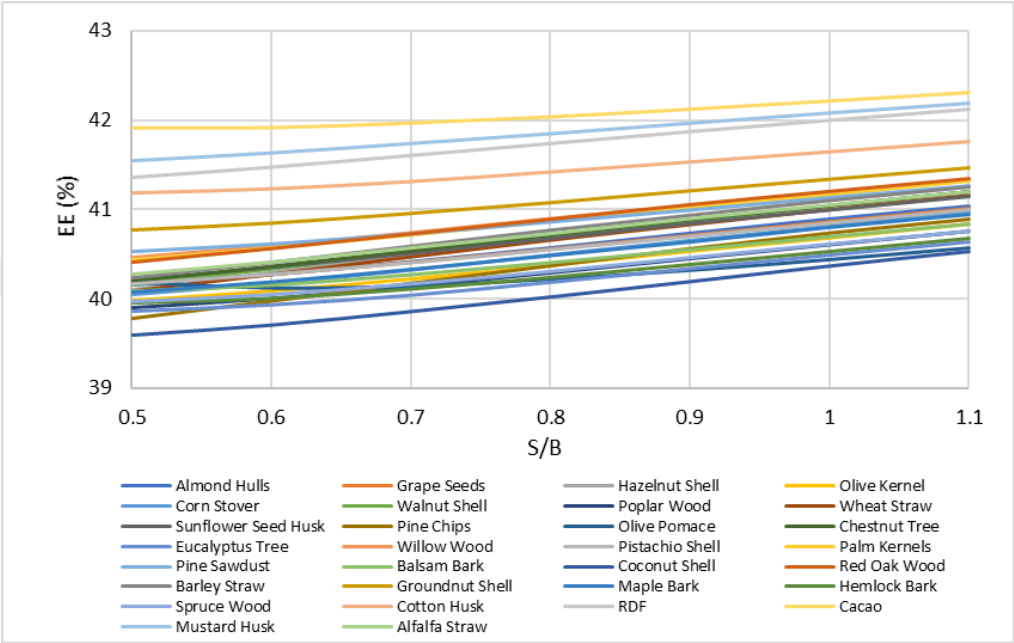
(a) EE, (b) V_{act}, (c) j, (d) biomass feed flow

Impact of varying BFBG temperature on the SOFC EE as illustrated in the Figure 4.4 (a). The EE value continuously decreased about 3-4% for each biomass samples while the temperature increased between 700-900 °C. The immense drop in EE and V_{act} as same with the CH_4 concentration change in syngas (Figure 4.2 (d)) and rise in j and biomass feed flow occurred at the temperature raising from 700 to 800 °C. These changes continued slower at temperature above 800 °C. Related to reduced CH_4 concentration in syngas with temperature as mentioned above supports the reverse water-gas shift reaction at higher temperature because of the increasing operating temperature of reformer. The endothermic reaction likely to occur does not cause the temperature to drop due to the low amount of CH_4. The decreasing trend of the SOFC EE can be explained with the increasing H_2O concentration in the anode inlet stream. The outputs depicted that the low temperature provides higher overall EE for SOFC. Even though temperature increase did not show a good effect on EE, tar in syngas that can be formed at lower temperature should be taken into account while adjusting the temperature value. Decreasing behavior of CH_4 concentration leads to reduce of $H_{2,cons}$ and $O_{2,cons}$ values as well as $nO_{2,in}$ which refers the molar flow of O_2 in air according to Eq. (3.12). These changes in molar flows caused the drop in partial pressure of O_2 and enhancement in partial pressure of H_2O. Thus, the j and biomass feed flow increased to acquire 120 kW DCP. In Figure 4.4 (b), V_{act} showed decline because increasing amount of j cause the losses in voltage as seen in the calculation of voltage losses Eq. (3.19) – (3.24). The obtained results showed consistency with the literature studies [143, 182-184]. Biomass feed flow was increased almost 1-2 kg/h with temperature for each sample as depicted in Figure 4.4 (d). Considering the decrease in voltage and increase in biomass feed flow electrical power production was conducted with lower EE at higher BFBG temperature as seen in Figure 4.4 (a).

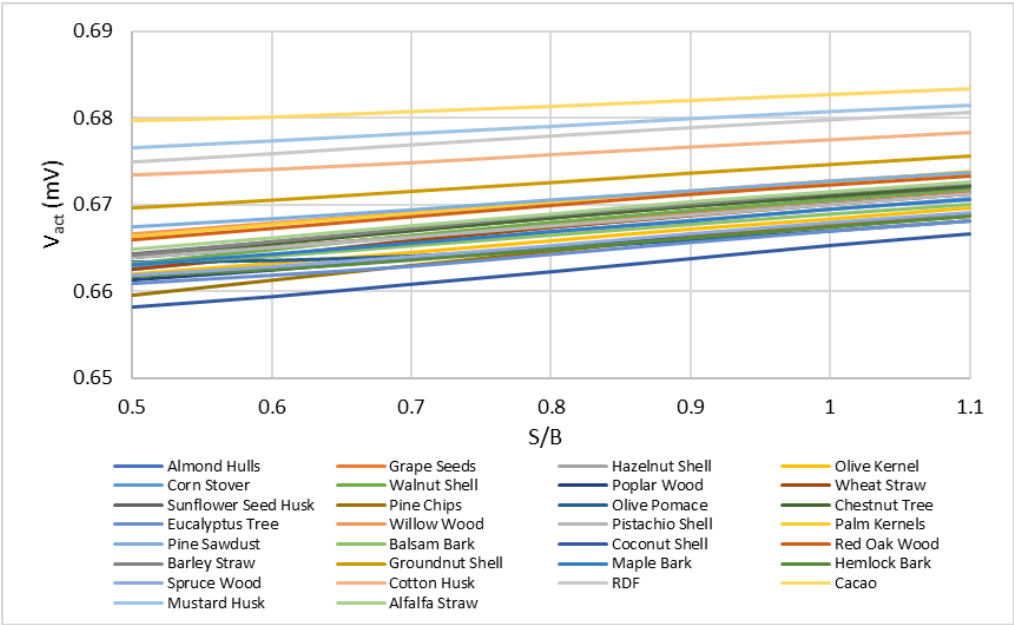
4.3.4. Effect of S/B Ratio on SOFC

Steam as gasifying agent leads to obtain a syngas with high H_2 content compared to others. SOFC has flexibility to impurities in fuel however higher H_2 content fuel is more desirable to produce electrical energy with higher efficiency. The tendency in EE, V_{act}, j and required amount of biomass as performance parameter of SOFC was observed to according to varying

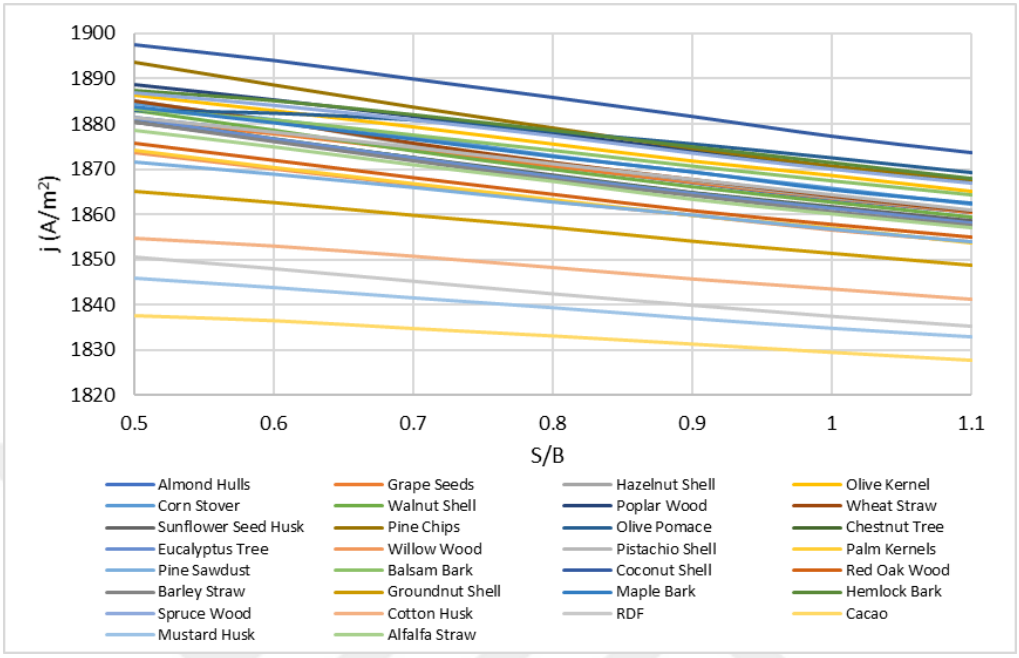
S/B ratio. The parametric study was carried out by fixing the BFBG and SOFC operating temperatures at 800 °C and 910 °C, respectively. Result can be seen in the Figure 4.5 for each biomass sample.



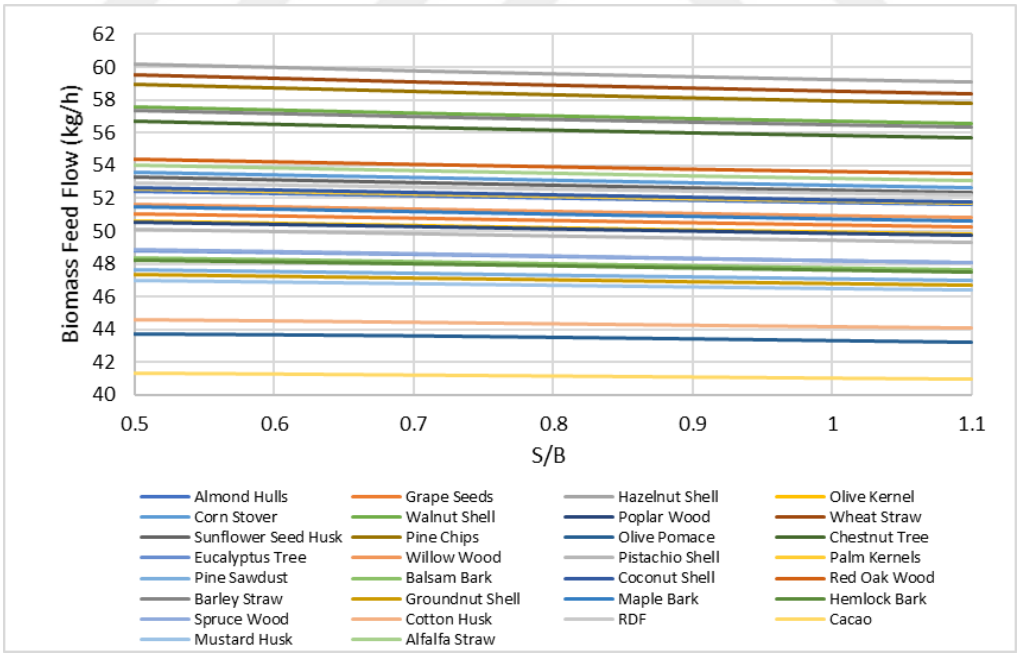
(a)



(b)



(c)



(d)

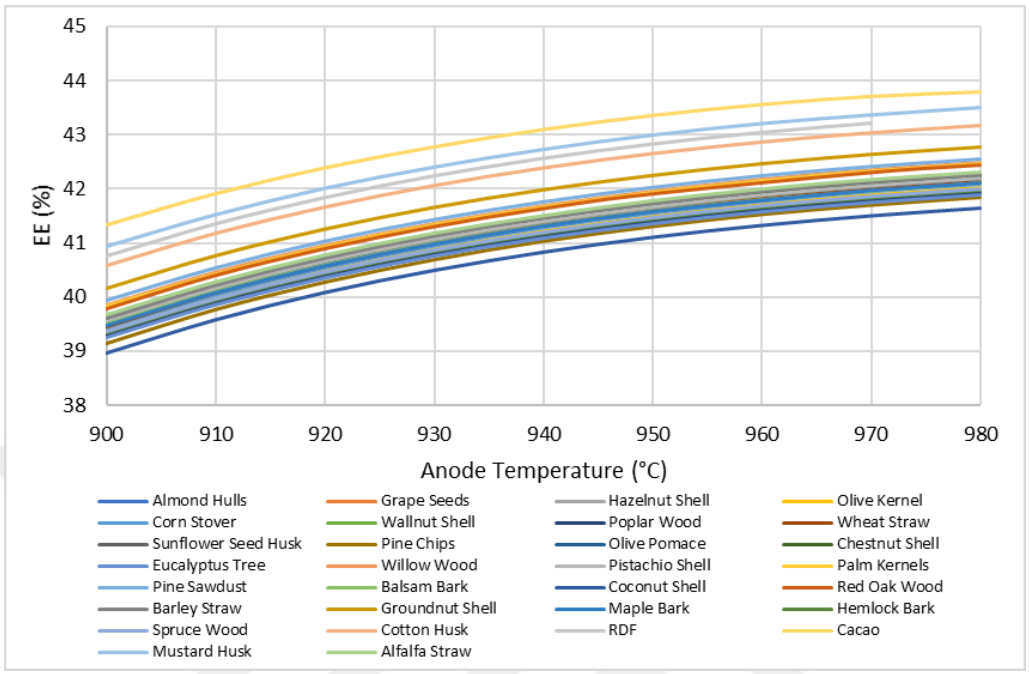
Figure 4.5 Effect of S/B ratio on SOFC

(a) EE, (b) V_{act}, (c) j, (d) biomass feed flow

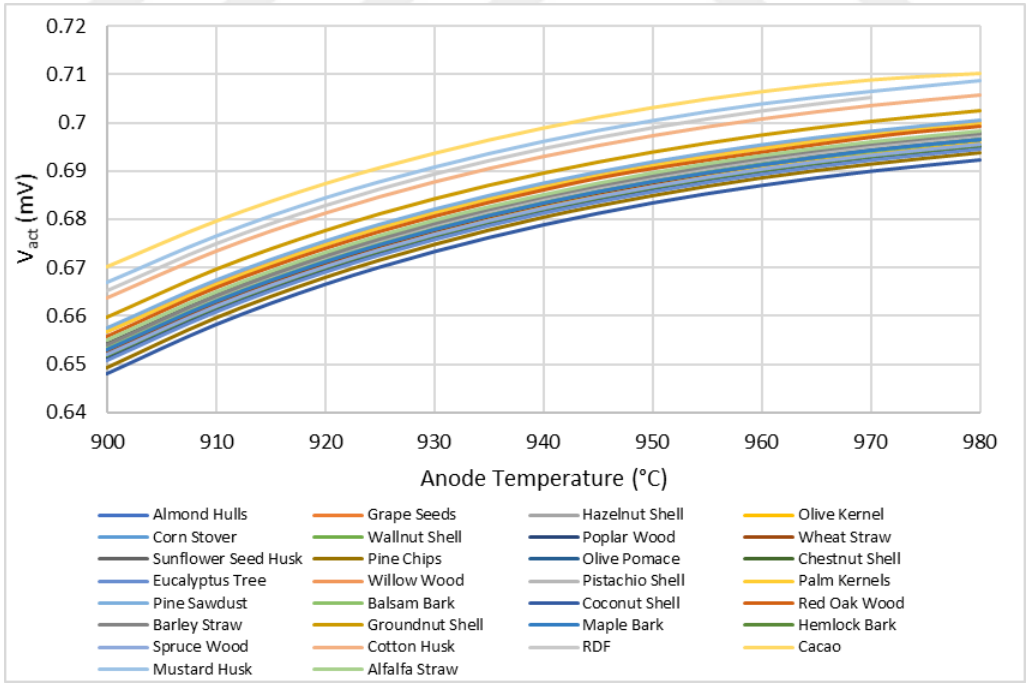
The impact of S/B ratio on the syngas composition was discussed above and results depicted that the H_2 and CO_2 concentrations increased in the syngas with increasing ratio. Even if there was insignificant drop in CH_4 concentration, it did not cause a negative impact on the performance of SOFC. Furthermore, increasing H_2 concentration almost 4-5% supported the electrochemical reactions in anode. The results presented in Figure 4.5. (b). illustrated that the V_{act} value increased related to the increase of the partial pressure of H_2 at the anode inlet. Due to the increased in V_{act}, the desired power generation (120 kW) was achieved with a lower amount of biomass and j accordingly as illustrated in Figure 4.5 (d). The lower amount of j provided a decrease in voltage losses that is also showed good impact on the V_{act}. Thus EE of SOFC increased for each sample and it raised above 42% for mustard husk, RDF and cacao samples particularly as depicted in Figure 4.5 (a). The obtained outputs showed similar manner with the literature [185].

4.3.5. Effect of Anode Temperature on SOFC

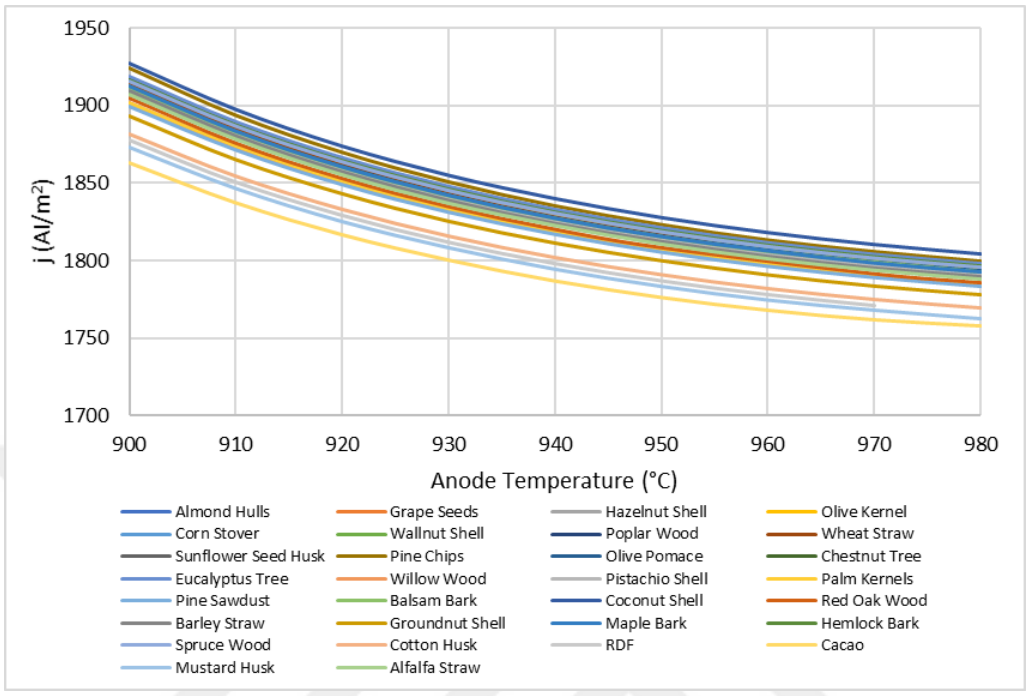
Anode is the main part that electrochemical reactions take place. The impact of anode operating temperature on the performance of the SOFC was investigated considering the reaction rate which highly affected by temperature. The anode operating temperature was changed between 900-980 °C, while the BFBG temperature and S/B ratio were kept constant at 800 and 0.5 respectively. To represent how anode temperature impacts EE, V_{act}, j and biomass feed flow as SOFC performance parameters, Figure 4.6 was plotted and illustrated their sensitivity to the temperature.


45
44
43
42
41
40
39
38
EE (%)
900
910
920
930
940
950
960
970
980
Anode Temperature (°C)
Almond Hulls
Grape Seeds
Hazelnut Shell
Olive Kernel
Corn Stover
Wallnut Shell
Poplar Wood
Wheat Straw
Sunflower Seed Husk
Pine Chips
Olive Pomace
Chestnut Shell
Eucalyptus Tree
Willow Wood
Pistachio Shell
Palm Kernels
Pine Sawdust
Balsam Bark
Coconut Shell
Red Oak Wood
Barley Straw
Groundnut Shell
Maple Bark
Hemlock Bark
Spruce Wood
Cotton Husk
RDF
Cacao
Mustard Husk
Alfalfa Straw

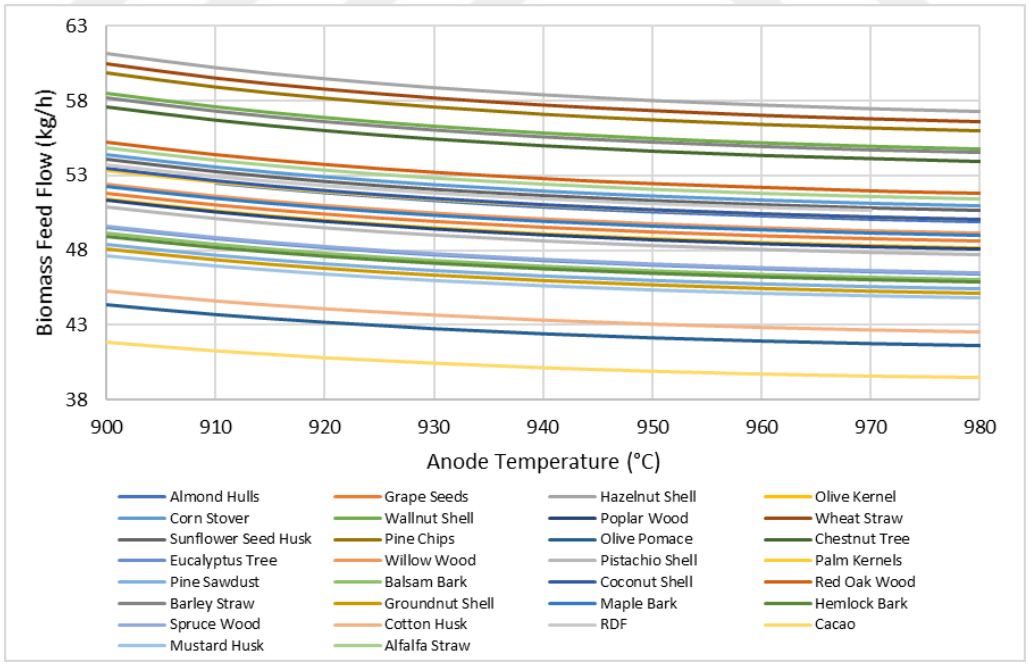
(a)


0.72
0.71
0.7
0.69
0.68
0.67
0.66
0.65
0.64
Vact (mV)
900
910
920
930
940
950
960
970
980
Anode Temperature (°C)
Almond Hulls
Grape Seeds
Hazelnut Shell
Olive Kernel
Corn Stover
Wallnut Shell
Poplar Wood
Wheat Straw
Sunflower Seed Husk
Pine Chips
Olive Pomace
Chestnut Shell
Eucalyptus Tree
Willow Wood
Pistachio Shell
Palm Kernels
Pine Sawdust
Balsam Bark
Coconut Shell
Red Oak Wood
Barley Straw
Groundnut Shell
Maple Bark
Hemlock Bark
Spruce Wood
Cotton Husk
RDF
Cacao
Mustard Husk
Alfalfa Straw

(b)



(c)



(d)

Figure 4.6 Effect of anode temperature on SOFC

(a) EE, (b) V_{act}, (c) j, (d) biomass feed flow

As depicted in Figure 4.6 (a) raising of the operating temperature of SOFC created a positive influence on the EE due to the increasing rate of the electrochemical reactions. The EE increased remarkably, between 2-3% for each biomass. The rising rate of the electrochemical reactions increased the O_2 flow into the anode part. The lower amount of j and biomass flow were found enough to reach 120 kW DCP as seen in Figure 4.6 (c) and (d). Thus, j value dropped with a parallel tendency to the required biomass feed flow. The decreasing amount of the biomass feed flow about 3-4 kg/h also influenced the voltage losses and EE at higher temperature. This increment in partial pressure of O_2 advanced the V_{act} value related to decreasing amount of j and voltage losses. Even though there was a substantial progress in SOFC performance with temperature increase, the SOFC that have high operating temperature needs to the more resistant material compared with the low temperature operation. Therefore, SOFC temperature should be optimized to reduce cost of high resistance material and maintain time.

4.4. ANN Model Results

4.4.1. Input Selection of the ANN Models

The conducted parametric studies showed that the operating parameters and selected biomass type remarkably influenced the overall system performance. It is very important to select the inputs among the parameters that affect the network significantly to create a suitable model. The input variables were determined in a wide range to develop generalized models. The chosen parameters that are O, C and H contents of biomass, S/B ratio and operating temperature of BFBG, operating temperature of SOFC anode and biomass feed flow can be seen with their ranges and increments in Table 4.5.

Table 4.5 Input parameters for the ANN model development

Parameter	Range	Increment
O Content (wt%)	31.47 – 45.61	-
H Content (wt%)	5.42 - 9.18	-
C Content (wt%)	40.75 – 54.70	-
Biomass Feed Flow (kg/h)	39.63 - 63.37	-
BFBG S/B Ratio	0.5-1.1	0.1
BFBG Temperature (°C)	700-900	25
SOFC Anode Temperature (°C)	900-980	10

The ranges for input parameters were determined considering suitable operating conditions for BFBG and SOFC. Biomass samples have different physicochemical characteristic as well as varying composition of O, C and H. The O, C and H contents of biomass samples were preferred from 31.47-45.61% for C, 40.75-54.70 for O and 5.42-9.18% for C to represent the comprehensive biomass ranges. The S/B ratio was changed between 0.5 and 1.1 with the increment of 0.1. The BFBG temperature range was selected among the 700-900 °C considering the reactions carry out in gasification. Moreover, anode operating temperature was increased from 900 to 980 °C with rise of 10 °C to create a realistic model. The range for the biomass flow rate was determined based on the data obtained from the simulation results. The value of biomass feed flow was adjusted to achieve 120 kW DCP for each operating condition. Simulations were run for constant O, C and H contents at varying S/B, BFBG and anode operating temperatures. A total of 15122 data sets were generated at the determined working conditions and biomass samples to be used in the ANN models.

Although sensitivity analysis showed that there is a correlation between input and output data sets, correlation matrix is a good and quick way to see the relations among them by visualizing as a heatmap. The correlation matrix was present in Figure 4.7 for input and output parameters of the ANN models using in this study. The color scheme was coded to indicate the positive, negative and zero correlations. Lowest negative correlations values (-1.0) were represented by black while highest positive correlation values (+1.0) colored by beige. A gradual coloring scale represented the values in between (-1.0 and +1.0) and zero

correlation was displayed as purple.

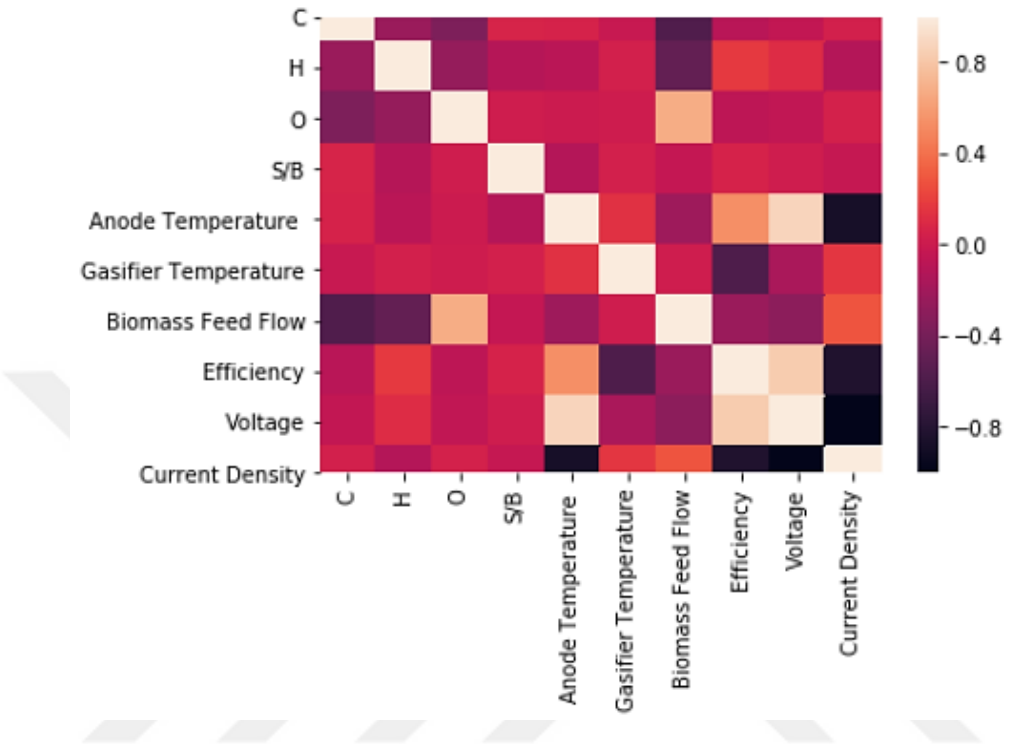


Figure 4.7 Correlation matrix for input and output parameters of the ANN models.

As illustrated in Figure 4.7, the correlation matrix displayed many significant correlations among the input and output parameters. It was observed that there was a negative correlation between the C and H content of the biomass and its feed flow rate, while there was a positive correlation between the O content. These results proved when using biomass samples with a high C and H content, a smaller amount of biomass is needed than those with a high O content. The correlation between O, C, H contents of biomass and EE, V_{act} and j values were represented by the colors which represent the zero and values close to it. This illustrates the nonlinear relationship between O, C, H as input parameters and EE, V_{act} and j values as output parameters. S/B ratio also showed the nonlinear relationship with each variable. Anode operating temperature and j were found in lowest negative correlation however it has a highest positive correlation with V_{act} and relatively high positive correlation with EE value. These correlation results showed a well consistency with the parametric studies which proved the positive effect of temperature increase on the EE and voltage and negative impact on the j (Section 4.3). The correlation between BFBG temperature and EE, V_{act} values demonstrated

a considerable negative while j has positive. The biomass feed flow has also high negative correlation with the EE and V_{act} values because low amount of voltage needs more biomass feed and system electrical efficiency decreases with flowing of more biomass. V_{act} and j value have lowest negative correlation because the rising of the j causes increment in voltage losses. Therefore, total V_{act} value drops with enhancing j value. As related to EE calculations (Eq. 3.35) higher voltage promotes the EE of the system, this relation proves the slightly positive correlation between them as seen in Figure 4.7. j and EE values was showed lowest negative relationship because higher amount of j means lower voltage as well as lower EE. As seen in correlation matrix most of the variables are not in a strong linear relationship that confirm the use of the ANN models to represent integrated system.

4.4.2. Structure of ANN Models

The sensitivity analysis results obtained from Aspen Plus simulations was used to create the ANN based models that predict EE, V_{act} and j values of the integrated BFBG-SOFC system individually. Design, training, test and validation processes of the models were performed in MATLAB R2021a using Neural Network Toolbox. The ANN architecture was created by connected input, output and hidden layers based on MLP structure. The dividing of data sets to use them for training, test and validation steps is one of the most important issues to create a powerful model. In this study, a total of 15122 datasets were randomly split for 55% training, 35% testing, and 10% validation to create each model. The FFBP training method with tangent sigmoid activation function was preferred to conduct training procedure. L-M algorithm was considered as a best optimizer due to its speed and reliability for convergence and selected to optimize networks. The layered structure was created with 7 neurons that represent the input variables of the ANNs in input layer, 8 neurons in hidden layer and one output for three different models as seen in Figure 4.8.

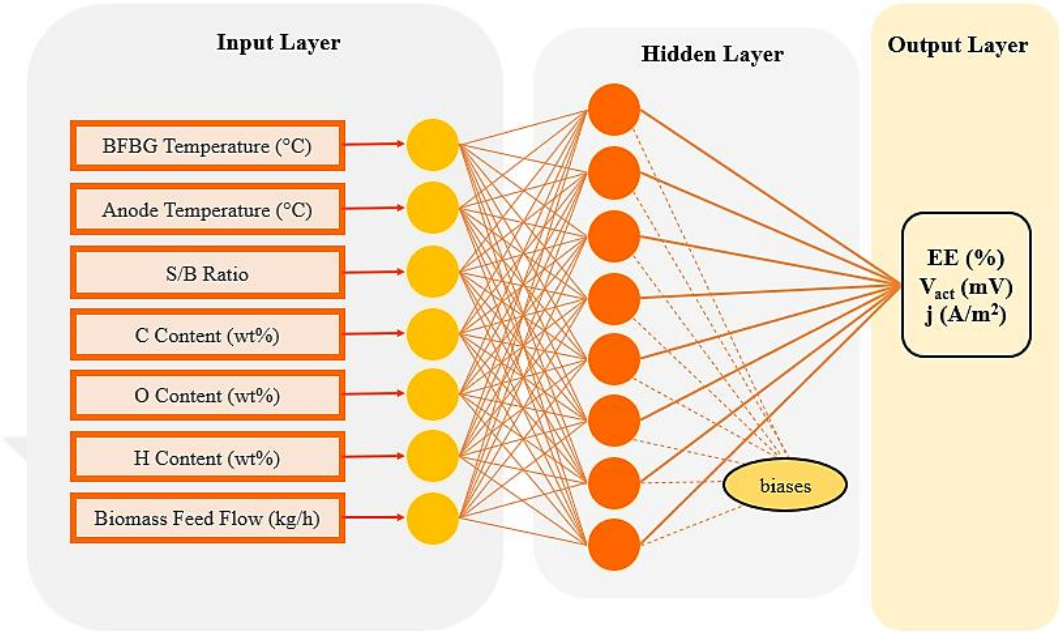


Figure 4.8 MLP structure of the developed ANN models

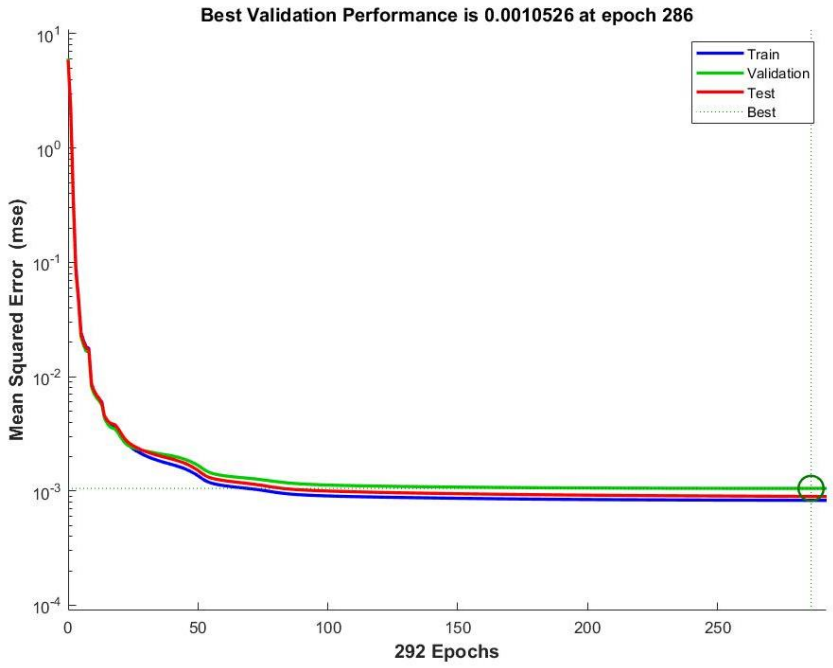
This neural network structure with 7, 8 and 1 neurons in input, hidden and output layers respectively were determined to be most suitable for prediction of the EE, V_{act} and j values. Data division, network structure, training and optimization algorithms were selected identical while epoch number was determined different for each ANN model. The specifications that belong to three different models were summarized in Table 4.6.

Table 4.6 Specifications of the ANN models

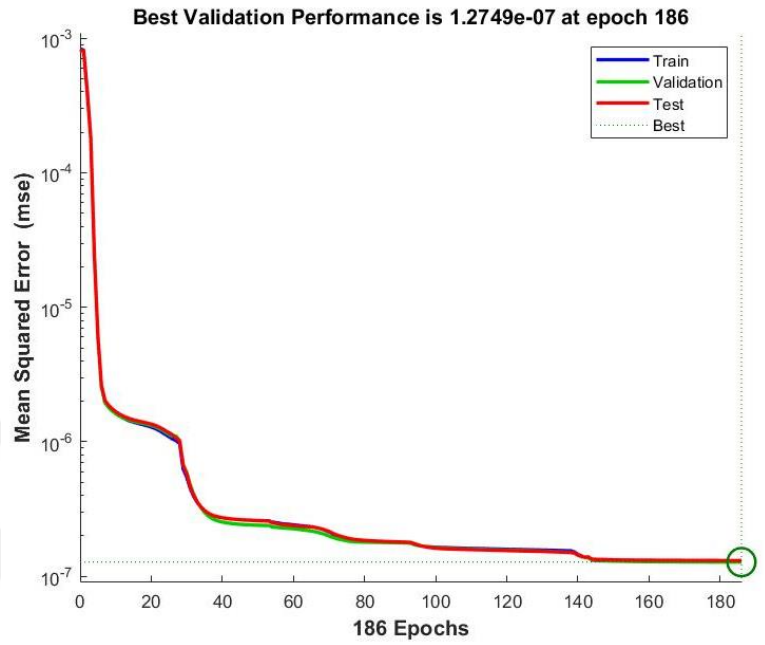
Properties	**Specification**
Number of neurons in the input layer	7
Number of neurons in the hidden layer	8
Number of neurons in the output layer	1
Network type and training algorithm	FFBP
Transfer function	Tangent sigmoid
Performance function	MSE
Optimization algorithm	L-M
Number of epochs (EE, V_{act}, j)	286, 186, 281
Size of data for each model	15122
Data division (training, test, validation), %	Random: 55, 35, 10

4.4.3. Performance Assessment of the ANN Models

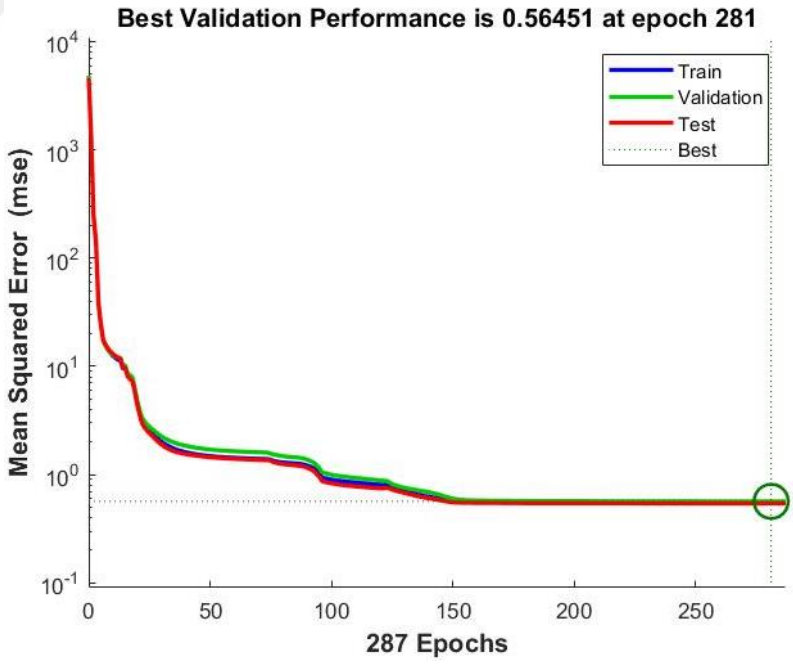
The hyperparameters of the ANN models was updated to acquire the minimum MSE values as the performance function for training, test and validation data sets. The models were trained with the randomly selected data then test and training sections were performed to evaluate the network performance using the data sets which have not seen in the training. Iterations were continued until the MSE values reaches minimum to obtain the predicted results at desired precision as seen in Figure 4.9 for each model.



(a)



(b)

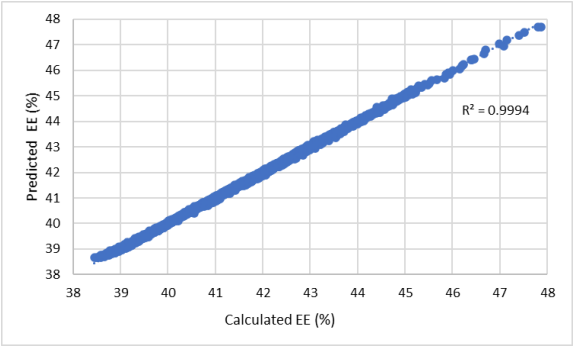


(c)

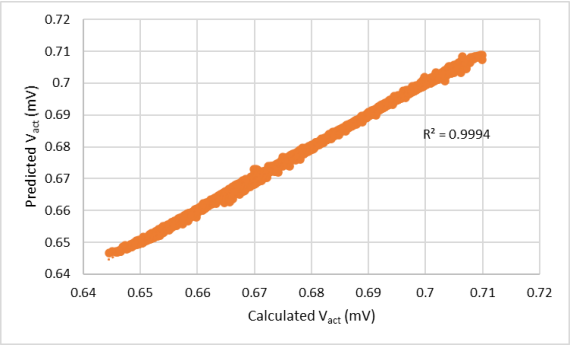
Figure 4.9 Performance analysis of training, test and validation data sets in terms of MSE (a) EE, (b) V_{act}, (c) j

Iterations were stopped at different epoch number because the models reached best fit with varying iteration number. As depicted in Figure 4.9 (a). the developed ANN model for EE prediction reaches the minimum error (0.0011) at epoch 286. After the best performance value was reached, the iterations were not continued any longer to prevent the over-fitting of the network. The MSE value was minimized as 1.2749×10^{-7} at epoch 186 for model that predicts V_{act} value of the integrated BFBG-SOFC system, can be seen in Figure 4.9 (b). The 0.5645 MSE value reached in 281 iterations proved that the estimation of j was successfully conducted using developed model as illustrated in Figure 4.9 (c). Likewise, the developed model for EE prediction, the iterations were finalized shortly after the reaching minimum MSE values for models developed for prediction of the V_{act} and j values as well. Drops in error values displayed the identical tendency for training, test and validation data sets. This consistent behavior proves that the models were well developed to perform the prediction processes successfully.

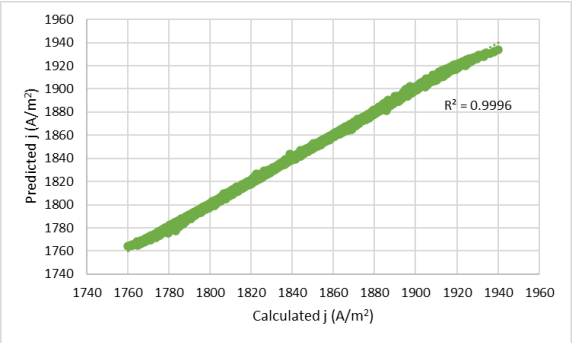
The R^2 value gives a correlation between estimated and real values. This method is commonly preferable to measure the prediction capability of the ANNs. For this study, the estimated and real values of EE, V_{act} and j values were compared and results were represented in Figures 4.10, 4.11 and 4.12 for the training, test and validation data sets respectively.



(a)



(b)



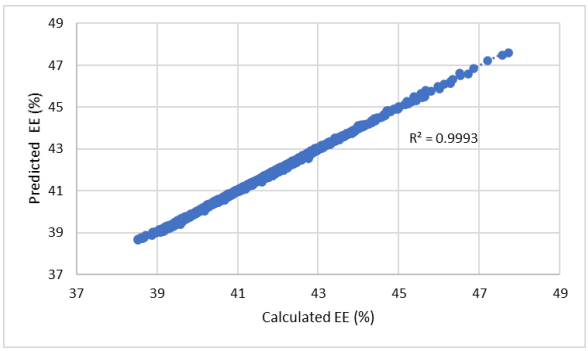
(c)

Figure 4.10 R^2 plot during ANN models training

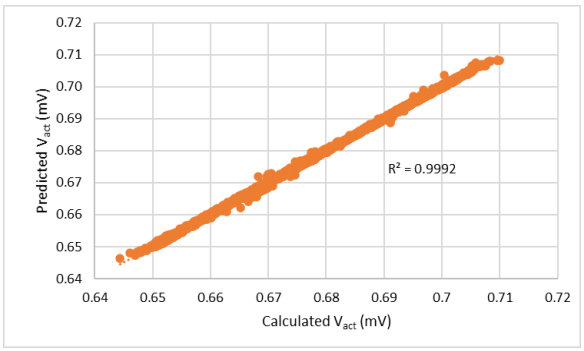
(a) EE, (b) V_{act}, (c) j

Results for training were represented with their respective R^2 for each model in Figure 4.12. The observed R^2 results illustrated that the networks were successfully estimated the EE, V_{act} and j values for the integrated BFBG-SOFC process during training. R^2 values were obtained greater than 0.999 for each model. It can be said that prediction capability of the models was proved in terms of R^2 for training processes.

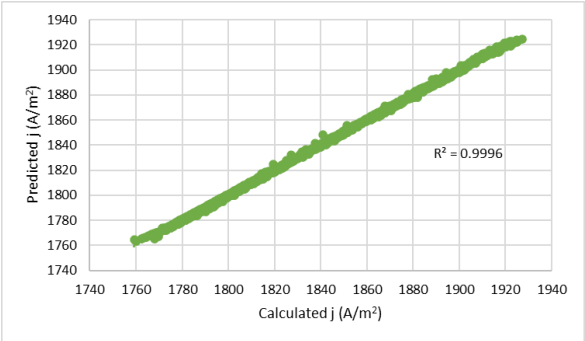
Although satisfying R^2 results were obtained for the training processes of the models, it is not adequate to prove that a generalized model has been created. Therefore, R^2 parameter was employed the analysis regression studies for test and validation processes as well.



(a)



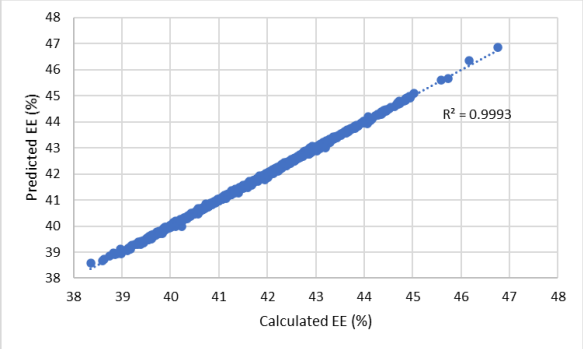
(b)

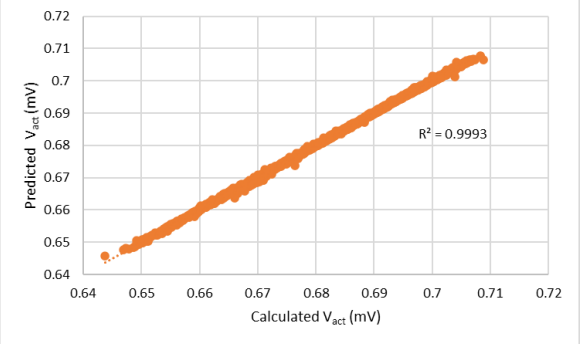


(c)

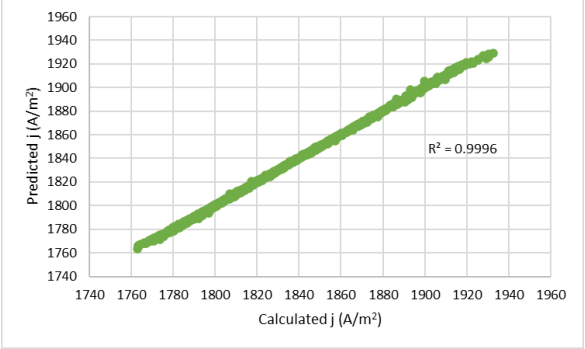
Figure 4.11 R^2 plot during ANN models testing

(a) EE, (b) V_{act}, (c) j





(a) (b)



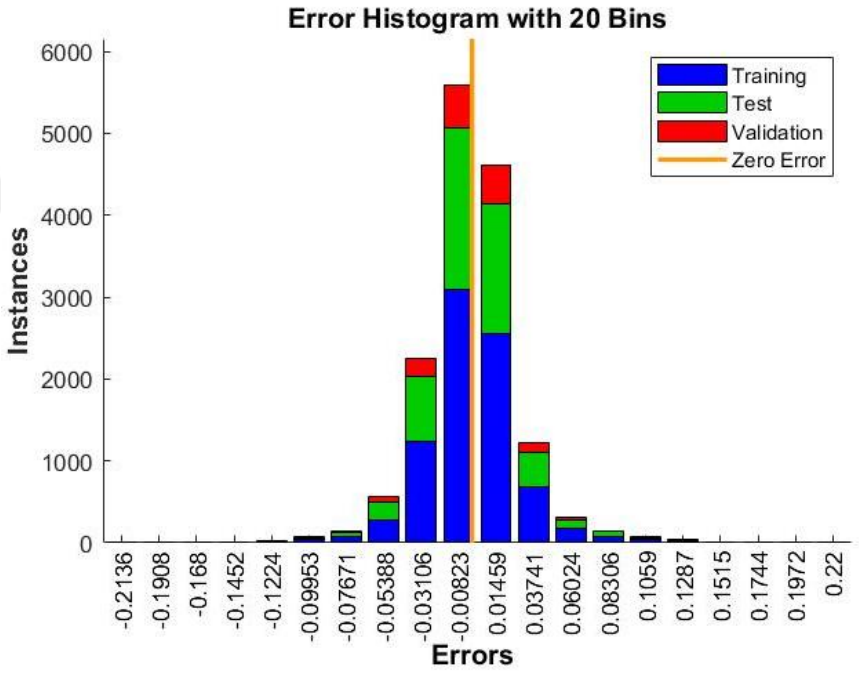
(c)

Figure 4.12 R^2 plot during ANN models validation

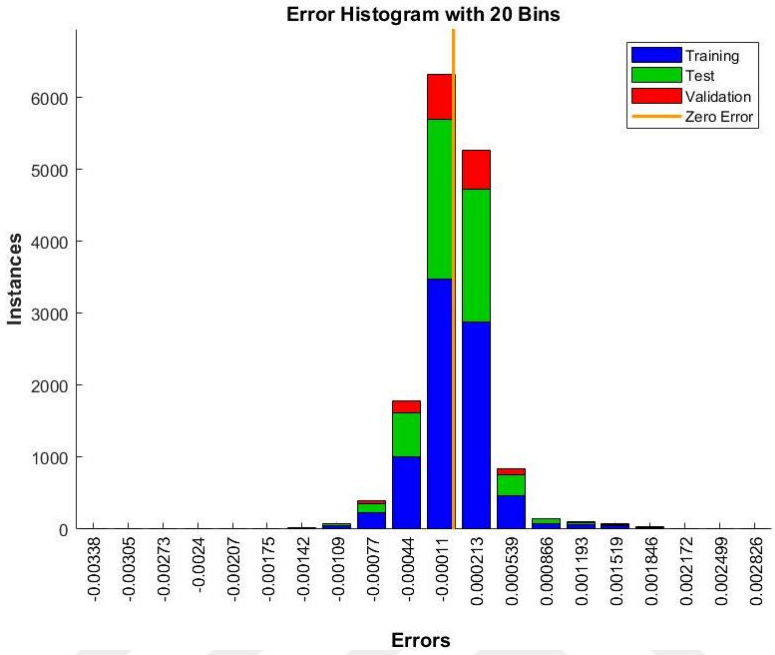
(a) EE, (b) V_{act}, (c) j

As depicted in Figure 4.11 and 4.12, R^2 between estimated and real values were found quite close to 1 for test and validation processes of each model. The fairly promising R^2 values from test (0.9993, 0.9992, 0.9996) and validation (0.9993, 0.9993, 0.9996) proved the high prediction accuracy of the models. The data sets showed homogeneous distributions around the trendlines for training, test and validation data sets of each model. This behavior shows that the model can establish consistent relationships between input and output parameters without memorizing. These results also showed that the established models well predicted the data sets have never been seen during the training without over-fitting.

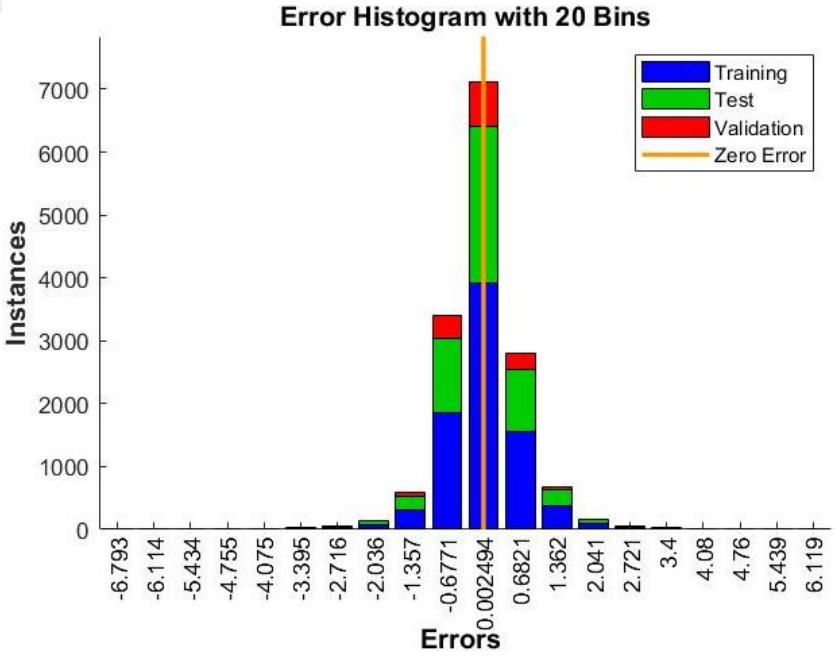
Moreover, the error between estimated and real values of EE, V_{act} and j were brought in Figure 4.13 as error histogram plots.



(a)



(b)



(c)

Figure 4.13 Error histogram plots

(a) EE, (b) V_{act}, (c) j

As seen in Figure 4.13. the error values displayed similar trend for training, test and validation data sets. The vertical bar numbers were determined as 20 on the histogram plot. The error values mostly collected around the zero error and the points close to it as depicted in Figure 4.13. The peak point of the error axis corresponds to zero. The prediction performance of each model is found trustworthy in convincing level.

The precision of estimation was also analyzed by applying statistical error evaluation terms that are ME, RMSE, MAPE and MRAE. The results of error evaluation in terms of four different statistical parameters were summarized in Table 4.7 for training, test and validation processes of each model.

Table 4.7 Error evaluation results

Parameters	Process	MAPE	RMSE	ME	MRAE
EE	**Training**	0.0484	0.0288	-0.0003	0.5830
	Test	0.0499	0.0299	-0.0011	0.1375
	Validation	0.0529	0.0324	-0.0007	0.1011
V_{act}	**Training**	0.0359	0.0004	8.41×10^{-7}	0.0786
	Test	0.0354	0.0004	0.6840	0.3852
	Validation	0.0352	0.0004	7.71×10^{-6}	0.0608
j	**Training**	0.0280	0.7395	-0.0026	0.0712
	Test	0.0280	0.7357	-0.0168	0.0552
	Validation	0.0278	0.7513	-0.0486	0.0950

The obtained error values were found very close to zero for training, test and validation data sets of each model. EE, V_{act} and j values were estimated with quite low errors, these results provide a confirmation for model prediction capability. Even though the system is complicated and influenced by many parameters, the ANN proved to be a powerful tool for modeling such systems. If the results are compared with the diverse applications that used ANN as a modeling tool, it was observed that the acquired results gave better outputs [186-190]. Thus, the obtained results indicated that the developed ANN models well represent the thermodynamic-based integrated BFBG-SOFC system.

5. CONCLUSION

Essential conclusions obtained from this thesis study are summarized as below:

- In this study, for the first time, a new integrated BFBG-SOFC model developed by using Aspen Plus.
- The developed thermodynamic based integrated BFBG-SOFC model was validated separately based on BFBG and SOFC with literature studies in Aspen Plus simulation environment successfully. Thus, the comprehensive data sets were generated from the Aspen Plus model, which obtained results compatible with the experimental data to train the ANN models.
- The effects of operating conditions on SOFC and BFBG performance were investigated in developed simulation model where 30 diverse biomass samples were used as fuel by performing the sensitivity analysis in Aspen Plus program.
- It was revealed from the evaluation of syngas composition under varying operating conditions that steam gasification in BFBG has well potential to produce high H_2 content syngas which can be proper fuel for SOFC.
- Raising of the operating temperature of SOFC created a positive influence on the EE due to the increasing rate of the electrochemical reactions. The EE increased remarkably, between 2-3% for each biomass.
- The increment in BFBG temperature created a negative impact on CH_4 concentration and accordingly EE, V_{act} and j values while the S/B ratio was increased the H_2 content substantially and EE for each sample and it rised above 42% for mustard husk, RDF and cacao samples particularly.
- The novel ANN models which developed to represent the integrated system estimated the EE, V_{act} and j values successfully. The results of the examination studies applied to measure the prediction capability of the models depicted that the developed ANN models are the effective tools to predict output parameters with good accuracy.
- The R^2 value was found to be greater than 0.999 for the training, testing and validation results of all models. Moreover, MAPE, RMSE, ME and MRAE which are the other statistical evaluation parameters, was obtained very close to zero.

- The ANN proved to be a powerful tool for modeling such complicated systems. Thus, the obtained results indicated that the developed ANN models well represent the thermodynamic-based integrated BFBG-SOFC system without to need any complex calculations and expensive simulation programs.

REFERENCES

[1] Indrawan, N. (2018) Advanced Biopower Generation Via Gasification of Biomass and Municipal Solid Waste. PhD Thesis, Oklahoma State University, Faculty of the Graduate College USA.

[2] Nhuchhen, D.R., Salam, P.A., (2012). Estimation of higher heating value of biomass from proximate analysis: A new approach. Fuel, 99, 55-63.

[3] Colpan, C.O. (2009) Thermal modeling of solid oxide fuel-cell based biomass gasification systems. PhD Thesis, Carleton University, Department of Mechanical and Aerospace Engineering, Ottawa, Ontario, Canada.

[4] Mahishi, M. (2006) Theoretical and experimental investigation of hydrogen production by gasification of biomass. PhD Thesis, University of Florida, USA.

[5] Shayan, E., Zare, V., Mirzaee, I., (2018). Hydrogen production from biomass gasification; a theoretical comparison of using different gasification agents. Energy conversión and management, 159, 30-41.

[6] Segurado, R., Pereira, S., Correia, D., Costa, M., (2019). Techno-economic analysis of a trigeneration system based on biomass gasification. Renewable and Sustainable Energy Reviews, 103, 501-514.

[7] Baruah, D., Baruah, D., (2014). Modeling of biomass gasification: A review. Renewable and Sustainable Energy Reviews, 39, 806-815.

[8] De Jong, W., Ünal, Ö., Andries, J., Hein, K., Spliethoff, H., (2003). Thermochemical conversion of brown coal and biomass in a pressurised fluidised bed gasifier with hot gas filtration using ceramic channel filters: measurements and gasifier modelling. Applied Energy, 74 (3-4), 425-437.

[9] Crocker, M., (2010). Thermochemical conversion of biomass to liquid fuels and chemicals, Royal Society of Chemistry, Cambridge.

[10] Guo, F., Dong, Y., Dong, L., Guo, C., (2014). Effect of design and operating parameters on the gasification process of biomass in a downdraft fixed bed: An experimental study. International Journal of Hydrogen Energy, 39 (11), 5625-5633.

[11] Abuadala, A., Dincer, I., Naterer, G.F., (2010). Exergy analysis of hydrogen production from biomass gasification. International Journal of Hydrogen Energy, 35 (10), 4981-4990.

[12] Basu, P., (2018). Biomass gasification, pyrolysis and torrefaction: practical design and theory, Third Edition, Academic press.

[13] Gómez-Barea, A., Leckner, B., (2010). Modeling of biomass gasification in fluidized bed. Progress in energy and combustion science, 36 (4), 444-509.

[14] Luque, R., Speight, J., (2014). Gasification for synthetic fuel production: fundamentals, processes and applications, Elsevier.

[15] O'hayre, R., Cha, S.-W., Colella, W., Prinz, F.B., (2016). Fuel cell fundamentals, Third Edition, John Wiley & Sons, New Jersey.

[16] Azizi, M.A. (2018) Solid Oxide Fuel Cell-Gas Turbine Hybrid Power Systems: Energy Analysis, Control Assessments, Fluid Dynamics Analysis and Dynamic Modeling for Stationary and Transportation Applications. PhD Thesis, University of California, Mechanical and Aerospace Engineering, Irvine, USA.

[17] Ahmed, T.Y., Ahmad, M.M., Yusup, S., Inayat, A., Khan, Z., (2012). Mathematical and computational approaches for design of biomass gasification for hydrogen production: A review. Renewable and Sustainable Energy Reviews, 16 (4), 2304-2315.

[18] Hauck, M., Herrmann, S., Spliethoff, H., (2017). Simulation of a reversible SOFC with Aspen Plus. International Journal of Hydrogen Energy, 42 (15), 10329-10340.

[19] Patra, T.K., Sheth, P.N., (2015). Biomass gasification models for downdraft gasifier: A state-of-the-art review. Renewable and Sustainable Energy Reviews, 50, 583-593.

[20] Ramos, A., Monteiro, E., Rouboa, A., (2019). Numerical approaches and comprehensive models for gasification process: A review. Renewable and Sustainable Energy Reviews, 110, 188-206.

[21] Ozonoh, M., Oboirien, B., Higginson, A., Daramola, M., (2020). Performance evaluation of gasification system efficiency using artificial neural network. Renewable Energy, 145, 2253-2270.

[22] Serrano, D., Golpour, I., Sánchez-Delgado, S., (2020). Predicting the effect of bed materials in bubbling fluidized bed gasification using artificial neural networks (ANNs) modeling approach. Fuel, 266, 117021.

[23] George, J., Arun, P., Muraleedharan, C., (2018). Assessment of producer gas composition in air gasification of biomass using artificial neural network model. International Journal of Hydrogen Energy, 43 (20), 9558-9568.

[24] Puig-Arnavat, M., Hernández, J.A., Bruno, J.C., Coronas, A., (2013). Artificial neural network models for biomass gasification in fluidized bed gasifiers. biomass and bioenergy, 49, 279-289.

[25] Baruah, D., Baruah, D., Hazarika, M., (2017). Artificial neural network based modeling of biomass gasification in fixed bed downdraft gasifiers. biomass and bioenergy, 98, 264-271.

[26] Dirbaz, M. (2020) A Neural Network Based Model for Biomass Gasification in Fluidized Bed. PhD Thesis, Illinois Institute of Technology, Department of Chemical and Biological Engineering, Chicago, Illinois, USA.

[27] Yu, J. (2018) Experimental and numerical investigation on tar production and recycling in fixed bed biomass gasifiers. Missouri University of Science and Technology, Chemical and Biochemical Engineering, USA.

[28] Matthew, O. (2019) Modeling and Simulation of Natural Gas Fired Quadruple Cycle for Power Generation. PhD Thesis, Catholic University of America, USA.

[29] Doherty, W., Reynolds, A., Kennedy, D., (2010). Computer simulation of a biomass gasification-solid oxide fuel cell power system using Aspen Plus. Energy, 35 (12), 4545-4555.

[30] Barelli, L., Bidini, G., Gallorini, F., Ottaviano, P., (2013). Design optimization of a SOFC-based CHP system through dynamic analysis. International Journal of Hydrogen Energy, 38 (1), 354-369.

[31] Min, G., Park, Y.J., Hong, J., (2020). 1D thermodynamic modeling for a solid oxide fuel cell stack and parametric study for its optimal operating conditions. Energy conversión and management, 209, 112614.

[32] Lin, Y., Ma, X., Yu, Z., Cao, Y., (2014). Investigation on thermochemical behavior of co-pyrolysis between oil-palm solid wastes and paper sludge. Bioresource technology, 166, 444-450.

[33] Sansaniwal, S., Pal, K., Rosen, M., Tyagi, S., (2017). Recent advances in the development of biomass gasification technology: A comprehensive review. Renewable and Sustainable Energy Reviews, 72, 363-384.

[34] Rahib, Y., Boushaki, T., Sarh, B., Chaoufi, J., (2021). Combustion and pollutant emission characteristics of argan nut shell (ANS) biomass. Fuel Processing Technology, 213, 106665.

[35] Safarian, S., Saryazdi, S.M.E., Unnthorsson, R., Richter, C., (2020). Artificial neural network integrated with thermodynamic equilibrium modeling of downdraft biomass gasification-power production plant. Energy, 213, 118800.

[36] Siedlecki, M., De Jong, W., Verkooijen, A.H., (2011). Fluidized bed gasification as a mature and reliable technology for the production of bio-syngas and applied in the production of liquid transportation fuels—a review. Energies, 4 (3), 389-434.

[37] Safarian, S., Unnthorsson, R., Richter, C., (2020). Performance analysis and environmental assessment of small-scale waste biomass gasification integrated CHP in Iceland. Energy, 197, 117268.

[38] Pala, L.P.R., Wang, Q., Kolb, G., Hessel, V., (2017). Steam gasification of biomass with subsequent syngas adjustment using shift reaction for syngas production: An Aspen Plus model. Renewable Energy, 101, 484-492.

[39] Das, S., Lee, S.-H., Kumar, P., Kim, K.-H., Lee, S.S., Bhattacharya, S.S., (2019). Solid waste management: Scope and the challenge of sustainability. Journal of Cleaner Production, 228, 658-678.

[40] Diyoke, C., Gao, N., Aneke, M., Wang, M., Wu, C., (2018). Modelling of down-draft gasification of biomass–An integrated pyrolysis, combustion and reduction process. Applied Thermal Engineering, 142, 444-456.

[41] Siwal, S.S., Zhang, Q., Sun, C., Thakur, S., Gupta, V.K., Thakur, V.K., (2020). Energy production from steam gasification processes and parameters that contemplate in biomass gasifier–A review. Bioresource technology, 297, 122481.

[42] Mountouris, A., Voutsas, E., Tassios, D., (2006). Solid waste plasma gasification: Equilibrium model development and exergy analysis. Energy conversión and management, 47 (13-14), 1723-1737.

[43] Ruiz, J.A., Juárez, M., Morales, M., Muñoz, P., Mendívil, M., (2013). Biomass gasification for electricity generation: Review of current technology barriers. Renewable and Sustainable Energy Reviews, 18, 174-183.

[44] Foscolo, P.U., Germanà, A., Jand, N., Rapagnà, S., (2007). Design and cold model testing of a biomass gasifier consisting of two interconnected fluidized beds. Powder Technology, 173 (3), 179-188.

[45] Schuster, G., Löffler, G., Weigl, K., Hofbauer, H., (2001). Biomass steam gasification–an extensive parametric modeling study. Bioresource technology, 77 (1), 71-79.

[46] Hosseini, M., Dincer, I., Rosen, M.A., (2012). Steam and air fed biomass gasification: comparisons based on energy and exergy. International Journal of Hydrogen Energy, 37 (21), 16446-16452.

[47] Udomsirichakorn, J., Salam, P.A., (2014). Review of hydrogen-enriched gas production from steam gasification of biomass: the prospect of CaO-based chemical looping gasification. Renewable and Sustainable Energy Reviews, 30, 565-579.

[48] Iliuta, I., Leclerc, A., Larachi, F., (2010). Allothermal steam gasification of biomass in cyclic multi-compartment bubbling fluidized-bed gasifier/combustor–New reactor concept. Bioresource technology, 101 (9), 3194-3208.

[49] Kaur, R., Gera, P., Jha, M.K., Bhaskar, T., (2019). Biohydrogen, Thermochemical route for biohydrogen production, Elsevier, 187-218.

[50] Baskar, C., Baskar, S., Dhillon, R.S., (2012). Biomass conversion: The interface of biotechnology, chemistry and materials science, Springer Science & Business Media,

[51] Monteiro, E., Ismail, T.M., Ramos, A., Abd El-Salam, M., Brito, P., Rouboa, A., (2018). Experimental and modeling studies of Portuguese peach stone gasification on an autothermal bubbling fluidized bed pilot plant. Energy, 142, 862-877.

[52] Basu, P., (2010). Biomass gasification and pyrolysis: practical design and theory, Academic press.

[53] Couto, N., Rouboa, A., Silva, V., Monteiro, E., Bouziane, K., (2013). Influence of the biomass gasification processes on the final composition of syngas. Energy Procedia, 36, 596-606.

[54] Molino, A., Chianese, S., Musmarra, D., (2016). Biomass gasification technology: The state of the art overview. Journal of Energy Chemistry, 25 (1), 10-25.

[55] Ptasinski, K.J., (2016). Efficiency of biomass energy: an exergy approach to biofuels, power, and biorefineries, John Wiley & Sons.

[56] Brown, R.C., (2019). Thermochemical processing of biomass: conversion into fuels, chemicals and power, John Wiley & Sons.

[57] Benedikt, F., Kuba, M., Schmid, J.C., Müller, S., Hofbauer, H., (2019). Assessment of correlations between tar and product gas composition in dual fluidized bed steam gasification for online tar prediction. Applied Energy, 238, 1138-1149.

[58] Loha, C., Gu, S., De Wilde, J., Mahanta, P., Chatterjee, P.K., (2014). Advances in mathematical modeling of fluidized bed gasification. Renewable and Sustainable Energy Reviews, 40, 688-715.

[59] Seo, M.W., Goo, J.H., Kim, S.D., Lee, S.H., Choi, Y.C., (2010). Gasification characteristics of coal/biomass blend in a dual circulating fluidized bed reactor. Energy & Fuels, 24 (5), 3108-3118.

[60] Kumar, K.V., Bharath, M., Raghavan, V., Prasad, B., Chakravarthy, S., Sundararajan, T., (2017). Gasification of high-ash Indian coal in bubbling fluidized bed using air and steam–An experimental study. Applied Thermal Engineering, 116, 372-381.

[61] Pio, D., Tarelho, L., Matos, M., (2017). Characteristics of the gas produced during biomass direct gasification in an autothermal pilot-scale bubbling fluidized bed reactor. Energy, 120, 915-928.

[62] Hwang, I.S., Sohn, J., Do Lee, U., Hwang, J., (2021). CFD-DEM simulation of air-blown gasification of biomass in a bubbling fluidized bed gasifier: Effects of equivalence ratio and fluidization number. Energy, 219, 119533.

[63] Pio, D., Tarelho, L., Pinto, R., Matos, M., Frade, J., Yaremchenko, A., et al., (2018). Low-cost catalysts for in-situ improvement of producer gas quality during direct gasification of biomass. Energy, 165, 442-454.

[64] de Souza-Santos, M.L., (2010). Solid fuels combustion and gasification: modeling, simulation, CRC Press, USA.

[65] Zennaro, R., Ricci, M., Bua, L., Querci, C., Carnelli, L., d'Arminio Monforte, A., (2013). Syngas: The Basis of Fischer–Tropsch. Greener Fischer-Tropsch Processes for Fuels and Feedstocks, 17-51.

[66] Halama, S., Spliethoff, H., (2016). Reaction Kinetics of Pressurized Entrained Flow Coal Gasification: Computational Fluid Dynamics Simulation of a 5 MW Siemens Test Gasifier. Journal of Energy Resources Technology, 138 (4).

[67] Liao, L., Zheng, J., Zhang, Y., Li, C., Yuan, C., (2021). Impact of torrefaction on entrained-flow gasification of pine sawdust: An experimental investigation. Fuel, 289, 119919.

[68] Hall, J., Kerr, R., (2003). Innovation dynamics and environmental technologies: the emergence of fuel cell technology. Journal of Cleaner Production, 11 (4), 459-471.

[69] Stambouli, A.B., Traversa, E., (2002). Solid oxide fuel cells (SOFCs): a review of an environmentally clean and efficient source of energy. Renewable and Sustainable Energy Reviews, 6 (5), 433-455.

[70] Flores, J.J.A., Rodríguez, M.L.Á., Vera, J.V.A., Quiñones, J.G.R., Martínez, S.J.G., Zarraga, R.A., (2021). Advances in the knowledge of the double perovskites derived from

the conformation and substitution of the material Sr2MgMoO6-δ as anode with potential application in SOFC cell. International Journal of Hydrogen Energy, In-press.

[71] Stambouli, A.B., Traversa, E., (2002). Fuel cells, an alternative to standard sources of energy. Renewable and Sustainable Energy Reviews, 6 (3), 295-304.

[72] Staffell, I., Scamman, D., Abad, A.V., Balcombe, P., Dodds, P.E., Ekins, P., et al., (2019). The role of hydrogen and fuel cells in the global energy system. Energy & Environmental Science, 12 (2), 463-491.

[73] Yuksel, Y.E., Ozturk, M., Dincer, I., (2020). Performance investigation of a combined biomass gasifier-SOFC plant for compressed hydrogen production. International Journal of Hydrogen Energy, 45 (60), 34679-34694.

[74] Ghorbani, B., Mehrpooya, M., Mousavi, S.A., (2019). Hybrid molten carbonate fuel cell power plant and multiple-effect desalination system. Journal of Cleaner Production, 220, 1039-1051.

[75] Benveniste, G., Pucciarelli, M., Torrell, M., Kendall, M., Tarancon, A., (2017). Life Cycle Assessment of microtubular solid oxide fuel cell based auxiliary power unit systems for recreational vehicles. Journal of Cleaner Production, 165, 312-322.

[76] Sengodan, S., Choi, S., Jun, A., Shin, T.H., Ju, Y.-W., Jeong, H.Y., et al., (2015). Layered oxygen-deficient double perovskite as an efficient and stable anode for direct hydrocarbon solid oxide fuel cells. Nature materials, 14 (2), 205-209.

[77] Zeng, Z., Qian, Y., Zhang, Y., Hao, C., Dan, D., Zhuge, W., (2020). A review of heat transfer and thermal management methods for temperature gradient reduction in solid oxide fuel cell (SOFC) stacks. Applied Energy, 280, 115899.

[78] Singhal, S.C., (2002). Solid oxide fuel cells for stationary, mobile, and military applications. Solid State Ionics, 152, 405-410.

[79] Meadowcroft, A.D., Howroyd, S., Kendall, K., Kendall, M., (2013). Testing micro-tubular SOFCs in unmanned air vehicles (UAVs). ECS Transactions, 57 (1), 451.

[80] Fernandes, M., Andrade, S.d.P., Bistritzki, V., Fonseca, R., Zacarias, L., Gonçalves, H., et al., (2018). SOFC-APU systems for aircraft: A review. International Journal of Hydrogen Energy, 43 (33), 16311-16333.

[81] Liu, Y., Shao, Z., Mori, T., (2021). Development of nickel based cermet anode materials in solid oxide fuel cells–Now and future. Materials Reports: Energy, 1 (1), 100003.

[82]http://www.nrel.gov/rredc/biomass_resource.html.

[83] Ramadhani, F., Hussain, M.A., Mokhlis, H., Hajimolana, S., (2017). Optimization strategies for Solid Oxide Fuel Cell (SOFC) application: A literature survey. Renewable and Sustainable Energy Reviews, 76, 460-484.

[84] Akkaya, A.V., (2007). Electrochemical model for performance analysis of a tubular SOFC. International journal of energy research, 31 (1), 79-98.

[85] Dollard, W., (1992). Solid oxide fuel cell developments at Westinghouse. Journal of power sources, 37 (1-2), 133-139.

[86] Tu, B., Wen, H., Yin, Y., Zhang, F., Su, X., Cui, D., et al., (2020). Thermodynamic analysis and experimental study of electrode reactions and open circuit voltages for methane-fuelled SOFC. International Journal of Hydrogen Energy, 45 (58), 34069-34079.

[87] Zheng, J., Zhu, H., Li, W., Ma, Z., Ou, X., Fan, Y., et al., (2021). Numerical study on the electron-blocking effect and optimized operation parameters of ceria-SOFCs with the pure Sm doping CeO2 electrolyte. International Journal of Hydrogen Energy, 46 (24), 13318-13329.

[88] Rosli, A., Somalu, M., Osman, N., Hamid, N., (2021). Physical characterization of LSCF-NiO as cathode material for intermediate temperature solid oxide fuel cell (IT-SOFCs). Materials Today: Proceedings.

[89] Ghaffarpour, Z., Mahmoudi, M., Mosaffa, A., Farshi, L.G., (2018). Thermoeconomic assessment of a novel integrated biomass based power generation system including gas turbine cycle, solid oxide fuel cell and Rankine cycle. Energy conversión and management, 161, 1-12.

[90] Colpan, C.O., Dincer, I., Hamdullahpur, F., (2007). Thermodynamic modeling of direct internal reforming solid oxide fuel cells operating with syngas. International Journal of Hydrogen Energy, 32 (7), 787-795.

[91] Gadsbøll, R.Ø., Thomsen, J., Bang-Møller, C., Ahrenfeldt, J., Henriksen, U.B., (2017). Solid oxide fuel cells powered by biomass gasification for high efficiency power generation. Energy, 131, 198-206.

[92] Mazaheri, N., Akbarzadeh, A., Madadian, E., Lefsrud, M., (2019). Systematic review of research guidelines for numerical simulation of biomass gasification for bioenergy production. Energy conversion and management, 183, 671-688.

[93] Strezov, V., Anawar, H.M., (2019). Renewable Energy Systems from Biomass, CRC Press.

[94] Shabbar, S., Janajreh, I., (2013). Thermodynamic equilibrium analysis of coal gasification using Gibbs energy minimization method. Energy conversión and management, 65, 755-763.

[95] Singh, D.K., Tirkey, J.V., (2021). Modeling and multi-objective optimization of variable air gasification performance parameters using Syzygium cumini biomass by integrating ASPEN Plus with Response surface methodology (RSM). International Journal of Hydrogen Energy, 46 (36), 18816-18831.

[96] Islam, M.W., (2020). Effect of different gasifying agents (steam, H2O2, oxygen, CO2, and air) on gasification parameters. International Journal of Hydrogen Energy, 45 (56), 31760-31774.

[97] Doherty, W. (2014) Modelling of biomass gasification integrated with a solid oxide fuel cell system. PhD Thesis, Technological University Dublin, School of Mechanical and Design Engineering, Dublin.

[98] Dharwal, R., Kaur, L., (2016). Applications of artificial neural networks: a review. Indian J Sci Technol, 9 (47), 1-8.

[99] Rahman, M.M., Charoenlarpnopparut, C., Suksompong, P., (Year). Classification and pattern recognition algorithms applied to E-Nose. IEEE, 2015 2nd International Conference on Electrical Information and Communication Technologies (EICT), 44-48.

[100] Pannu, A., (2015). Artificial intelligence and its application in different areas. Artificial Intelligence, 4 (10), 79-84.

[101] Gardner, M.W., Dorling, S., (1998). Artificial neural networks (the multilayer perceptron)—a review of applications in the atmospheric sciences. Atmospheric environment, 32 (14-15), 2627-2636.

[102] Theodoridis, S., (2015). Neural networks and deep learning. Machine Learning, 875-936.

[103] Kermani, B.G., Schiffman, S.S., Nagle, H.T., (2005). Performance of the Levenberg–Marquardt neural network training method in electronic nose applications. Sensors and Actuators B: Chemical, 110 (1), 13-22.

[104] Okolie, J.A., Epelle, E.I., Nanda, S., Castello, D., Dalai, A.K., Kozinski, J.A., (2021). Modeling and process optimization of hydrothermal gasification for hydrogen production: A comprehensive review. The Journal of Supercritical Fluids, 105199.

[105] Kartal, F., Özveren, U., (2020). A deep learning approach for prediction of syngas lower heating value from CFB gasifier in Aspen plus®. Energy, 209, 118457.

[106] Sezer, S., Özveren, U., (2021). Investigation of syngas exergy value and hydrogen concentration in syngas from biomass gasification in a bubbling fluidized bed gasifier by using machine learning. International Journal of Hydrogen Energy, 46 (39), 20377-20396.

[107] Milewski, J., Świrski, K., (2009). Modelling the SOFC behaviours by artificial neural network. International Journal of Hydrogen Energy, 34 (13), 5546-5553.

[108] Cao, L., Iris, K., Xiong, X., Tsang, D.C., Zhang, S., Clark, J.H., et al., (2020). Biorenewable hydrogen production through biomass gasification: A review and future prospects. Environmental research, 186, 109547.

[109] Küçük, M., Demirbaş, A., (1997). Biomass conversion processes. Energy conversión and management, 38 (2), 151-165.

[110] McKendry, P., (2002). Energy production from biomass (part 1): overview of biomass. Bioresource technology, 83 (1), 37-46.

[111] Xu, S., Chen, J., Peng, H., Leng, S., Li, H., Qu, W., et al., (2021). Effect of biomass type and pyrolysis temperature on nitrogen in biochar, and the comparison with hydrochar. Fuel, 291, 120128.

[112] Wang, F., Ouyang, D., Zhou, Z., Page, S.J., Liu, D., Zhao, X., (2021). Lignocellulosic biomass as sustainable feedstock and materials for power generation and energy storage. Journal of Energy Chemistry, 57, 247-280.

[113] Ehite, E.H., Drumm, E., Abdoulmoumine, N., (2021). The effect of hemicellulose on the interparticle frictional behavior of lignocellulosic biomass particulates. Particuology, 55, 16-22.

[114] Zhang, L., Yang, Z., Li, S., Wang, X., Lin, R., (2020). Comparative study on the two-step pyrolysis of different lignocellulosic biomass: Effects of components. Journal of Analytical and Applied Pyrolysis, 152, 104966.

[115] Wong, W.-Y., Lim, S., Pang, Y.-L., Shuit, S.-H., Chen, W.-H., Lee, K.-T., (2020). Synthesis of renewable heterogeneous acid catalyst from oil palm empty fruit bunch for glycerol-free biodiesel production. Science of The Total Environment, 727, 138534.

[116] Obernberger, I., Brunner, T., Bärnthaler, G., (2006). Chemical properties of solid biofuels—significance and impact. biomass and bioenergy, 30 (11), 973-982.

[117] Garcia-Perez, M., Chaala, A., Pakdel, H., Kretschmer, D., Roy, C., (2007). Vacuum pyrolysis of softwood and hardwood biomass: comparison between product yields and bio-oil properties. Journal of Analytical and Applied Pyrolysis, 78 (1), 104-116.

[118] Miles, T.R., Miles Jr, T., Baxter, L., Bryers, R., Jenkins, B., Oden, L. (1995) Alkali deposits found in biomass power plants: A preliminary investigation of their extent and nature. Volume 1. Thesis University, Academic Department.

[119] Results from EC project SEFCO, 2004, https://phyllis.nl/Browse/Standard/ECN-Phyllis#2736.

[120] Dogru, M., Howarth, C., Malik, A., Olgun, H., (1999). Use of bio-nut shells for gasification. U.S. Department of Energy Office of Scientific and Technical Information, 4 biomass conference of the Americas, Oakland,USA, 1051-1057.

[121] Koukios, E., Arvelakis, S., Georgali, B., (1999). Physico-chemical upgrading of agroresidues as solid biofuels. U.S. Department of Energy Office of Scientific and Technical Information, 4 biomass conference of the Americas, Oakland, USA, 299-304.

[122] Magasiner, N., de Kock, J., (1987). Design criteria for fibrous fuel fired boilers. Energy world (Monthly), (150), 4-12.

[123] Masiá, A.T., Buhre, B., Gupta, R., Wall, T., (2007). Characterising ash of biomass and waste. Fuel Processing Technology, 88 (11-12), 1071-1081.

[124] EU H2020 project Biofficiency, 2019, https://phyllis.nl/Browse/Standard/ECN-Phyllis#3586.

[125] Safarian, S., Saryazdi, S.M.E., Unnthorsson, R., Richter, C., (2020). Dataset of biomass characteristics and net output power from downdraft biomass gasifier integrated power production unit. Data in brief, 33, 106390.

[126] Barducci, G., Daddi, P., Polzinetti, G., (1995). Thermic and electric power production and use from gasification of biomass and RDF: Experience at CFBG plant at Greve in Chianti. National Renewable Energy Lab., Golden, CO (United States), 2 meeting on biomass of the Americas, Portland, OR, USA.

[127] Evans, R., Knight, R., Onischak, M., Babu, S., (1988). Development of biomass gasification to produce substitute fuels. Pacific Northwest Lab., Richland, WA (USA), USA.

[128] Ghaly, A., Ergüdenler, A., Laufer, E., (1993). Agglomeration characteristics of alumina sand-straw ash mixtures at elevated temperatures. biomass and bioenergy, 5 (6), 467-480.

[129] Kurkela, E., (1996). Formation and removal of biomass-derived contaminants in fluidized-bed gasification processes. Technical Research Centre of Finland, Espoo (Finland), Finland, 135.

[130] Illerup, J.B., Rathmann, O., (1996). CO2 gasification of wheat straw, barley straw, willow and giganteus, 873(EN), Forskningscenter Risoe. Risoe-R, Denmark.

[131] García, R., Pizarro, C., Lavín, A.G., Bueno, J.L., (2012). Characterization of Spanish biomass wastes for energy use. Bioresource technology, 103 (1), 249-258.

[132] Ries, M. (2017) Environmental and Economic Impacts of Small-Scale Biomass Gasification. Master Thesis, UNIVERSITY OF MINNESOTA, USA.

[133] Doherty, W., Reynolds, A., Kennedy, D., (2009). The effect of air preheating in a biomass CFB gasifier using ASPEN Plus simulation. biomass and bioenergy, 33 (9), 1158-1167.

[134] Lv, P., Chang, J., Xiong, Z., Huang, H., Wu, C., Chen, Y., et al., (2003). Biomass air− steam gasification in a fluidized bed to produce hydrogen-rich gas. Energy & Fuels, 17 (3), 677-682.

[135] Cheung, M., (2004). Modelling of the Nickel and Cobalt Kinetics During Pressure Acid Leaching of Laterites Using Aspen Plus 11.1 TM and OLI, University of Toronto.

[136] Watanasiri, S., Anavi, S., Wadsley, M.W., (1993). Modeling metallurgical processes using a chemical-engineering simulator. Fluid phase equilibria, 82, 55-62.

[137] Zhu, T.A. (2021) Aspen Plus Model Simulation and Financial Analysis of Pyrrhotite Processing Technology Options. Master Thesis, University of Toronto, Department of Chemical Engineering, Canada.

[138] Melgar, A., Pérez, J.F., Laget, H., Horillo, A., (2007). Thermochemical equilibrium modelling of a gasifying process. Energy conversion and management, 48 (1), 59-67.

[139] Freitas, A.C., Guirardello, R., (2014). Comparison of several glycerol reforming methods for hydrogen and syngas production using Gibbs energy minimization. International Journal of Hydrogen Energy, 39 (31), 17969-17984.

[140] Mojaver, P., Jafarmadar, S., Khalilarya, S., Chitsaz, A., (2020). Investigation and optimization of a Co-Generation plant integrated of gasifier, gas turbine and heat pipes using

minimization of Gibbs free energy, Lagrange method and response surface methodology. International Journal of Hydrogen Energy, 45 (38), 19027-19044.

[141] Braun, R.J. (2002) Optimal design and operation of solid oxide fuel cell systems for small-scale stationary applications. PhD Thesis, University of Wisconsin, Mechanical Engineering, Madison, USA.

[142] Mu, L. (2010) Detailed fuel cell modeling for coal-based integrated gasification fuel cell system design and analysis. PhD Thesis, University of California, Mechanical and Aerospace Engineering, Irvine.

[143] Dey, T., Singdeo, D., Pophale, A., Bose, M., Ghosh, P.C., (2014). SOFC power generation system by bio-gasification. Energy Procedia, 54, 748-755.

[144] Zhang, W., Croiset, E., Douglas, P.L., Fowler, M., Entchev, E., (2005). Simulation of a tubular solid oxide fuel cell stack using AspenPlusTM unit operation models. Energy conversión and management, 46 (2), 181-196.

[145] Anderson, T., Vijay, P., Tade, M.O., (2014). An adaptable steady state Aspen Hysys model for the methane fuelled solid oxide fuel cell. Chemical Engineering Research and Design, 92 (2), 295-307.

[146] Özveren, U. (2013) Theoretical and experimental investigation of biomass and coal gasification. PhD Thesis, Marmara University, Chemical Engineering, Istanbul,Turkey.

[147] O'Hayre, R., Cha, S., Colella, W., Prinz, F., (2009). Fuel Cell Fundamentals, Fuel Cell Characterization, Second Edition, John Wiley & Sons, Inc., New Jersey, 237-238.

[148] Song, C., (2002). Fuel processing for low-temperature and high-temperature fuel cells: Challenges, and opportunities for sustainable development in the 21st century. Catalysis today, 77 (1-2), 17-49.

[149] Achenbach, E., (1994). Three-dimensional and time-dependent simulation of a planar solid oxide fuel cell stack. Journal of power sources, 49 (1-3), 333-348.

[150] Song, T.W., Sohn, J.L., Kim, J.H., Kim, T.S., Ro, S.T., Suzuki, K., (2005). Performance analysis of a tubular solid oxide fuel cell/micro gas turbine hybrid power system based on a quasi-two dimensional model. Journal of power sources, 142 (1-2), 30-42.

[151] Bessette II, N.F., Wepfer, W.J., Winnick, J., (1995). A mathematical model of a solid oxide fuel cell. Journal of the Electrochemical Society, 142 (11), 3792.

[152] Chan, S., Khor, K., Xia, Z., (2001). A complete polarization model of a solid oxide fuel cell and its sensitivity to the change of cell component thickness. Journal of power sources, 93 (1-2), 130-140.

[153] Arpino, F., Massarotti, N., (2009). Numerical simulation of mass and energy transport phenomena in solid oxide fuel cells. Energy, 34 (12), 2033-2041.

[154] Todd, B., Young, J., (2002). Thermodynamic and transport properties of gases for use in solid oxide fuel cell modelling. Journal of power sources, 110 (1), 186-200.

[155] Fuller, E.N., Schettler, P.D., Giddings, J.C., (1966). New method for prediction of binary gas-phase diffusion coefficients. Industrial & Engineering Chemistry, 58 (5), 18-27.

[156] Din, Z.U., Zainal, Z., (2016). Biomass integrated gasification–SOFC systems: Technology overview. Renewable and Sustainable Energy Reviews, 53, 1356-1376.

[157] Cordiner, S., Feola, M., Mulone, V., Romanelli, F., (2007). Analysis of a SOFC energy generation system fuelled with biomass reformate. Applied Thermal Engineering, 27 (4), 738-747.

[158] Subotić, V., Baldinelli, A., Barelli, L., Scharler, R., Pongratz, G., Hochenauer, C., et al., (2019). Applicability of the SOFC technology for coupling with biomass-gasifier systems: Short-and long-term experimental study on SOFC performance and degradation behaviour. Applied Energy, 256, 113904.

[159] Aravind, P., de Jong, W., (2012). Evaluation of high temperature gas cleaning options for biomass gasification product gas for solid oxide fuel cells. Progress in energy and combustion science, 38 (6), 737-764.

[160] Pereira, E.G., Da Silva, J.N., de Oliveira, J.L., Machado, C.S., (2012). Sustainable energy: a review of gasification technologies. Renewable and Sustainable Energy Reviews, 16 (7), 4753-4762.

[161] Çolak, A.B., (2021). A novel comparative analysis between the experimental and numeric methods on viscosity of zirconium oxide nanofluid: Developing optimal artificial neural network and new mathematical model. Powder Technology, 381, 338-351.

[162] Bahiraei, M., Heshmatian, S., Moayedi, H., (2019). Artificial intelligence in the field of nanofluids: A review on applications and potential future directions. Powder Technology, 353, 276-301.

[163] Alpaydin, E., (2020). Introduction to machine learning, Fourth Edition, MIT press.

[164] Sarkar, B., Sengupta, A., De, S., DasGupta, S., (2009). Prediction of permeate flux during electric field enhanced cross-flow ultrafiltration—a neural network approach. Separation and purification technology, 65 (3), 260-268.

[165] Moghaddam, A.H., Moghaddam, M.H., Esfandyari, M., (2016). Stock market index prediction using artificial neural network. Journal of Economics, Finance and Administrative Science, 21 (41), 89-93.

[166] Igwe, K., Oyedum, O., Aibinu, A., Ajewole, M., Moses, A., (2021). Application of artificial neural network modeling techniques to signal strength computation. Heliyon, 7 (3), e06047.

[167] Feng, J., Lu, S., (Year). Performance analysis of various activation functions in artificial neural networks. IOP Publishing, Journal of Physics: Conference Series, 1237, 022030.

[168] Daher, R. (2005) Application of artificial intelligence in gas turbine control and modelling. Master Thesis, Carleton University, Mechanical and Aerospace Engineering Ottawa, Ontario, Canada.

[169] Chen, T.-c., Han, D.-j., Au, F.T., Tham, L., (Year). Acceleration of Levenberg-Marquardt training of neural networks with variable decay rate. IEEE, Proceedings of the International Joint Conference on Neural Networks, 2003, 3, 1873-1878.

[170] Loha, C., Chattopadhyay, H., Chatterjee, P.K., (2013). Energy generation from fluidized bed gasification of rice husk. Journal of renewable and sustainable energy, 5 (4), 043111.

[171] Rupesh, S., Muraleedharan, C., Arun, P., (2016). ASPEN plus modelling of air–steam gasification of biomass with sorbent enabled CO2 capture. Resource-efficient technologies, 2 (2), 94-103.

[172] Jarungthammachote, S., Dutta, A., (2008). Equilibrium modeling of gasification: Gibbs free energy minimization approach and its application to spouted bed and spout-fluid bed gasifiers. Energy conversión and management, 49 (6), 1345-1356.

[173] Veyo, S.E., Lundberg, W.L., (Year). Solid oxide fuel cell power system cycles. American Society of Mechanical Engineers Digital Collection, ASME 1999 international gas turbine and aeroengine congress and exhibition.

[174] Gómez-Barea, A., Ollero, P., Leckner, B., (2013). Optimization of char and tar conversion in fluidized bed biomass gasifiers. Fuel, 103, 42-52.

[175] Faraji, M., Saidi, M., (2021). Hydrogen-rich syngas production via integrated configuration of pyrolysis and air gasification processes of various algal biomass: Process simulation and evaluation using Aspen Plus software. International Journal of Hydrogen Energy, 46 (36), 18844-18856.

[176] Monteiro, E., Ismail, T.M., Ramos, A., Abd El-Salam, M., Brito, P., Rouboa, A., (2017). Assessment of the miscanthus gasification in a semi-industrial gasifier using a CFD model. Applied Thermal Engineering, 123, 448-457.

[177] Couto, N.D., Silva, V.B., Monteiro, E., Rouboa, A., (2015). Assessment of municipal solid wastes gasification in a semi-industrial gasifier using syngas quality indices. Energy, 93, 864-873.

[178] De Jong, W., van Ommen, J.R., (2014). Biomass as a sustainable energy source for the future, Wiley Online Library.

[179] Pinto, F., Lopes, H., André, R.N., Dias, M., Gulyurtlu, I., Cabrita, I., (2007). Effect of experimental conditions on gas quality and solids produced by sewage sludge cogasification. 1. Sewage sludge mixed with coal. Energy & Fuels, 21 (5), 2737-2745.

[180] Couto, N., Monteiro, E., Silva, V., Rouboa, A., (2016). Hydrogen-rich gas from gasification of Portuguese municipal solid wastes. International Journal of Hydrogen Energy, 41 (25), 10619-10630.

[181] Pinto, F., André, R.N., Carolino, C., Miranda, M., Abelha, P., Direito, D., et al., (2015). Effects of experimental conditions and of addition of natural minerals on syngas production from lignin by oxy-gasification: Comparison of bench-and pilot scale gasification. Fuel, 140, 62-72.

[182] Hosseinpour, J., Chitsaz, A., Eisavi, B., Yari, M., (2018). Investigation on performance of an integrated SOFC-Goswami system using wood gasification. Energy, 148, 614-628.

[183] Bellomare, F., Rokni, M., (2013). Integration of a municipal solid waste gasification plant with solid oxide fuel cell and gas turbine. Renewable Energy, 55, 490-500.

[184] Abuadala, A.G. (2010) Investigation of sustainable hydrogen production from steam biomass gasification. PhD Thesis, University of Ontario Institute of Technology, Mechanical Engineering, Canada.

[185] Wongchanapai, S., Iwai, H., Saito, M., Yoshida, H., (2012). Performance evaluation of an integrated small-scale SOFC-biomass gasification power generation system. Journal of power sources, 216, 314-322.

[186] Maran, J.P., Priya, B., (2015). Modeling of ultrasound assisted intensification of biodiesel production from neem (Azadirachta indica) oil using response surface methodology and artificial neural network. Fuel, 143, 262-267.

[187] Maran, J.P., Priya, B., (2015). Comparison of response surface methodology and artificial neural network approach towards efficient ultrasound-assisted biodiesel production from muskmelon oil. Ultrasonics Sonochemistry, 23, 192-200.

[188] Okoro, E.E., Obomanu, T., Sanni, S.E., Olatunji, D.I., Igbinedion, P., (2021). Application of artificial intelligence in predicting the dynamics of bottom hole pressure for under-balanced drilling: Extra tree compared with feed forward neural network model. Petroleum, In-press.

[189] Sirdesai, N.N., Singh, A., Sharma, L.K., Singh, R., Singh, T., (2018). Determination of thermal damage in rock specimen using intelligent techniques. Engineering Geology, 239, 179-194.

[190] Sun, F., Xie, G., Li, S., (2021). An artificial-neural-network based prediction of heat transfer behaviors for in-tube supercritical CO2 flow. Applied Soft Computing, 102, 107110.